Stochastic Geometry Approach on Modelling Finite Millimetre Wave Outdoor Cellular Networks

Thiaza Thasthakeer

A thesis submitted in fulfilment of the requirements for the degree of Doctor of Philosophy in Electrical and Electronic Engineering, the University of Auckland, 2021.

Abstract

This thesis focuses on modelling future high capacity cellular networks operating in millimetre wave (mmWave) frequency bands. An analytical approach has been proposed for network modelling rather than system-level simulations. The increasing complexity of cellular networks due to their continuous evolution has made conventional system-level simulations time-consuming. Recently stochastic geometry has been recognised as a tractable and efficient analytical tool for network modelling and quantifying key performance metrics.

The stochastic geometry approach involves representing base stations and user locations as a spatial point process. It allows us to investigate trends in performance related to base station density and user distribution. Network performance characteristics mainly depend on the nature of the point process model. Therefore it is important that the chosen model should closely represent practical cellular network deployments. The goal of this research is to adopt an accurate spatial point process model to design cellular networks. Previously the Poisson Point Process (PPP) model has been used as a way of representing these practical cellular networks. However, this model has some deficiencies, and the Binomial Point Process (BPP) overcomes these deficiencies to some extent.

This research uses the BPP model to analyse the performance of high capacity cellular networks operating at millimetre wave frequencies. By considering the unique features of mmWave communications, such as different channel characteristics for the line-of-sight (LOS) and the non-line-of-sight (NLOS) links and high directional antenna gains provided by antenna arrays, we have developed stochastic geometry frameworks to analyse both downlink and uplink coverage probability for a reference receiver.

The BPP is defined in a finite region with a fixed number of nodes. Initially, a simple finite disk region has been considered as the network's geographical region, and then later, the analysis has been extended to a more general arbitrary region.

The results indicate that the performance difference between an arbitrary shape and a disk shape is almost negligible for a centrally located user. Therefore a simple disk region can be an acceptable shape to model finite cellular systems for a centrally located user. Furthermore, we have also analysed the performance trends representing the impact of antenna arrays, the base station (BS) density, and LOS and NLOS links in the coverage analysis.

Acknowledgements

First and foremost, I am incredibly grateful to my main supervisor Professor Kevin Sowerby for his invaluable supervision, guidance and patience throughout my PhD program. I would also like to extend my gratitude to my co-supervisor, Dr Michael Neve, for his guidance and encouragement towards completing this research.

I would like to thank my friends and colleagues from the electrical department for their support, companionship, and cherished time spent together on campus and in social settings.

Finally, I would like to thank my parents and brother, whose love and encouragement have always been the source of inspiration throughout my studies.

List of Acronyms

mmWave	Millimetre Wave
UDN	Ultra Dense Networks
SINR	Signal-to-Interference-plus-Noise-Ratio
BS	Base Station
UE	User Equipment
PPP	Poisson Point Process
BPP	Binomial Point Process
PDF	Probability Density Function
CDF	Cumulative Distribution Function
LOS	Line-of-Sight
NLOS	Non-Line-of-Sight
MGF	Moment Generating Function
PGFL	Probability Generating Functional
AoD	Angle of Departure
FPC	Fractional Power Control
MIMO	Multiple Input Multiple Output
CA	Carrier Aggregation
WiMAX	Worldwide Interoperability for Microwave Access
LTE-A	Long Term Evolution - Advanced
LTE-U	Long Term Evolution - Unlicensed

List of Notations

$\mathbb{R}^2$	Two-dimensional Euclidean domain
$\forall$	For all
Φ	Set of points defined by a point process
Φ_x	Specific point process formalised by subscript x
s_x	A set of points formalised by subscript x
λ_p	Poisson point process node density
$\boldsymbol{X}, \boldsymbol{Y}$	Arbitrary vectors describing the locations of the nodes, denoted by bold capital letters
$\boldsymbol{O}$	Vector denoting the origin
$\boldsymbol{Y} \in \Phi \setminus \boldsymbol{X}$	This can be interpreted as, a node located at $\boldsymbol{Y}$ is an element in Φ, which excludes the node at $\boldsymbol{X}$
$\|\|\boldsymbol{X} - \boldsymbol{Y}\|\|$	Distance between two vectors
$\mathcal{A}$, $\|\mathcal{A}\|$	Network region and area
R	Radius of a disk region
$h_{\boldsymbol{X}}$	Fading gain of the transmitted signal of a node located at $\boldsymbol{X}$
N_t	Number of base stations
ω	Blockage parameter
β	Nakagami fading parameter
α	Path loss exponent
α_L, α_N, β_L, β_N	LOS and NLOS path loss exponents and Nakagami fading parameters.
$\Gamma(.)$	Gamma function
τ	SINR threshold
ϵ	Power control factor
θ_i	Interior angle between two adjacent sides of the polygon
L	Number of sides in a polygon
p_t	Base station transmit power
σ^2	Thermal noise power

$G_{\boldsymbol{X}}, G_{\boldsymbol{Y}}$	Antenna gains of the desired and interfering signals
$G_{\text{act}}(.), G_{\text{mcos}}(.)$	Actual and multi-cosine antenna gains
N, φ, d, λ, ϑ	Refers to antenna parameters as follows; Number of array elements, spatial AoD, antenna element spacing, wavelength and physical AoD
$\mathbb{E}_X[.]$	Expectation operation with respect to X
$\mathcal{L}_X(.)$	Laplace transform of the PDF of the random variable X

Contents

List of Figures

List of Tables

Chapter 1

Introduction

Combined with a growing trend in bandwidth-hungry applications, the significant increase in smart mobile devices has resulted in a looming spectrum crisis [1]. Ericsson reported that there are 7.8 billion mobile devices globally in 2017, which will increase to 9.1 billion mobile devices in 2023. Also, the average data traffic generated by an active smartphone is 2.9 GB per month in 2017, which is anticipated to increase to 17 GB per month in 2023 [2]. There is a strong consensus in academia and industry that the present cellular network evolution cannot fulfil the expected high demand [3]. Therefore to meet the ever-increasing traffic demand, three main approaches have been proposed in recent literature. The first approach is to improve the spectral efficiency by using advanced physical layer techniques, such as multiple input multiple output (MIMO) or carrier aggregation (CA). While MIMO improves the spectral efficiency by placing multiple antennas at the transmitter and receiver, the CA aggregates multiple frequency blocks in order to increase the data rate [4, 5]. These techniques are relatively well developed and are part of the WiMAX and LTE-A wireless standards [6]. In the case of conventional cellular frequencies in the sub-6 GHz range, packing a massive number of antennas on a Base Station (BS) and a mobile device is limited because the antenna size decreases with frequency [6], and the carrier aggregation is limited to available spectrum in the sub-6 GHz range.

The second approach is to provide more spectrum to cellular networks. With the limited available spectrum in the sub-6 GHz range, there are two possible options. One is to exploit the readily available unlicensed spectrum in the 5 GHz band (the same spectrum is shared by the Wi-Fi standard as well), standardised as LTE for Unlicensed (LTE-U) [7]. This standard is well developed. Recently T-Mobile rolled out LTE-U networks in six cities in the US [8]. Another option is to utilise the significant amount of spectrum available in the range of 30 GHz to 300 GHz, referred to as millimetre wave (mmWave) frequencies [9]. A large amount of new spectrum in mmWave bands is becoming increasingly attractive as a potential solution for the next generation high capacity networks. These high frequencies exhibit very different propagation characteristics from sub-6 GHz frequencies. Millimetre wave frequencies have very high signal attenuation and greater diffraction loss, limiting the cell range to up to 200 m [9, 10].

The third approach is network densification to bring the users close as possible to the BSs, this is achieved by the dense deployment of small cells, and these networks are termed as Ultra-Dense Networks (UDN). These small access nodes are with small transmission power deployed either by customers or operators [11]. The UDNs can be defined as those networks where there are more cells than active users [12]. Combining the last two approaches by deploying ultra-dense networks in the mmWave band can be a promising approach to meet future traffic demand, which is currently under active research [13, 14]. Deployment of UDN in mmWave bands has many open challenges to be addressed and should be defined clearly before the network becomes commercially available.

This thesis focuses on modelling the downlink and uplink performances of mmWave cellular networks. An important performance-related metric in a cellular network is the probability of coverage, which can be interpreted as the probability that the signal strength is below the minimum required signal strength of a random user to make a successful connection with a base station. Mathematically, it can be defined as the Signal-to-Interference-plus-Noise-Ratio (SINR) being greater than a predefined threshold for successful communication [6]. All the performance metrics, such as the probability of coverage, spectral efficiency, and throughput, are

primarily a function of the SINR [15]. As a result, this research primarily concerned about the characterisation of the SINR in the mmWave UDN.

The first challenge for performance analysis is network modelling. The Wyner model [16] has commonly been used to model and analyse cellular networks due to its analytical tractability, but with a significant simplification of a practical cellular system, assuming fixed user locations and homogeneous interference intensity. In comparison, real system user locations are random, and the interference level varies over a cell range [17]. Another way to model cellular networks is with a hexagonal grid pattern using Monte Carlo simulations; in practice, however, the locations of the BSs do not strictly follow the grid pattern [3] – instead, they follow random topology. Recently another modelling approach has been adopted, that is, to model BS locations as a random spatial model with complete spatial randomness [18]. However, real cellular networks are deployed in a more strategic manner than either a complete random independent deployment or a regular grid pattern deployment. A better model would possess more spatial variations than the regular grid model, but not to the extreme provided by the random spatial model. However, the properties of random spatial models enable tractable analytical models to be developed using a stochastic geometry approach, overcoming the need for exhaustive simulations required by the regular grid models [18].

Under the random spatial model, the BSs can be distributed as a point process, this means that they are randomly scattered in a plane with independent locations[1]. The Poisson Point Process (PPP) is the most popular choice due to its simplicity and tractability [20], where a random number of BSs are independently distributed in an infinite region [19]. However, in reality, cellular networks are planned with a fixed number of BSs in a geographically bounded region. This creates a necessity to adopt a more suitable distribution to represent cellular networks. Another choice in such cases is modelling the network with the Binomial Point Process (BPP) because the BPP specifies a fixed number of nodes in a geographically bounded

[1]Note that not all point processes are scattered in a plane with independent locations. There are exemptions; for example, in Matérn cluster point process, the daughter points are uniformly scattered on a ball centred at each parent point [19, p. 57].

region [21]. Therefore in this thesis, we[2] focus on system design and performance evaluation by incorporating the unique features of mmWave communications by modelling the network using the binomial point process.

1.1 Research Contributions

This thesis has developed an analytical model to analyse a mmWave cellular systems' performance trends of both uplink and downlink communications. As highlighted in the introduction, our research's main contribution is to use a more realistic point process model to design the mmWave cellular systems. Therefore in this thesis, we have analysed a finite mmWave cellular systems using the BPP. To the best of our knowledge, finite mmWave cellular systems with BPP have not been investigated in previous literature produced to date. In the following section, we elaborate on the research problems and this thesis's corresponding contributions.

The first research problem we tackle in this thesis is the downlink performance analysis of mmWave cellular systems (Chapter 4). Since we consider a finite point process, we need to define a finite network region. In this regard, we have considered a finite two-dimensional disk region as the geographical network region. The main contributions this thesis makes regarding this research problem are summarised as follows:

- A mathematical framework for evaluating an outdoor mmWave cellular network's downlink performance using stochastic geometry tools has been presented. Unlike previous literature on mmWave system evaluation, where the BSs are assumed to be distributed according to a PPP, in this research, a new system model with a uniform BPP has been assumed to model the locations of the BSs accurately. In this setup, a user is associated with the BS that has the smallest path loss;

[2]This thesis is a single-authored document, but the term "we" is used instead of "I" because the contributions arise collectively from the author and her supervisors.

- The coverage probability and achievable rate of a reference user have been derived for a mmWave cellular network. The mmWave cellular network has been modelled by incorporating the unique characteristics of mmWave communications such as different line-of-sight (LOS) and non-line-of-sight (NLOS) link characteristics and a more realistic array antenna model, termed as multi-cosine antenna model, proposed in [22];

- To compute the coverage probability, as the intermediate steps, the user association probabilities, serving BS's distance distributions, interfering BSs' distance distributions, and the Laplace transform of the interference have been evaluated;

- Numerical results are provided to validate the accuracy of the proposed analytical models. The results show the impact of antenna array size, location-dependant user performance, the effect of blockage parameter, the effect of BS count and the impact of the LOS and the NLOS links in the coverage performance analysis; and

- Also, a comparative performance analysis of the PPP and BPP models has been conducted.

Having analysed the downlink performance in a finite disk region, the second research problem we tackle is to analyse the performance in a more generalised shape (Chapter 5). The main contributions this thesis makes regarding this research problem are summarised as follows:

- In this analysis, we consider a regular L-sided convex polygon. This chapter is an extension of Chapter 4. We focus on the coverage probability derivations, using similar modelling assumptions to those seen in Chapter 4; and

- We have compared user performance in a regular polygon with a user in a disk region. The results illustrate that the performance difference between polygons with different sides and disk regions is almost similar. Therefore

considering a finite disk region can be a better way to model a finite region, enabling better analytical tractability than a regular polygon.

The third research problem we focus on is the uplink performance analysis (Chapter 6). Based on the conclusions derived in Chapter 5, the finite geographical region to model the uplink performance is considered as a disk region. The uplink coverage analysis is more complicated than the downlink analysis; the additional challenges involved in modelling uplink communications are discussed in Chapter 6. The contributions this thesis makes to this research problem can be summarised as follows:

- Similar to the downlink performance analysis in chapters 4 and 5, we have developed a stochastic geometry framework for evaluating the uplink performance of an outdoor mmWave cellular system. We have assumed a uniform BPP in order to model the network nodes accurately. In this case, a user associates with the BS, which has the smallest path loss;
- Coverage probability has been derived for the uplink transmission of finite mmWave cellular network by incorporating the unique features of mmWave communications such as high directional antenna arrays and the different link characteristic for LOS and NLOS links;
- Fractional power control (FPC) at the user equipment has been adopted to minimise the user equipment's battery power consumption and to control the interference power in the uplink transmission;
- Also, as in the previous chapters, to compute the coverage probability, we need to derive certain intermediate definitions, namely, (i) association probabilities, (ii) distance distributions between a reference user (user of interest) and its tagged BS, (iii) distance distributions between the interfering users and the reference BS (BS of interest) and (iv) the Laplace transform of the interference. The association probabilities and the tagged BS's distance distributions can be utilised directly from Chapter 4. However, the interference

modelling on uplink communications is different from the downlink communications. Therefore, the interfering users' distance distributions and the Laplace transform of interference for the uplink communications have been derived in this chapter;

- Similar to the downlink scenario, we have compared the performance between the PPP and BPP models under the uplink case; and
- Based on the system design, finally, the impact of the antenna array size, blockage parameter, BS count, network area and the FPC factor have been investigated.

1.2 Thesis Outline

The remainder of the thesis is organised as follows. Chapter 2 provides the relevant theoretical background on stochastic geometry and key concepts relating to mmWave cellular systems. Chapters 4 to 6 then presents this thesis's research contributions. In Chapter 4, the downlink performance analysis of mmWave cellular systems in a finite disk region is investigated. Chapter 5, presents an extension to the work of Chapter 4 by modelling the downlink performance in an arbitrary finite region, and Chapter 6 presents the uplink performance analysis of finite mmWave cellular systems. Finally, Chapter 7 concludes this thesis by presenting the main results and highlighting possible future research directions.

Chapter 2

Background

This chapter presents the essential theoretical background related to this research. Firstly, mmWave cellular systems' fundamentals, which includes the essential properties of mmWave communications, have been presented. Then the fundamentals of stochastic geometry, which are relevant to the analytical models we have presented in this thesis, have been outlined.

2.1 Fundamentals of Millimetre Wave Communications

As mentioned in Chapter 1, mmWave frequencies (which are theoretically defined as being between 30 and 300 GHz) have different propagation characteristics compared to the sub-6 GHz frequencies. These propagation characteristics brings additional challenges to be addressed before deploying the cellular networks in real environment. Therefore it is essential to incorporate these peculiar features of mmWave communications in to our system design as presented in the following sections.

2.1.1 Large-scale Path Loss

The path loss can be modelled as

$$L(r) = L(r_0) + 10\alpha \log_{10}\left(\frac{r}{r_0}\right) + \mathcal{S} \quad \text{in dB} \tag{2.1}$$

where r is distance between a BS and a user, $L(r_0)$ is the close-in free space path loss, α is the path loss exponent and $\mathcal{S}$ is a random variable for log-normal shadowing. The close-in free space path loss can be computed by Friis's equation, which is

$$L(r_0) = 20 \log_{10}\left(\frac{4\pi r_0}{\lambda}\right) \quad \text{in dB}, \tag{2.2}$$

where λ is the carrier wavelength r_0 is the close-in distance considered as $r_0 = 1$ metre in [23].

Most of the mmWave coverage analysis literature [24, 25] adopts a simplified path loss model, which this thesis will also employ in the subsequent chapters. A simplified path loss model is given as

$$L(r) = r^{\alpha}, \tag{2.3}$$

where α is the path loss exponent.

Due to the presence of blockages in the environment, different path loss laws apply to the LOS and NLOS links. Based on the extensive measurements using directional antennas in [23, 26, 27] the LOS path loss exponent is found to be equal to 2, i.e. $\alpha_L = 2$, whereas the LOS paths are clear paths with no obstacles in between the transmitter and the receiver. On the other hand, the NLOS links path loss exponent is found to be larger than the LOS path loss exponent, due to the presence of blocking in the NLOS paths. Based on the measurements in the New York and Austin city it has been concluded that the NLOS path loss

TABLE 2.1: Penetration losses for different materials and frequencies [28].

		Attenuation (dB)		
Material	**Thickness (cm)**	**<3 GHz** [29, 30]	**40 GHz** [31]	**60 GHz** [29]
Drywall	2.5	5.4	—	6.0
Office white-board	1.9	0.5	—	9.6
Clear glass	0.3/0.4	6.4	2.5	3.6
Mesh glass	0.3	7.7	—	10.2
Chipwood	1.6	—	0.6	—
Wood	0.7	5.4	3.5	—
Plasterboard	1.5	—	2.9	—
Mortar	10	—	160	—
Brick wall	10	—	178	—
Concrete	10	17.7	175	—

exponent is $\alpha_N = 4.5$, $\alpha_N = 3.3$ and $\alpha_N = 4.7$ at 28 GHz, 38 GHz and 73 GHz frequencies, respectively [23]. In this thesis we have assumed the LOS and NLOS path loss exponents to be $\alpha_L = 2$ and $\alpha_N = 4$, respectively.

2.1.2 Effects of Blockage

The presence of blockages results in two outcomes that are penetration losses and multi-path components. Millimetre wave frequencies do not penetrate most solid materials compared to the sub-6 GHz frequencies. Table 2.1 summarises the penetration losses for different materials measured at sub-6 GHz and mmWave frequencies. As can be observed in Table 2.1, mmWave frequencies exhibit very high signal attenuation for certain building materials such as brick and concrete, which may keep outdoor mmWave signals away from indoor users.

Furthermore, high penetration loss occurs when mmWave signals go through the human body and trees; penetration losses through trees and the human body can be as much as 20 dB [32, 33] and 20–35 dB [34, 35], respectively. These losses can significantly decrease the coverage probability of mmWave networks.

The next phenomena that occurs due to blocking is the impact of the multi-path components. Millimetre wave channel has fewer multi-path components than a sub-6 GHz channel; for example, in the Manhattan area the average number of multi-path components was found to be approximately five and three at 28 GHz and 73 GHz, respectively [23]. Due to this, the small-scale fading[1] has less impact on mmWave signals compared to the effect of Rayleigh fading[2] on sub-6 GHz frequencies. By understanding the minor impact of small-scale fading in mmWave communications, we can observe that it is important to choose an appropriate fading models to represent the mmWave channels. Thus, we have incorporated the Nakagami-m fading model as described below.

Nakagami-m fading: The Nakagami fading model is a generalised distribution to describe fading, whereas different fading parameters can be applied to LOS and NLOS links. Its probability density function (PDF) is given as [37, p. 24]

$$p(z,\Omega) = \frac{2}{\Gamma(m)}\left(\frac{m}{\Omega}\right)^{m} z^{2m-1}\exp\left(-\frac{m}{\omega}z^{2}\right); \quad z>0, m\geq 0.5 \tag{2.4}$$

where z is the received signal level, $\Gamma(.)$ is the gamma function, m is the parameter which represents the severity of the fading and Ω is the average signal power. The Nakagami fading model is versatile, whereas $m = 1$, and $m \to \infty$ represent the Rayleigh fading, and no-fading cases, respectively.

2.1.3 Antenna Beamforming

From (2.2), it is evident that the path loss increases with the carrier frequency. Therefore in order to compensate the high path loss that occurs in the mmWave cellular systems, it is expected that mmWave cellular systems will be deployed with large antenna arrays at the base stations and mobile stations. In mmWave communications systems large number of antenna elements can be packed within

[1]Small-scale fading is the random fluctuations of the signal amplitude over short distance due to effects of the multi-path components [36, p. 509].

[2]Rayleigh fading represents a severe fading environment, whereas most applicable when there is no dominant LOS path between the transmitter and receiver [37, p. 20].

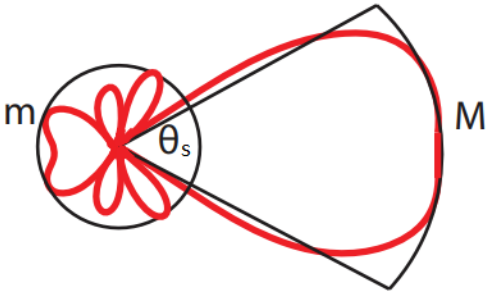

FIGURE 2.1: Sectored antenna model [38].

a small hardware to provide directional beamforming. This is because antenna elements' size decrease with the increase of frequency.

For analytical tractability, most mmWave cellular system models have considered a simplified sectored antenna model (also known as the flat-top antenna model) as initially proposed in [38]. Here the antenna gain pattern is divided into discrete regions based on the angle off the boresight direction as in Fig. 2.1. Hence, the antenna gain can be expressed as

$$G = \begin{cases} \mathrm{M} & |\theta_s| \leq \omega_b \\ \mathrm{m} & \text{elsewhere,} \end{cases} \tag{2.5}$$

where M, m, ω_b and θ_s refer to main lobe gain, back lobe gain, main lobe beamwidth and steering angle, respectively. The aforementioned antenna model fails to capture the actual antenna radiation pattern. Therefore in this thesis we have considered a better approximation to the actual antenna model developed in [22]. The details of the antenna modelling assumption has been given in Section 4.1.4.

2.2 Stochastic Geometry for Cellular Network Analysis

This section presents the fundamentals of stochastic geometry and the point process models used in this thesis. Unlike stochastic geometry, another conventional approach is the system-level simulations, which can analyse the cellular network's performance in any detail. Nevertheless, every required scenario needs to be simulated individually through specific system parameters is one of the main drawbacks of simulations as it is a much time-consuming task [39]. Hence to overcome these limitations, it is desirable to have an accurate and efficient analytical tool to model the cellular systems. Recently, stochastic geometry has proven to be an excellent candidate. Stochastic geometry is the mathematical study of random points defined on some (often Euclidean) space [19, pp. 3-4]. In the context of wireless networks, the random points may represent the locations of network nodes such as transmitters and receivers, and the Euclidean space is usually the two-dimensional plane, which represents a geographical region. Stochastic geometry analysis provides a path for analytical modelling using the statistical properties of the point process models. It provides an approach for characterising the key performance metrics of cellular networks [40, p. 9].

2.2.1 Point Process Models

A point process can be referred to as a collection of nodes located in a certain space [19, pp. 3-4]. A collection of nodes in wireless networks represents BSs and user equipment (UEs) [3]. The locations of these nodes are completely random in nature [41, p. 36]. From the modelling perspective, it is appropriate to assume the mobile user locations as a complete random process, but BSs are deployed in a more strategic manner. However, as presented in [42], the results from the point process models closely match actual 4G deployments and a coverage map of a real LTE network and a point process model is shown in Fig. 2.2 [18]. Random spatial models enable the development of tractable analytical tools that estimate

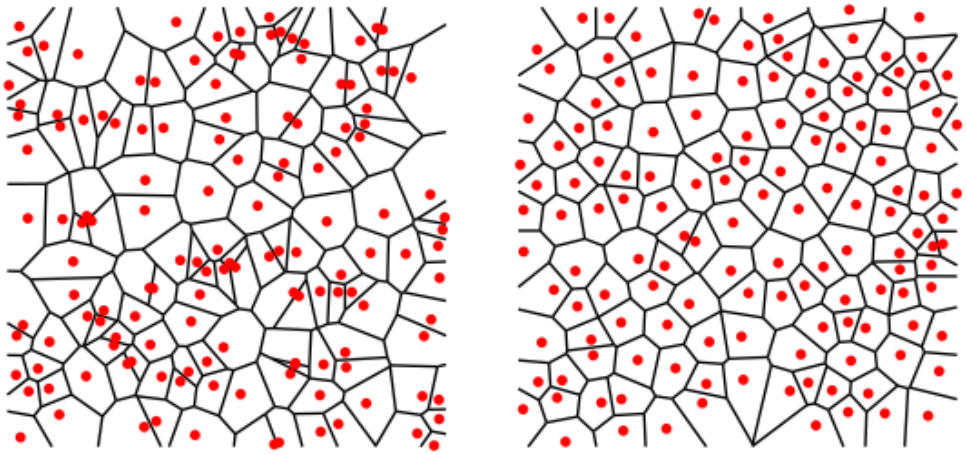

FIGURE 2.2: Point process model (left) compared with the actual LTE BSs [18].

the performance of cellular network deployments; this would otherwise require repeated simulation analysis for sets of specific BS locations.

In stochastic geometry-based cellular network modelling, different types of point process models have been adopted. Out of all of these point process models, the PPP is most commonly used and has been adopted by almost all the mm-wave cellular network models [24, 25, 38, 43–47].

2.2.1.1 Poisson Point Process

A Poisson point process is characterised via the Poisson distribution. It has the following properties:

- In a given sub region A, the number of points ($\Psi(A)$) is a Poisson random variable $\forall\ A \in \mathbb{R}^2$, such that the probability that $\Psi(A)$ equals to n is given by

$$\mathbb{P}[\Psi(A) = n] = \frac{\exp\left(-\mu(A)\right)\mu(A)^n}{n!} \tag{2.6}$$

  where $\mu(A)$ is the expected value of $\Psi(A)$; and

- For any m disjoint sets $A_1, A_2, ..., A_m$, the number of points $\Psi(A_1), ..., \Psi(A_m)$ are independent random variables.

Furthermore, the PPP is termed as a homogeneous PPP, if the points are independently and uniformly distributed with uniform intensity λ such that

$$\mu(A) = \lambda l(A) \tag{2.7}$$

where $l(A)$ is a Lebesgue measure (i.e. size) of A. Conversely, while an inhomogeneous PPP also has independence between disjointed sets, but the points are not uniformly distributed [18, 48].

When it comes to stochastic geometry-based network modelling, PPP is the most common choice due to its simplicity and analytical tractability. Its properties such as stationary (invariant to translation) and isotropic (invariant to rotation) enables to analyse the location independent performance [3]. This reduces the analytical complexity, such that typically a user is assumed to be at the centre of the network and all the statistical characteristics observed at this user are same for all the other users in the network. Even though this location independent performance analysis reduces the analytical complexity, the PPP based model cannot be used to analyse the location dependant performance. It is evident that the performance of a user at the centre of a network and at the boundary will have different statistical characteristics. Therefore it is crucial to have a better model, which can be utilised to analyse the location dependant performance [3].

From the definition of the PPP, it is evident that it is a process defined in an infinite space with a random number of nodes. However, the real cellular environment is a finite geographical region with a fixed number of network nodes. Therefore it is necessary to adopt a more suitable point process, which can closely represents the real cellular environment. A possible choice in this case is to model the network using the BPP.

2.2.1.2 Binomial Point Process

The BPP can be defined as, a fixed number of points n is identically and independently distributed on a compact set $W \subset \mathbb{R}^2$. The number of points in a sub region $A \subset W$ is binomially distributed with parameters n, and $p = |A|/|W|$ [19, Def. 2.4.4]. Similar to PPP, if the points are distributed randomly, independently and uniformly, the process is referred to as uniform BPP. In contrast to the PPP, however, the BPP allows us to analyse the performance based on the user's location in a finite geographical region. It introduces more complexity than the PPP model offers, but it will be more appropriate to use the BPP due to its aforementioned advantages compared to the PPP. Figures 2.3 and 2.4 show the distribution of PPP and BPP models for three different realisations in a unit square-like region. It can be observed that the PPP gives three different counts for the number of nodes, for the same BS density set-up, whereas in the BPP model the count remains constant for all three realisations.

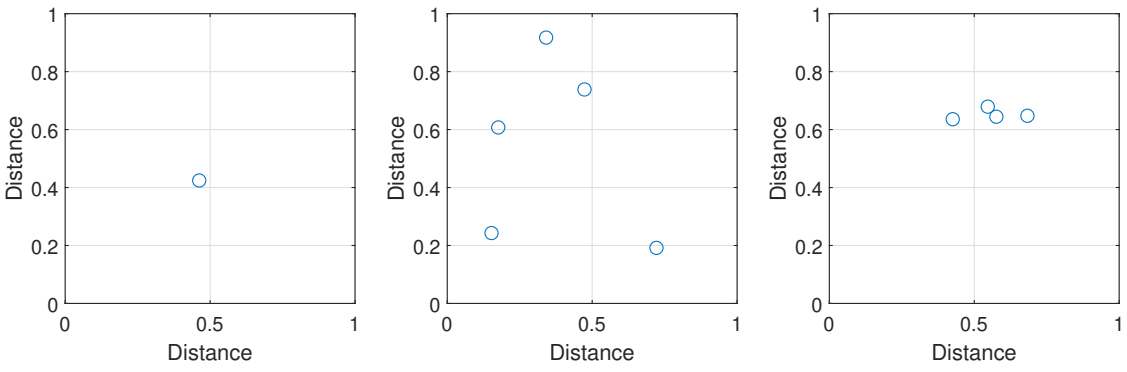

FIGURE 2.3: PPP in a square-like region. This represents the homogeneous PPP for a square-like geographical unit area for three different realisations for a constant BS density (BS density = 6). The unit area plotted is a subset of a theoretically infinite area.

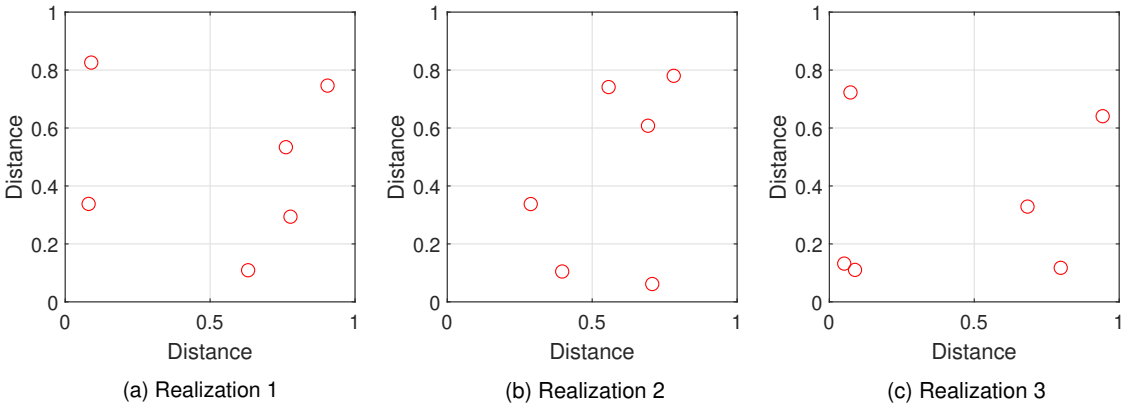

FIGURE 2.4: BPP in a square-like region. This represents the uniform BPP for a square-like geographical unit area for three different realisations for a fixed number of BSs (Number of BSs = 6).

2.3 Key Performance Metric

The Signal-to-Interference-plus-Noise-Ratio (SINR) is the most fundamental metric to evaluate the network performance, as it captures the quality of the received signal by considering both the propagation environment and interferers [49]. In this research, the key SINR related performance metric coverage probability will be employed to analyse the mmWave cellular network performance. The coverage probability is defined as [18]

$$\mathbb{P}[\text{SINR} > \tau] \tag{2.8}$$

where, τ is the SINR threshold for successful decoding at the receiver. It can be interpreted as, the probability that an arbitrary user can achieve the target SINR.

This thesis focuses on both downlink and uplink performance analysis of mmWave cellular systems. As an example the expression for the downlink SINR can be written as

$$\text{SINR} = \frac{L(x)^{-1} h_{\boldsymbol{X}} p_t G_{\boldsymbol{X}}}{(\sigma^2 + I)}; \tag{2.9}$$

$$I = \sum_{\boldsymbol{Y} \in \Phi \setminus \boldsymbol{X}} h_{\boldsymbol{Y}} p_t G_{\boldsymbol{Y}} L(y)^{-1}$$

where I is the total interference from all interfering BSs except the serving BS. Let us denote the locations of the serving BS and interfering BSs as[3] $\boldsymbol{X}$ and $\boldsymbol{Y}$ with distance x and y to the reference user (reference user is the user of interest), respectively. Φ refers to a set of points defined by a point process, here a set of points refer to BSs. The functions $L(x)$ and $L(y)$ represents the path losses given by (2.3) of the desired and interfering signals, respectively. The parameters $h_{\boldsymbol{X}}$ and $h_{\boldsymbol{Y}}$ are the fading gains of the desired and interfering signals representing random channel effects, $G_{\boldsymbol{X}}$ and $G_{\boldsymbol{Y}}$ are the antenna gains of the desired and interfering signals, p_t is the BS transmit power and σ^2 is the thermal noise power. Thermal noise power can be written as, $\sigma^2 = KTB$, where K is the Boltzmann constant, T is the room temperature and B is the bandwidth. The next section presents the downlink SINR coverage probability derivation for a simple model; the notations used are consistent with the above-presented SINR expression (2.9).

2.4 Coverage Probability for a Simple Model

This section provides the derivations of coverage probability for simple models of both PPP and BPP. Through these derivations, the main tools and theorems necessary to derive coverage probability have been explained. These fundamental analytical approaches have been used in chapters 4 to 6 to develop the mathematical frameworks representing the mmWave cellular networks proposed in this thesis.

2.4.1 Coverage Probability with Poisson Point Process

Let us consider a simple downlink scenario, in which we assume that BSs are located according to a homogeneous PPP Φ with density λ_p. As defined in (2.8)

[3]In this thesis we denote a vector describing the location of a point inside a point process with bold capital letters ($\boldsymbol{X}, \boldsymbol{Y}$, etc.).

coverage probability conditioning on the nearest BS being at distance x from the reference user at the origin $\boldsymbol{O}$ can be written as

$$P_{\text{cov,p}} = \mathbb{E}[\mathbb{P}[\text{SINR} > \tau] \mid x] = \int_0^\infty \mathbb{P}[\text{SINR} > \tau] f_p(x) dx \tag{2.10}$$

where $\mathbb{E}[.]$ denotes the expectation and $f_p(x)$ is the probability density function (PDF) of its distance to the nearest BS and is computed as follows:

The void probability of a PPP in an area $\mathcal{A}$ is given by $\exp(-\lambda_p \mathcal{A})$ [18], so the probability that no BSs are closer than x is given by, $\exp(-\lambda_p \pi x^2)$. Therefore the cumulative distribution function (CDF) $F_p(x)$ of its distance to the nearest BS is, $1 - \exp(-\lambda_p \pi x^2)$. The PDF $f_p(x)$ of its distance to the nearest BS is the derivation of the CDF and can be expressed as

$$f_p(x) = \frac{dF_p(x)}{dx} = 2\pi\lambda_p x \exp(-\lambda_p \pi x^2). \tag{2.11}$$

Substituting (2.9) and (2.11) in (2.10) gives

$$\begin{aligned} P_{\text{cov,p}} &= \int_0^\infty \mathbb{P}\left[\frac{x^{-\alpha} h_{\boldsymbol{X}}}{I} > \tau\right] 2\pi\lambda_p x \exp(-\lambda_p \pi x^2) dx \\ &= \int_0^\infty \mathbb{P}\left[h_{\boldsymbol{X}} > \tau x^\alpha I\right] 2\pi\lambda_p x \exp(-\lambda_p \pi x^2) dx \end{aligned} \tag{2.12}$$

where the path loss function is assumed as distance dependent power law path loss $L(x) = x^\alpha$, where α is the path loss exponent. Furthermore the antenna gains of the desired and interfering signals $G_{\boldsymbol{X}}$ and $G_{\boldsymbol{Y}}$, and the transmit power p_t are set to unity. Thermal noise power σ^2 has been excluded.

The inner probability term can be simplified further as

$$\mathbb{P}\left[h_{\boldsymbol{X}} > \tau x^{\alpha} I\right] \overset{(a)}{=} 1 - \mathbb{E}[(1 - \exp\left(-\eta\tau x^{\alpha} I\right))^{\beta}] \overset{(b)}{=} \sum_{n=1}^{\beta} (-1)^{n+1} \binom{\beta}{n} \mathbb{E}[(\exp\left(-\eta\tau x^{\alpha} I\right))] \tag{2.13}$$

where (a) follows from, the fading gain $h_{\boldsymbol{X}}$ is assumed to follow the Nakagami fading. The Nakagami fading follows gamma distribution[4] [50, p. 162], so the analytical computation is derived by using the properties of gamma distribution. From [51], for a normalised gamma random variable γ with parameter β, the probability $P(\gamma < C \in R^{+})$ is upper bounded by $P(\gamma < C \in R^{+}) < [1 - \exp\left(-\eta C\right)]^{\beta}$, where $\eta_L = \beta(\beta!)^{(\frac{-1}{\beta})}$. Furthermore (b) follows from the binomial theorem expansion.

In (2.13), $\mathbb{E}[(\exp\left(-\eta\tau x^{\alpha} I\right))]$ is the Laplace transform of interference. The Laplace transform is defined as an expected value. If X is a random variable, then the Laplace transform of X[5] is given by the expectation [19, p. 81], i.e. $\mathcal{L}_X(s) = \mathbb{E}[\exp\left(-sX\right)]$. With this understanding, the $\mathbb{E}[(\exp\left(-\eta\tau x^{\alpha} I\right))]$ can be written as

$$\mathbb{E}[(\exp\left(-\eta\tau x^{\alpha} I\right))] = \overset{(\text{PPP})}{\mathcal{L}_I}(\eta\tau x^{\alpha}). \tag{2.14}$$

The Laplace transform of interference $\overset{(\text{PPP})}{\mathcal{L}_I}(.)$ can be simplified further by using the probability generating functional (PGFL). The PGFL can be used for converting an expectation of a product of the points in the PPP into an integral and it is defined as follows.

PGFL of a homogeneous PPP, with intensity λ_p can be written as [18]

$$\text{PGFL} = \mathbb{E}\left[\prod_{X \in \Phi} g(X)\right] = \exp\left(-\lambda_p \int_{\mathbb{R}^2} (1 - g(X)) dx\right). \tag{2.15}$$

Now using the PGFL of PPP, the $\overset{(\text{PPP})}{\mathcal{L}_I}(.)$ can be written as

[4] If the amplitude is Nakagami fading, then the received power follows a gamma distribution.

[5] Throughout this thesis, when reference is made to taking the Laplace transform of a random variable this is accomplished by taking the Laplace transform of the PDF of the random variable.

$$\overset{(\mathrm{PPP})}{\mathcal{L}_I}(\eta\tau x^{\alpha}) = \mathbb{E}[(\exp(-\eta\tau x^{\alpha} I))] = \mathbb{E}_{\Phi,h_{\boldsymbol{Y}}}[(\exp(-\eta\tau x^{\alpha} \sum_{\boldsymbol{Y}\in\Phi\setminus\boldsymbol{X}} h_{\boldsymbol{Y}} y^{-\alpha}))]$$

$$= \mathbb{E}_{\Phi}\left[\prod_{\boldsymbol{Y}\in\Phi\setminus\boldsymbol{X}} \mathbb{E}_{h_{\boldsymbol{Y}}}\left[\exp(-\eta\tau x^{\alpha} h_{\boldsymbol{Y}} y^{-\alpha})\right]\right]$$

$$= \exp\left(-\lambda_p \int_{\mathbb{R}^2\setminus\mathcal{B}(\boldsymbol{O},x)} \left(1 - \mathbb{E}_{h_{\boldsymbol{Y}}}\left[\exp(-\eta\tau x^{\alpha} h_{\boldsymbol{Y}} y^{-\alpha})\right]\right) dy\right)$$

$$\overset{(a)}{=} \exp\left(-2\pi\lambda_p \int_{x}^{\infty} \left(1 - \mathbb{E}_{h_{\boldsymbol{Y}}}\left[\exp(-\eta\tau x^{\alpha} h_{\boldsymbol{Y}} y^{-\alpha})\right]\right) y dy\right) \quad (2.16)$$

where (a) follows from converting to polar coordinates. Here, $\mathcal{B}(\boldsymbol{O}, x)$ refers to a ball[6] centred at the origin $\boldsymbol{O}$ with radius x, whereas the interfering BSs should be farther than the serving BS at distance x.

In (2.16), $\mathbb{E}_{h_{\boldsymbol{Y}}}\left[\exp(-\eta\tau x^{\alpha} h_{\boldsymbol{Y}} y^{-\alpha})\right]$ can be interpreted as the moment generating function (MGF). For a random variable γ, the moment generating function is given by [52, p. 187]

$$M_{\gamma}(s) = \mathbb{E}_{\gamma}[\exp(-s\gamma)] \quad (2.17)$$

where $\mathbb{E}_{\gamma}[.]$ denotes the expectation with respect to the random variable γ. In this thesis the channel fading gain is assumed to follow the Nakagami fading, which, in turn, follows the gamma distribution. Hence, the MGF for a gamma random variable with parameter β can be written as [52, p. 187]

$$M_{\gamma}(s) = \mathbb{E}_{\gamma}[\exp(-s\gamma)] = \left(1 + \frac{s\gamma}{\beta}\right)^{-\beta}. \quad (2.18)$$

With the above defined MGF, the Laplace transform of interference in (2.16) can be written as

[6]Representing a 2-dimensional disk, the term ball is used to be consistent with previous studies [21].

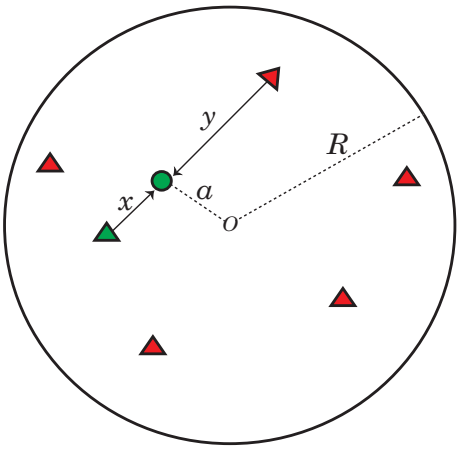

FIGURE 2.5: Illustration of a downlink transmission in a finite disk region. Reference user at distance a from the centre is served by a BS at distance x. Interfering BSs are distance y away from the reference user.

$$\mathcal{L}_I^{(\mathrm{PPP})}(\eta\tau x^{\alpha}) = \exp\left(-2\pi\lambda_p \int_x^{\infty} \left(1 - \frac{1}{\left(1+\frac{\eta\tau x^{\alpha} y^{-\alpha}}{\beta}\right)^{\beta}}\right) y dy\right). \tag{2.19}$$

Substituting (2.19) and (2.13) in (2.12) provides the expression for the coverage probability as

$$P_{\mathrm{cov,p}} = \int_0^{\infty} \sum_{n=1}^{\beta} (-1)^{n+1} \binom{\beta}{n} \exp\left(-2\pi\lambda_p \int_x^{\infty} \left(1 - \frac{1}{\left(1+\frac{\eta\tau x^{\alpha} y^{-\alpha}}{\beta}\right)^{\beta}}\right) y dy\right) 2\pi\lambda_p x \exp\left(-\lambda_p \pi x^2\right) dx \tag{2.20}$$

2.4.2 Coverage Probability with Binomial Point Process

As similar in the PPP based model, let us consider a simple downlink scenario. The binomial point process is based on a finite region with a fixed number of nodes. Therefore in this analysis, we have considered a simple disk region with radius R as shown in Fig. 2.5 with N_t number of BSs. The reference receiver can be placed anywhere in the finite region and its assumed to be at distance a from the centre of the disk region.

As similar in Section 2.4.1, coverage probability under the BPP can be written as

$$P_{\text{cov,b}} = \int_0^{R+a} \mathbb{P}\left[\frac{x^{-\alpha} h_{\boldsymbol{X}}}{I} > \tau\right] f_b(x) dx \tag{2.21}$$

where $f_b(x)$ is the PDF of its distance to the nearest BS and is computed from the definition of the void probability of the BPP. The void probability under the BPP is defined as the probability that there is no point in an arbitrary compact subset $K \subset W$ and is given by [53, Def. 2.1]

$$\mathbb{P}[\text{No BSs in } |K|] = \left(1 - \frac{|K|}{|W|}\right)^{N_t} \tag{2.22}$$

where $|.|$ denotes the area. Hence, for the given disk region with radius R, the CDF of its distance to the nearest BS at distance x from the reference user, which is at distance a from the origin can be written as,

$$F_b(x) = \begin{cases} 1 - \left(1 - \frac{A}{\pi R^2}\right)^{N_t} & 0 \leq x \leq R - a \\ 1 - \left(1 - \frac{B}{\pi R^2}\right)^{N_t} & R - a \leq x \leq R + a \end{cases} \tag{2.23}$$

where $A = \pi x^2$ and $B = 2J \int_0^x t dt + \int_J^{2\pi - J} \int_0^{R_\theta} t dt d\theta$ are the areas as shown in Fig. 2.6. Also $J = \cos^{-1}(\frac{a^2 + x^2 - R^2}{2ax})$, and $R_\theta = \sqrt{R^2 - a^2 \sin^2\theta} + a\cos\theta$.

The CDFs,

$$F_1(x) = \frac{A}{\pi R^2} \tag{2.24}$$

and

$$F_2(x) = \frac{B}{\pi R^2} \tag{2.25}$$

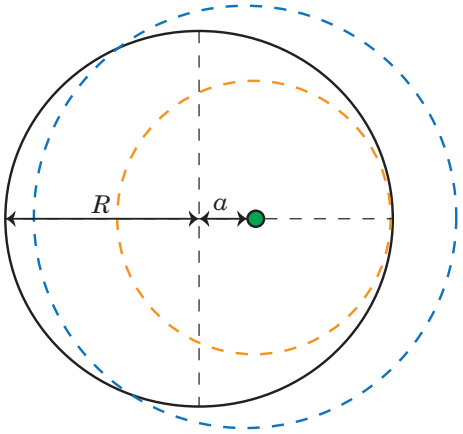

FIGURE 2.6: Diagram of the intersection area, between the disk region of radius R and the region formed by the serving BS. A user (green solid circle) is at distance a from the centre of the disk region . If the serving BS is inside the orange circle, then the intersection area becomes A. If the serving BS is outside the orange circle, then the intersection area between the finite disk region (black circle) and the region formed by the serving BS (blue circle) becomes B.

are termed as the conditional CDF of a BS with distance x from an arbitrary receiver at distance a from the centre of the disk region. And the corresponding PDFs can be written as

$$f_1(x) = \frac{dF_1(x)}{dx} \tag{2.26}$$

and

$$f_2(x) = \frac{dF_2(x)}{dx}. \tag{2.27}$$

The PDF of its distance to the nearest BS is the derivation of the CDF and can be expressed as

$$f_b(x) = \frac{dF_b(x)}{dx} = \begin{cases} f_{b,1}(x) = N_t \left(1 - \frac{A}{\pi R^2}\right)^{(N_t-1)} \frac{1}{\pi R^2} \frac{dA}{dx} & 0 \le x \le R - a \\ f_{b,2}(x) = N_t \left(1 - \frac{B}{\pi R^2}\right)^{(N_t-1)} \frac{1}{\pi R^2} \frac{dB}{dx} & R - a \le x \le R + a. \end{cases} \tag{2.28}$$

Having defined the distance distributions, the next step is to simplify the inner probability term in (2.21) and this can be simplified as in (2.13).

Next, the Laplace transform of interference under the BPP can simplified as

$$\begin{aligned}
\overset{(\mathrm{BPP})}{\mathcal{L}_I}(\eta\tau x^{\alpha}) &= \mathbb{E}[(\exp(-\eta\tau x^{\alpha} I))] = \mathbb{E}_{\Phi,h_{\boldsymbol{Y}}}[(\exp(-\eta\tau x^{\alpha} \sum_{\boldsymbol{Y}\in\Phi\setminus\boldsymbol{X}} h_{\boldsymbol{Y}} y^{-\alpha}))] \\
&= \mathbb{E}_{\Phi}\left[\prod_{\boldsymbol{Y}\in\Phi\setminus\boldsymbol{X}} \mathbb{E}_{h_{\boldsymbol{Y}}}\left[\exp(-\eta\tau x^{\alpha} h_{\boldsymbol{Y}} y^{-\alpha})\right]\right] \\
&\overset{(a)}{=} \left(\int_{x}^{R+a} \mathbb{E}_{h_{\boldsymbol{Y}}}\left[\exp(-\eta\tau x^{\alpha} h_{\boldsymbol{Y}} y^{-\alpha})\right] f_i(y)dy\right)^{(N_t-1)} \\
&\overset{(b)}{=} \left(\int_{x}^{R+a} \frac{1}{\left(1+\frac{\eta\tau x^{\alpha} y^{-\alpha}}{\beta}\right)^{\beta}} f_i(y)dy\right)^{(N_t-1)}
\end{aligned} \tag{2.29}$$

where (a) is obtained by converting from Cartesian to polar coordinates, and (b) follows from the moment generating function of the gamma random variable. Here, $f_i(y)$ is the interfering BSs' distance distribution. Depending on the position of the serving BS the interfering BS's distance distribution can be either one of the three cases as shown in Fig. 2.7. By substituting the appropriate PDFs and CDFs, the distance distributions of interfering BSs can be written as [21]

$$f_i(y) = \begin{cases} \frac{f_1(y)}{1-F_1(x)} & 0 < x \leq R-a,\ x < y \leq R-a \\ \frac{f_2(y)}{1-F_1(x)} & 0 < x \leq R-a,\ R-a < y \leq R+a \\ \frac{f_2(y)}{1-F_2(x)} & R-a < x < R+a,\ x < y \leq R+a \end{cases} \tag{2.30}$$

where $F_1(.)$, $F_2(.)$, $f_1(.)$ and $f_2(.)$ are given by (2.24), (2.25), (2.26) and (2.27).

Next, the coverage probability under the BPP can be written with the above-defined distance distributions and the Laplace transform of the interference as

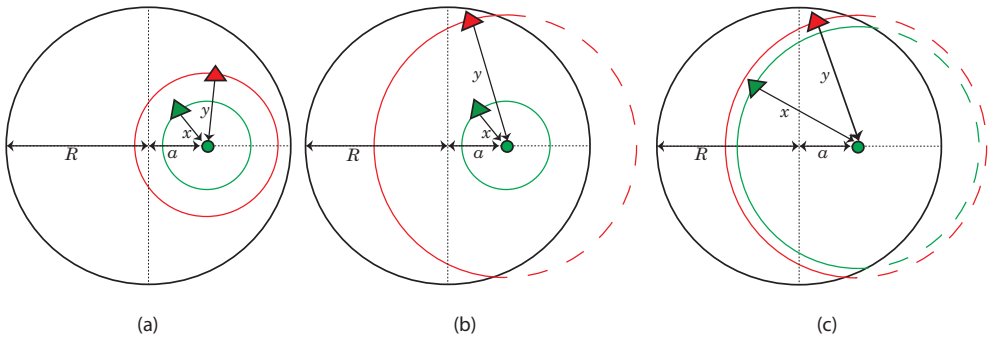

FIGURE 2.7: Distance of serving and interfering BSs for three different cases. The green triangle, red triangle and the green circle represent the serving BS, interfering BS and the reference user, respectively. Plot (a): $0 < x \leq R-a,\ x < y \leq R-a$, Plot (b): $0 < x \leq R-a,\ R-a < y \leq R+a$ and Plot (c): $R-a < x < R+a,\ x < y \leq R+a$.

$$P_{\text{cov,b}} = \int_0^{R-a} \sum_{n=1}^{\beta} (-1)^{n+1} \binom{\beta}{n} \left(\int_x^{R-a} \frac{1}{\left(1+\frac{\eta\tau x^{\alpha} y^{-\alpha}}{\beta}\right)^{\beta}} \frac{f_1(y)}{1-F_1(x)} dy + \int_{R-a}^{R+a} \frac{1}{\left(1+\frac{\eta\tau x^{\alpha} y^{-\alpha}}{\beta}\right)^{\beta}} \frac{f_2(y)}{1-F_1(x)} dy \right)^{(N_t-1)} f_{b,1}(x)dx + \int_{R-a}^{R+a} \sum_{n=1}^{\beta} (-1)^{n+1} \binom{\beta}{n} \left(\int_x^{R+a} \frac{1}{\left(1+\frac{\eta\tau x^{\alpha} y^{-\alpha}}{\beta}\right)^{\beta}} \frac{f_2(y)}{1-F_2(x)} dy \right)^{(N_t-1)} f_{b,2}(x)dx. \tag{2.31}$$

If the user at the centre of the disk region, (2.31) can be simplified by substituting $a = 0$ and can be written as

$$P_{\text{cov,b}} = \int_0^{R} \sum_{n=1}^{\beta} (-1)^{n+1} \binom{\beta}{n} \left(\int_x^{R} \frac{1}{\left(1+\frac{\eta\tau x^{\alpha} y^{-\alpha}}{\beta}\right)^{\beta}} \frac{f_1(y)}{1-F_1(x)} dy \right)^{(N_t-1)} f_{b,1}(x)dx. \tag{2.32}$$

From the above derivations, it can be observed that in order to derive the coverage probability, the intermediate expressions, namely, the distance distributions and the Laplace transform of interference, should be defined. In chapters 4 to 6, a

similar approach has been followed; that is, to compute the coverage probability as the first step, the distance distributions and Laplace transform of interference will be derived.

Chapter 3

Literature Review

This section presents the related studies on mmWave cellular networks that are modelled based on the stochastic geometry approach. This section has been divided into two major categories. Section 3.1 overviews the literature on the suitability of mmWave spectrum for cellular networks, and Section 3.2 overviews related studies on mmWave cellular network models based on stochastic geometry approach.

3.1 Suitability of Millimetre Wave Spectrum for Cellular Networks

As highlighted in Chapter 1, the worldwide need for more cellular spectrum has attracted researchers to study the applicability of mmWave frequencies for use in cellular networks. The large available bandwidth from 30 GHz to 300 GHz [28] has already been considered in various commercial wireless systems [54, 55]. However, the applicability of these frequencies to cellular communications has only been considered recently due to the challenges posed by the additional propagation losses and greater diffraction losses that occur at these frequencies compared to the lower cellular frequency band. In Feb 2018 the Federal Communications

Commission (FCC) granted Samsung the world's first approval for 28 GHz base stations which will be used in the rollout of 5G in the United States [56].

The challenges in mmWave signals are addressed in [57]. Millimetre wave signals are extremely susceptible to blockages present in the propagation environment. Signal strength degrades severely due to the high penetration loss compared to the sub-6 GHz bands [57]. These characteristics of the propagation environment significantly affect the signal quality of mmWaves; hence it should be included in the mmWave system modelling process [38].

Having discussed the challenges in mmWave communications, the suitability of these waves in cellular networks has been studied in [10, 58]. Recent field measurements conducted at 28 GHz and 38 GHz in urban and suburban environments reveal that consistent coverage can be achieved with a 200 metres cell radius, provided that high gain steerable directional antennas are employed [10]. Also, shorter wavelengths enable more antennas to be packed into an array to support high directional adaptive beamforming, which can compensate for the severe frequency-dependent path losses in mmWave propagation [28]. The deployment of these directional antennas, together with the mmWave signals' high signal path loss reduces the out-of-cell interferences, which enables the deployment of more dense networks.

3.2 Analytical Modelling of Millimetre Wave Cellular Networks with Random Spatial Models

The system-level performance of cellular networks is usually modelled by relying on numerical simulations, which are typically time-consuming and do not provide direct insight into the effect of various parameters [24]. On the other hand, the analytical modelling of cellular networks is difficult due to the lack of tractability for modelling the BSs and interference. A new mathematical approach has

gained popularity due to a tractable analytical approach, known as stochastic geometry [24].

Stochastic geometry deals with random spatial patterns and point process theory. The most widely used point process for mmWave cellular network modelling is the Poisson point process due to its mathematical and computational simplicity [59].

3.2.1 Millimetre Wave Cellular Network Models with Poisson Point Process

The mathematical flexibility of the PPP-based modelling has attracted researchers [24, 25, 38, 43] to study the system level performance of mmWave cellular networks with the aid of stochastic geometry. The approach used to model conventional cellular networks needs to be modified so as to fit into mmWave cellular network models. In particular, it is necessary to incorporate suitable modelling parameters such as link state models, path loss models, antenna design and fading characteristics. The following sections present the studies related to downlink and uplink mmWave cellular network models, which have incorporated the aforementioned modelling parameters.

3.2.1.1 Downlink Coverage Analysis of Millimetre Wave Cellular Networks

The initial work in analysing mmWave cellular networks' downlink communications with the aid of stochastic geometry was done in [38]. In [38], network was modelled using a PPP. Two link states for LOS and NLOS communication were proposed with an exponential probability function, which incorporates the blockage characteristics in an environment. The exponential probability function is then approximated to a step function with a LOS equivalent ball approximation region. Also, the propagation characteristics such as different path loss functions and fading characteristics have been considered with different parameters for LOS and NLOS links. To compensate for the high path loss in mmWave communications

directional adaptive beamforming is applied both at BSs and UEs by approximating the actual array patterns to a step function (also referred to as a sectored or flat-top antenna model). It was concluded in [38], with the above-specified network features significantly higher data rates can be achieved compared to the conventional cellular networks. Also, the impact of base station density has been demonstrated; it reveals that increasing the BSs beyond a limit will degrade the system performance. An analogous network model to [38] has been considered in [24] with additional modifications to give more insight for mmWave networks. Specifically, an extra state in the link state modelling is adopted, with an outage probability resulting in a two-ball approximation region. This is to accommodate the signal outages present in mmWave frequencies due to high propagation losses. Millimetre wave downlink coverage analysis of a heterogeneous cellular network is presented in [25], a similar sectored antenna model has been considered, but the beamforming alignment errors have been incorporated. Also, the two ball approximation in [24] has been generalised to D-ball approximation.

3.2.1.2 Uplink Coverage Analysis of Millimetre Wave Cellular Networks

A majority of the studies on millimetre wave cellular systems performance analysis have focused on investigating downlink performance analysis [24, 25, 38, 60–62]. Comparatively limited studies have focused on the uplink performance analysis of the mmWave cellular networks [44–47]. In [44] the authors investigated coverage analysis for an uplink mmWave cellular network by modelling the BS and UE locations as a PPP. The SINR coverage analysis has been investigated by considering fractional power control (FPC) and the unique characteristics of mmWave cellular networks such as blockage model and antenna model. The findings in [44] have also been extended to multi-tier mmWave cellular networks in [45]. In [46] along with considering mmWave unique features and FPC, the uplink performance analysis has been investigated with clustered users, whereas BS locations and UE locations follow PPP and Poisson cluster process, respectively. In [47], the authors investigated system performance considering a two-tier PPP based

heterogeneous network, where the conventional sub-6 GHz macrocells coexisting with the mmWave small cells.

3.2.1.3 Antenna Modelling of Millimetre Wave Cellular Networks

To overcome the significant propagation losses in mmWave networks, large scale antenna arrays will likely be required. Therefore it is necessary to incorporate realistic models to represent array antenna systems reflecting the important antenna aspects such as the number of array elements and the Angle of Departures (AoDs) of the transmitted signals. Most PPP based mmWave cellular network models [24, 25, 38, 61–63] use a flat-top antenna model as an approximation in the characterization of antenna arrays. However, this approximation does not represent the roll-off characteristics of the antenna radiation pattern, the AoDs and the impact of array size (i.e., the number of antenna elements).

Two other antenna models have been proposed as alternatives, namely the sinc and cosine antenna models [60]. It has been demonstrated that the sinc model provides a slightly better approximation compared to the cosine model. But the cosine model provides better analytical tractability than the sinc model. Hence, the cosine model provides a good balance in terms of accuracy and analytical tractability. However, the main drawback of this cosine model is that the side lobe antenna gains are neglected and, unfortunately, the side lobe gains are likely to impact the performance of the network as it becomes denser. Very recently, a novel array antenna model has been proposed, namely the multi-cosine pattern [22]. This model is based on the cosine model, but it is modified to represent the side lobe gains of the array antennas.

3.2.2 Binomial Point Process for Modelling Millimetre Wave Cellular Networks

The main concern with the infinite PPP model is that it assumes a random number of BSs distributed in an infinite region [18], whereas the real cellular networks

operates in a finite region with finite a number of nodes. To overcome this limitation partially, in [62] a finite PPP model has been considered for a finite region with a random number of nodes. However, in reality, cellular networks are planned with a fixed number of BSs in a geographically bounded region. This motivates the adoption of a more suitable distribution to represent cellular networks. A popular choice in such cases is the binomial point process (BPP) distribution [21]. In [21] it has been suggested that the BPP would be more suitable to model a mmWave network communications where the receiver of interest may experience interference from a fixed number of BSs due to blocking. The BPP specifies a fixed number of nodes in a geographically bounded region [53, Def. 2.1]. Unfortunately, performance analysis under the BPP model is more challenging, compared to the PPP model, because the statistical properties assumed for the PPP model are not valid for the BPP model. For example, the aggregate interference experienced at the centre of the network is different from that at the network boundaries [21], so the location independence performance is no longer valid under the BPP model. It is shown in [21] that a centrally located receiver and an arbitrarily located receiver will experience different SINR distributions. The applicability of the BPP for wireless networks has been reviewed in [21, 53, 64–68]. These studies have been used in this thesis as a guideline to aid the development of a BPP-based model of a mmWave cellular network.

Chapter 4

Downlink Coverage Analysis on a Disk Region

This chapter investigates the downlink performance of an outdoor mmWave cellular network, modelled using the BPP. The BPP overcomes the limitations of the PPP by allowing to model a finite network region with a fixed number of nodes. In this chapter, we have assumed a finite two-dimensional disk region as the network region. Later in Chapter 5, the model will be extended to an arbitrary region. By considering the unique features of mmWave communications such as directional antenna arrays and different link characteristics, this chapter proposes tractable expressions to evaluate the coverage and rate performance in mmWave cellular networks for a reference receiver located anywhere arbitrary in the defined disk region, while numerical results are provided to validate the accuracy of the proposed analytical models. The rest of the chapter is organised as follows. Section 4.1 describes the system model; including the network model, blockage and channel model, selection strategy, antenna model, and the performance metric. Section 4.2 presents the main technical derivations of this chapter, together with analytical results from the coverage and rate probability analyses. Section 4.3 presents the numerical and simulation results. Finally, Section 4.4 concludes the chapter.

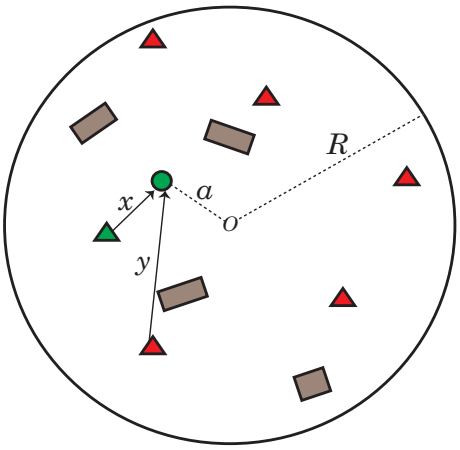

FIGURE 4.1: Finite disk region with $N_t = 6$. The green triangle, red triangles, the green circle and grey rectangles represent the serving BS, interfering BSs, the reference receiver and the random blockages, respectively.

4.1 System Model

This section presents the system modelling assumptions, which we have incorporated to model the mmWave cellular systems.

4.1.1 Network Model

This chapter focuses on conducting downlink performance analysis of an outdoor mmWave cellular network in a two-dimensional finite disk region $\mathcal{A}$ with radius R, as shown in Fig. 4.1. It is assumed that N_t BSs are distributed according to a uniform BPP, Φ. The user of interest, referred as the reference UE is located at $\boldsymbol{D}$ with distance $a = ||\boldsymbol{D} - \boldsymbol{O}||$ from the origin $\boldsymbol{O}$, the serving BS of the reference UE, referred as the reference BS is located at $\boldsymbol{X}$ with distance $x = ||\boldsymbol{X} - \boldsymbol{D}||$ from the reference UE and an interfering BS is located at $\boldsymbol{Y}$ with distance $y = ||\boldsymbol{Y} - \boldsymbol{D}||$ from the reference UE. Furthermore, it is also assumed that all BSs are active, serving their corresponding mobile users by simultaneously reusing the same resources.

4.1.2 Blockage and Channel Model

Cellular network environment is surrounded by randomly distributed blockages, therefore it is necessary to incorporate the effects of these blockages in the system model, as shown in Fig. 4.1. In this thesis, the blockage model proposed in [38] has been adopted to characterise the blockage effects on the system performance. In that model, the blockages are assumed to be buildings and distributed according to a process of random shapes. Based on this model a user can be either LOS or NLOS to its associated base station and the probability of a link being LOS or NLOS are respectively given by, $p(r) = e^{-\omega r}$ and $1 - p(r)$, where r represents the distance between a user and a BS, and ω is the blockage parameter, which is determined by the density and the average size of the blockages. Furthermore, as indicated in [69], it is also assumed that the blockage effects for different links are independent and ignoring such correlations cause a minor loss of accuracy in the SINR calculations. Thus, from this assumption the network might consist of finite number of LOS and NLOS BSs, which are denoted by N_{tL} and N_{tN}, respectively. Also, due to blocking of the buildings, we have assumed that indoor to outdoor penetration loss to be high enough such that an outdoor user can not receive any signal from an indoor base station.

A distance dependent power law path loss $l = x^{\alpha}$ has been assumed, where α equals to α_L with probability $p(r)$ for LOS links and α_N with probability $1 - p(r)$ for NLOS links. Furthermore, Nakagami fading has been assumed. The fading power can be modelled as a normalised Gamma random variable $\Gamma(\beta, \frac{1}{\beta})$. Different parameters of Nakagami fading β_L and β_N are assumed for LOS and NLOS links.

4.1.3 Selection Strategy

It is assumed that, a user will be connected to the base station, that has the smallest path loss $l = x^{\alpha}$. The BS can be either LOS or NLOS. With this assumption the serving BS can either be the nearest BS in the LOS set or the nearest one in the NLOS set.

4.1.4 Antenna Model

It is expected that millimetre wave cellular network BSs will be deployed with antenna arrays to cope with the significant propagation losses. In [60], a Uniform Linear Array (ULA) antenna has been considered as a possible candidate. The array gain function of the "actual" ULA is given by [60], equation (6) as[1]

$$G_{\text{act}}(\varphi) = \frac{\sin^2(\pi N \varphi)}{N \sin^2(\pi \varphi)} \tag{4.1}$$

where N is the number of antenna array elements and $\varphi = \frac{d}{\lambda}\cos\vartheta$ is defined in [60] as the spatial AoD, ϑ is the physical AoD, d is the antenna element spacing and λ is the wavelength. As shown in [60] φ can be assumed to be uniformly distributed in $[\frac{-d}{\lambda}, \frac{d}{\lambda}]$. But this assumption is not valid for a bounded region, whereas the spatial AoD distribution will depend on the transmitter and receiver locations. But including these dependency will make the analytical model more complex. Therefore as similar to the PPP based networks, we have assumed the AoD to be distributed uniformly in $[\frac{-d}{\lambda}, \frac{d}{\lambda}]$. To avoid gratings lobes d should be less than or equal to $\frac{\lambda}{2}$. Thus φ is assumed to be distributed in [-0.5, 0.5]. This assumption provides a good approximation for even a bounded network region. The accuracy of this assumption has been presented in Section 4.3.

In [60] cosine and sinc array antenna models have been proposed as a close approximation to the actual array antenna patterns. Both the models provide almost similar results, but the cosine model provides better analytical tractability compared to the sinc model, but it fails to represent the side lobe gains of the antenna array. Very recently a multi-cosine antenna model considering the side lobe antenna gains has been proposed in [22] and it demonstrates much better approximations in terms of both the antenna pattern and the coverage probability. Therefore in this thesis multi-cosine antenna pattern has been considered to model the finite mmWave cellular network.

[1]Note that in [60], equation (6), the array gain function of the actual ULA is normalised with factor $\frac{1}{N}$. Also, φ and ϑ are equivalent to ϑ_x and ϕ_x in [60], respectively.

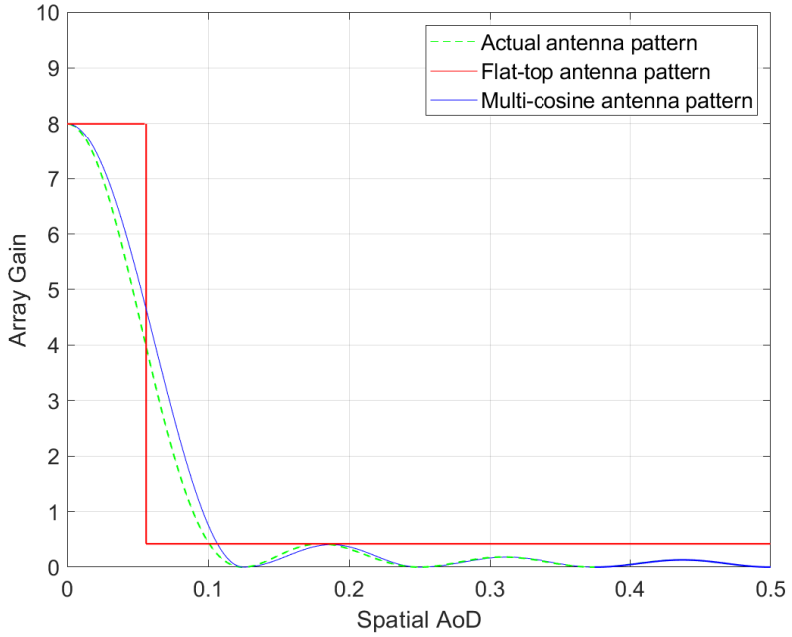

FIGURE 4.2: Visualisation of three different antenna patterns for $N = 8$.

The multi-cosine antenna pattern is given by

$$G_{\text{mcos}}(\varphi) = \begin{cases} G_0 \cos^2\left(\frac{\pi N \varphi}{2}\right) & \text{if } \mid \varphi \mid \leq \frac{1}{N} \\ G_k \cos^2\left(\pi N(\mid \varphi \mid -\varphi_k)\right) & \text{if } \frac{k}{N} < \mid \varphi \mid \leq \frac{k+1}{N} \\ 0 & \text{otherwise,} \end{cases} \tag{4.2}$$

where $G_k = G_{\text{act}}(\varphi_k), \varphi_k = \frac{2k+1}{2N}$ for $k > 0$ and $G_0 = N$ as defined in [22], equation (2). A graph of the actual, multi-cosine and the flat-top[2] antenna patterns is shown in Fig. 4.2. Furthermore, we assume that the reference receiver has a single receive antenna. Also we assume that the reference BS adjust its beam steering angles to achieve maximum array gain based on channel estimations. Therefore the total directivity gain of the desired signal is the maximum gain, which is equal to $G_0 = N$.

[2]In flat-top antenna pattern, the maximum and the minimum power gains are assumed to be the maximum main lobe gain and the maximum first side lobe gain of the actual antenna pattern, respectively [60] as shown in Fig. 4.2.

4.1.5 Performance Metric

As highlighted in Section 2.3, SINR has been considered as the key performance metric. This chapter will be focusing on downlink network performance analysis and the downlink SINR of a user at distance x from its serving BS can be expressed as

$$\text{SINR} = \frac{x^{-\alpha} h_{\boldsymbol{X}} p_t G_{\text{mcos}}(\varphi_{\boldsymbol{X}})}{(\sigma^2 + I)} \tag{4.3}$$

$$I = \sum_{\boldsymbol{Y} \in \Phi \setminus \boldsymbol{X}} h_{\boldsymbol{Y}} p_t G_{\text{mcos}}(\varphi_{\boldsymbol{Y}}) y^{-\alpha} \tag{4.4}$$

where I is the total interference from all interfering BSs except the serving BS at $\boldsymbol{X}$. The parameters $h_{\boldsymbol{X}}$ and $h_{\boldsymbol{Y}}$ are the fading gains of the desired and interfering signals representing random channel effects, $G_{\text{mcos}}(\varphi_{\boldsymbol{X}})$ and $G_{\text{mcos}}(\varphi_{\boldsymbol{Y}})$ are the antenna gains of the desired and interfering signals, p_t is the BS transmit power and σ^2 is the thermal noise power. The antenna gain of the desired signal is the maximum gain, which is equal to $G_{\text{mcos}}(\varphi_{\boldsymbol{X}}) = N$, where N is the number of array elements.

4.2 Coverage and Rate Analysis

This section presents the probability of coverage and rate for the proposed millimetre wave network in Section 4.1. To compute the coverage probability the following intermediate definitions should be derived namely association probabilities, serving BS's distance distributions and interfering BSs' distance distributions.

4.2.1 Association Probabilities

A user can be associated with either the nearest LOS or NLOS base station. In order to find these probabilities, the nearest distance distributions should be defined. Let x_L be the distance from the reference user to its nearest LOS base station. Distance x_L can be the nearest, only if there is at least one LOS BS in

$\mathcal{A}$ and no LOS BSs located within $\mathcal{B}(\mathbf{D}, x)^3 \cap \mathcal{A}$, denoted by $\mathcal{I}_L$. Therefore the nearest LOS distance distribution can be written as

$$\begin{aligned}\mathbb{P}[\ ||x_L > r||\ ] &= \frac{\mathbb{P}[\ n(\mathcal{C}_L \cap \mathcal{I}_L) = 0\ \&\ N_{tL} \geq 1\ ]}{\mathbb{P}[\ N_{tL} \geq 1\ ]} \\ &= \frac{\mathbb{P}[\ n(\mathcal{C}_L \cap \mathcal{I}_L) = 0\ ]\,\mathbb{P}[\ n(\mathcal{C}_L \backslash \mathcal{I}_L) \geq 1\ ]}{\mathbb{P}[\ N_{tL} \geq 1\ ]} \\ &\overset{(a)}{=} \frac{\mathbb{P}[\ n(\mathcal{C}_L \cap \mathcal{I}_L) = 0\ ] - \mathbb{P}[\ n(\mathcal{C}_L \cap \mathcal{A}) = 0\ ]}{\mathbb{P}[\ N_{tL} \geq 1\ ]} \overset{(b)}{=} \frac{(1 - F_L(x))^{N_t} - a_L}{1 - a_L} \end{aligned} \tag{4.5}$$

where $\mathcal{C}_L$ denotes the set which contains the LOS BSs, (a) follows from

$$\mathbb{P}[\ n(\mathcal{C}_L \cap \mathcal{A}) = 0\ ] = \mathbb{P}[\ n(\mathcal{C}_L \cap \mathcal{I}_L) = 0\ ]\,\mathbb{P}[\ n(\mathcal{C}_L \cap \mathcal{A} \backslash \mathcal{I}_L) = 0\ ]$$

and (b) follows from the definition of void probabilities [53, Def. 2.1]. The distance distributions $F_L(x)$ and a_L are given by (4.6) and (4.8).

The cumulative distribution function (CDF) $F_L(x)$ is

$$F_L(x) = \begin{cases} F_{L,1}(x) = \frac{2\int_0^x tp(t)dt}{R^2} & 0 \leq x \leq R - a \\ F_{L,2}(x) = \frac{2J\int_0^x tp(t)dt + \int_J^{2\pi - J}\int_0^{R_\theta} tp(t)dtd\theta}{\pi R^2} & R - a < x \leq R + a \end{cases} \tag{4.6}$$

where $J = \cos^{-1}(\frac{a^2 + x^2 - R^2}{2ax})$, and $R_\theta = \sqrt{R^2 - a^2 \sin^2\theta} + a\cos\theta$.

And the corresponding probability density function (PDF) $f_L(x)$ is

$$f_L(x) = \begin{cases} f_{L,1}(x) = \frac{dF_{L,1}(x)}{dx} & 0 \leq x \leq R - a \\ f_{L,2}(x) = \frac{dF_{L,2}(x)}{dx} & R - a < x \leq R + a. \end{cases} \tag{4.7}$$

Next, a_L, which is the probability a user observes no LOS BS in the given disk region can be written as

[3] $\mathcal{B}(\mathbf{D}, x)$ denotes the disk centred at $\mathbf{D}$ of radius x. $\mathbf{D}$ denotes the location vector of the reference receiver from the centre of the disk region.

$$a_L \overset{(a)}{=} [1 - \frac{2\int_0^R tp(t)dt)}{R^2}]^{N_t}, \tag{4.8}$$

where (a) follows from the definition of void probabilities [53, Def. 2.1] and substituting for the area of a circle.

Then, the CDF of the distance to the nearest LOS BS can be written as

$$\overset{(\text{NEA})}{F_L}(x) = 1 - \mathbb{P}\left[\text{No LOS BSs closer than } x\right] = \frac{1 - (1 - F_L(x))^{N_t}}{1 - a_L}. \tag{4.9}$$

Based on the position of x the CDFs ($\overset{(\text{NEA})}{F_L}(x)$) and PDFs ($\overset{(\text{NEA})}{f_L}(x)$) of the distance to the nearest LOS BS can be written as

$$\overset{(\text{NEA})}{F_L}(x) = \begin{cases} \overset{(\text{NEA})}{F_{L,1}}(x) = \frac{1-\left(1-F_{L,1}(x)\right)^{N_t}}{1-a_L} & 0 \le x \le R-a \\ \overset{(\text{NEA})}{F_{L,2}}(x) = \frac{1-\left(1-F_{L,2}(x)\right)^{N_t}}{1-a_L} & R-a < x \le R+a \end{cases} \tag{4.10}$$

and

$$\overset{(\text{NEA})}{f_L}(x) = \begin{cases} \overset{(\text{NEA})}{f_{L,1}}(x) = \frac{d\,\overset{(\text{NEA})}{F_{L,1}}(x)}{dx} & 0 \le x \le R-a \\ \overset{(\text{NEA})}{f_{L,2}}(x) = \frac{d\,\overset{(\text{NEA})}{F_{L,2}}(x)}{dx} & R-a < x \le R+a. \end{cases} \tag{4.11}$$

Following a similar approach the CDFs and PDFs of the distance to the nearest NLOS BS can be written as

$$\overset{(\text{NEA})}{F_N}(x) = \begin{cases} \overset{(\text{NEA})}{F_{N,1}}(x) = \frac{1-\left(1-F_{N,1}(x)\right)^{N_t}}{1-a_N} & 0 \le x \le R-a \\ \overset{(\text{NEA})}{F_{N,2}}(x) = \frac{1-\left(1-F_{N,2}(x)\right)^{N_t}}{1-a_N} & R-a < x \le R+a \end{cases} \tag{4.12}$$

and

$$\overset{(\text{NEA})}{f_N}(x) = \begin{cases} \overset{(\text{NEA})}{f_{N,1}}(x) = \frac{d\,\overset{(\text{NEA})}{F_{N,1}}(x)}{dx} & 0 \le x \le R-a \\ \overset{(\text{NEA})}{f_{N,2}}(x) = \frac{d\,\overset{(\text{NEA})}{F_{N,2}}(x)}{dx} & R-a < x \le R+a \end{cases} \tag{4.13}$$

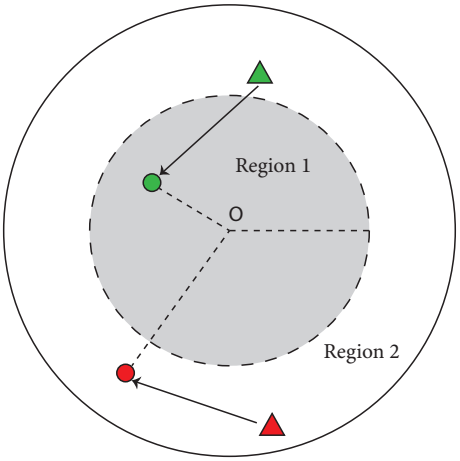

FIGURE 4.3: If a user is in Region 1, then distance distributions and association probabilities of its tagged BS will be as per the case $(R-a)^{\frac{\alpha_N}{\alpha_L}} > R+a$. If a user is in Region 2, then it takes the probabilities corresponding to the case $(R-a)^{\frac{\alpha_N}{\alpha_L}} < R+a$.

where

$$F_N(x) = \begin{cases} F_{N,1}(x) = \frac{2\int_0^x t(1-p(t))dt}{R^2} & 0 \le x \le R-a \\ F_{N,2}(x) = \frac{2J\int_0^x t(1-p(t))dt + \int_J^{2\pi-J}\int_0^{R_\theta} t(1-p(t))dtd\theta}{\pi R^2} & \\ & R-a < x \le R+a, \end{cases} \tag{4.14}$$

$$f_N(x) = \begin{cases} f_{N,1}(x) = \frac{dF_{N,1}(x)}{dx} & 0 \le x \le R-a \\ f_{N,2}(x) = \frac{dF_{N,2}(x)}{dx} & R-a < x \le R+a \end{cases} \tag{4.15}$$

and

$$a_N = [1 - \frac{2\int_0^R t(1-p(t))dt)}{R^2}]^{N_t}. \tag{4.16}$$

With the above derived nearest distributions next, the association probabilities can be derived. Depending on the position of the UE from the centre of the disk region and the fact that $\alpha_N > \alpha_L$, there can be two different cases for the association probabilities. This can be visualised in Fig. 4.3. The following sections provide the association probabilities of a UE connected to LOS and NLOS BS.

Theorem 4.1. *The probability that the reference user is associated with a LOS base station in the case* $(R-a)^{\frac{\alpha_N}{\alpha_L}} > R+a$ *is*

$$Y_{L,1} = N_t\Bigg(\int_0^{R-a} \Big(1 - F_{N,1}(x^{\frac{\alpha_L}{\alpha_N}})\Big)^{N_t} (1-F_{L,1}(x))^{(N_t-1)} f_{L,1}(x)dx + \int_{R-a}^{R+a} \Big(1 - F_{N,1}(x^{\frac{\alpha_L}{\alpha_N}})\Big)^{N_t} (1-F_{L,2}(x))^{(N_t-1)} f_{L,2}(x)dx \Bigg) \quad (4.17)$$

and in the case $(R-a)^{\frac{\alpha_N}{\alpha_L}} < R+a$ is

$$\begin{aligned} Y_{L,2} = N_t\Bigg(& \int_0^{R-a} \Big(1 - F_{N,1}(x^{\frac{\alpha_L}{\alpha_N}})\Big)^{N_t} (1-F_{L,1}(x))^{(N_t-1)} f_{L,1}(x)dx + \\ & \int_{R-a}^{(R-a)^{\frac{\alpha_N}{\alpha_L}}} \Big(1 - F_{N,1}(x^{\frac{\alpha_L}{\alpha_N}})\Big)^{N_t} (1-F_{L,2}(x))^{(N_t-1)} f_{L,2}(x)dx + \\ & \int_{(R-a)^{\frac{\alpha_N}{\alpha_L}}}^{R+a} \Big(1 - F_{N,2}(x^{\frac{\alpha_L}{\alpha_N}})\Big)^{N_t} (1-F_{L,2}(x))^{(N_t-1)} f_{L,2}(x)dx \Bigg). \end{aligned} \quad (4.18)$$

Proof: See Appendix A.1.

Theorem 4.2. *The probability that the reference user is associated with an NLOS base station in the case* $(R-a)^{\frac{\alpha_N}{\alpha_L}} > R+a$ *is*

$$\begin{aligned} Y_{N,1} = N_t\Bigg(& \int_0^{(R-a)^{\frac{\alpha_L}{\alpha_N}}} \Big(1 - F_{L,1}(x^{\frac{\alpha_N}{\alpha_L}})\Big)^{N_t} (1-F_{N,1}(x))^{(N_t-1)} f_{N,1}(x)dx + \\ & \int_{(R-a)^{\frac{\alpha_L}{\alpha_N}}}^{(R+a)^{\frac{\alpha_L}{\alpha_N}}} \Big(1 - F_{L,2}(x^{\frac{\alpha_N}{\alpha_L}})\Big)^{N_t} (1-F_{N,1}(x))^{(N_t-1)} f_{N,1}(x)dx + \\ & \int_{(R+a)^{\frac{\alpha_L}{\alpha_N}}}^{R-a} (1-F_{L,2}(R+a))^{N_t} (1-F_{N,1}(x))^{(N_t-1)} f_{N,1}(x)dx + \\ & \int_{R-a}^{R+a} (1-F_{L,2}(R+a))^{N_t} (1-F_{N,2}(x))^{(N_t-1)} f_{N,2}(x)dx \Bigg) \end{aligned} \quad (4.19)$$

and in the case $(R-a)^{\frac{\alpha_N}{\alpha_L}} < R+a$ is

$$Y_{N,2} = N_t \Bigg(\int_0^{(R-a)^{\frac{\alpha_L}{\alpha_N}}} \left(1 - F_{L,1}(x^{\frac{\alpha_N}{\alpha_L}})\right)^{N_t} (1 - F_{N,1}(x))^{(N_t-1)} f_{N,1}(x)dx + \int_{(R-a)^{\frac{\alpha_L}{\alpha_N}}}^{R-a} \left(1 - F_{L,2}(x^{\frac{\alpha_N}{\alpha_L}})\right)^{N_t} (1 - F_{N,1}(x))^{(N_t-1)} f_{N,1}(x)dx + \int_{R-a}^{(R+a)^{\frac{\alpha_L}{\alpha_N}}} \left(1 - F_{L,2}(x^{\frac{\alpha_N}{\alpha_L}})\right)^{N_t} (1 - F_{N,2}(x))^{(N_t-1)} f_{N,2}(x)dx + \int_{(R+a)^{\frac{\alpha_L}{\alpha_N}}}^{R+a} (1 - F_{L,2}(R+a))^{N_t} (1 - F_{N,2}(x))^{(N_t-1)} f_{N,2}(x)dx \Bigg). \quad (4.20)$$

Proof: Follows a similar approach to that seen in Appendix A.1

It should be noted that, the NLOS association probability is also equivalent to $1 -$ LOS association probability, i.e., $Y_{N,1} = 1 - Y_{L,1}$. and $Y_{N,2} = 1 - Y_{L,2}$. Based on the above defined association probabilities, the distance distributions of the serving BS are presented in the following section.

4.2.2 Serving BS's Distance Distributions

The serving BS can be either the nearest LOS or NLOS BS, which depends on the path gain provided by the serving BS. So, this section presents the serving BS's distance distribution conditioned on the link status of the serving BS.

Theorem 4.3. *Given that the reference receiver is associated with a LOS base station, the PDF of the distance to its serving base station in the case* $(R-a)^{\frac{\alpha_N}{\alpha_L}} > R + a$ *is given by*

$$f_{L,1}^{(\mathrm{SER})}(x) = \begin{cases} \frac{N_t}{Y_{L,1}} (1 - F_{L,1}(x))^{(N_t-1)} f_{L,1}(x) \left(1 - F_{N,1}(x^{\frac{\alpha_L}{\alpha_N}})\right)^{N_t} & 0 < x < R - a \\ \frac{N_t}{Y_{L,1}} (1 - F_{L,2}(x))^{(N_t-1)} f_{L,2}(x) \left(1 - F_{N,1}(x^{\frac{\alpha_L}{\alpha_N}})\right)^{N_t} & R - a < x < R + a \end{cases} \quad (4.21)$$

and in the case $(R-a)^{\frac{\alpha_N}{\alpha_L}} < R + a$ is

$$
\overset{(\mathrm{SER})}{f}_{L,2}(x) =
$$

$$
\begin{cases}
\frac{N_t}{Y_{L,2}}\left(1-F_{L,1}(x)\right)^{(N_t-1)} f_{L,1}(x)\left(1-F_{N,1}(x^{\frac{\alpha_L}{\alpha_N}})\right)^{N_t} & 0<x<R-a \\
\frac{N_t}{Y_{L,2}}\left(1-F_{L,2}(x)\right)^{(N_t-1)} f_{L,2}(x)\left(1-F_{N,1}(x^{\frac{\alpha_L}{\alpha_N}})\right)^{N_t} & R-a<x<(R-a)^{\frac{\alpha_N}{\alpha_L}} \\
\frac{N_t}{Y_{L,2}}\left(1-F_{L,2}(x)\right)^{(N_t-1)} f_{L,2}(x)\left(1-F_{N,2}(x^{\frac{\alpha_L}{\alpha_N}})\right)^{N_t} & (R-a)^{\frac{\alpha_N}{\alpha_L}}<x<R+a.
\end{cases}
\tag{4.22}
$$

Proof: See Appendix A.2.

Theorem 4.4. *Given that the reference receiver is associated with an NLOS base station, the PDF of the distance to its serving base station for the case* $(R-a)^{\frac{\alpha_N}{\alpha_L}} > R+a$ *is given by*

$$
\overset{(\mathrm{SER})}{f}_{N,1}(x) =
$$

$$
\begin{cases}
\frac{N_t}{Y_{N,1}}\left(1-F_{N,1}(x)\right)^{(N_t-1)} f_{N,1}(x)\left(1-F_{L,1}(x^{\frac{\alpha_N}{\alpha_L}})\right)^{N_t} & \\
\qquad\qquad 0<x<(R-a)^{\frac{\alpha_L}{\alpha_N}} & \\
\frac{N_t}{Y_{N,1}}\left(1-F_{N,1}(x)\right)^{(N_t-1)} f_{N,1}(x)\left(1-F_{L,2}(x^{\frac{\alpha_N}{\alpha_L}})\right)^{N_t} & \\
\qquad\qquad (R-a)^{\frac{\alpha_L}{\alpha_N}}<x<(R+a)^{\frac{\alpha_L}{\alpha_N}} & \\
\frac{N_t}{Y_{N,1}}\left(1-F_{N,1}(x)\right)^{(N_t-1)} f_{N,1}(x)\left(1-F_{L,2}(R+a)\right)^{N_t} & \\
\qquad\qquad (R+a)^{\frac{\alpha_L}{\alpha_N}}<x<R-a & \\
\frac{N_t}{Y_{N,1}}\left(1-F_{N,2}(x)\right)^{(N_t-1)} f_{N,2}(x)\left(1-F_{L,2}(R+a)\right)^{N_t} & \\
\qquad\qquad R-a<x<R+a &
\end{cases}
\tag{4.23}
$$

and in the case $(R-a)^{\frac{\alpha_N}{\alpha_L}} < R+a$ is

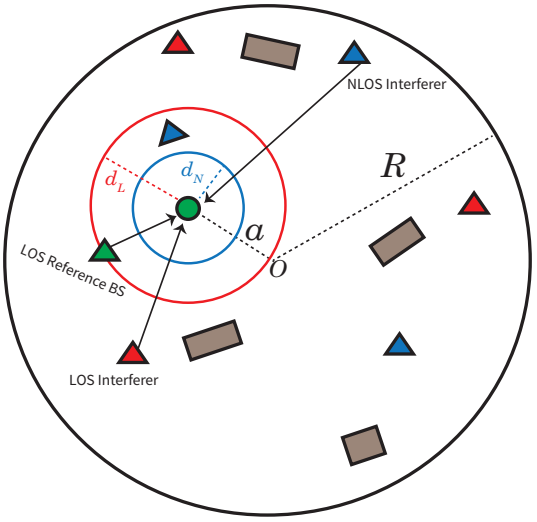

FIGURE 4.4: Given that the reference UE at distance a from the origin is served by an LOS BS with distance x to the user. Then the LOS and the NLOS interfering BSs will be $d_L = x$ and $d_N = x^{\frac{\alpha_L}{\alpha_N}}$ away from the reference UE, respectively.

$$
\overset{(\mathrm{SER})}{f}_{N,2}(x) =
$$

$$
\begin{cases}
\frac{N_t}{Y_{N,2}} \left(1 - F_{N,1}(x)\right)^{(N_t-1)} f_{N,1}(x) \left(1 - F_{L,1}(x^{\frac{\alpha_N}{\alpha_L}})\right)^{N_t} & 0 < x < (R-a)^{\frac{\alpha_L}{\alpha_N}} \\
\frac{N_t}{Y_{N,2}} \left(1 - F_{N,1}(x)\right)^{(N_t-1)} f_{N,1}(x) \left(1 - F_{L,2}(x^{\frac{\alpha_N}{\alpha_L}})\right)^{N_t} & (R-a)^{\frac{\alpha_L}{\alpha_N}} < x < R-a \\
\frac{N_t}{Y_{N,2}} \left(1 - F_{N,2}(x)\right)^{(N_t-1)} f_{N,2}(x) \left(1 - F_{L,2}(x^{\frac{\alpha_N}{\alpha_L}})\right)^{N_t} & R-a < x < (R+a)^{\frac{\alpha_L}{\alpha_N}} \\
\frac{N_t}{Y_{N,2}} \left(1 - F_{N,2}(x)\right)^{(N_t-1)} f_{N,2}(x) \left(1 - F_{L,2}(R+a)\right)^{N_t} & (R+a)^{\frac{\alpha_L}{\alpha_N}} < x < R+a.
\end{cases}
\tag{4.24}
$$

Proof: Follows a similar approach to that seen in Appendix A.2.

4.2.3 Interfering BSs' Distance Distributions

Due to the presence of blocking, interfering BSs can be partitioned into four categories, namely (i) LOS interferers given that a user is associated with a LOS BS, (ii) NLOS interferers given that a user is associated with a LOS BS, (iii) LOS interferers given that a user is associated with an NLOS BS and (iv) NLOS interferers given that a user is associated with an NLOS BS, see Figs. 4.4 and 4.5. Therefore

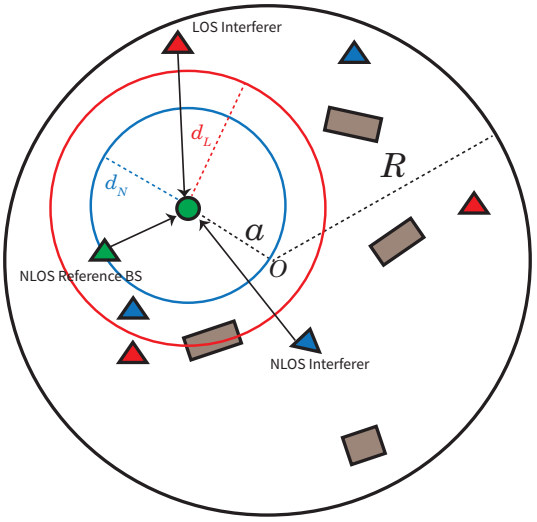

FIGURE 4.5: Given that the reference UE at distance a from the origin is served by an NLOS BS with distance x to the user. Then the LOS and the NLOS interfering BSs will be $d_L = x^{\frac{\alpha_N}{\alpha_L}}$ and $d_N = x$ away from the reference UE, respectively.

the distance distributions of the interfering BSs depend on both the link statuses of the serving BS and the interfering BS. Hence, the distance distributions of the interfering BSs can be written as in the following Lemma.

Theorem 4.5. *The PDF of the distance to the interfering BSs from the reference receiver is given by*

$$f^{(\mathrm{INT})}_{s,u}(y) = \frac{f_{s,k}(y)}{\int_{\mathbb{A}}^{\mathbb{B}} f_{s,k}(q)dq}; u = \{1,2\}, \mathbb{A} = \{A_{s,1}, A_{s,2}\},$$
$$\mathbb{B} = \{B_{s,1}, B_{s,2}\}, k = \{1,2\} \text{ and } s = \{L, N\}. \quad (4.25)$$

In (4.25), $u = 1$ and $u = 2$ corresponds to the cases $(R-a)^{\frac{\alpha_N}{\alpha_L}} > (R+a)$ and $(R-a)^{\frac{\alpha_N}{\alpha_L}} < (R+a)$, respectively. Further, $s = L$ and $s = N$ denotes the LOS and the NLOS interferers, respectively. Note that, depending on the location of the serving BS, the distances y of the interfering BSs can be in different distance ranges as shown in Tables 4.1, 4.2, 4.3 and 4.4. The distance distributions of the interferers' corresponding to different ranges of the aforementioned four categories

can be written by referring to these tables. Also, in these tables, the ditto mark (") indicates that the values above it are to be repeated for the given cell and the dash (—) symbol indicates a blank cell. Furthermore, $f_{s,k}(.)$ is given by equations (4.7) and (4.15).

Proof: See Appendix A.3.

TABLE 4.1: Conditioned on serving BS being LOS for the case $(R-a)^{\frac{\alpha_N}{\alpha_L}} > R+a$

	LOS interferers		**NLOS interferers**	
	$\mathrm{A}_{L,1} < y < B_{L,1}$	$\mathrm{A}_{L,2} < y < B_{L,2}$	$\mathrm{A}_{N,1} < y < B_{N,1}$	$\mathrm{A}_{N,2} < y < B_{N,2}$
$0 < x < (R-a)$	$f_{L,1}(y),\ A_{L,1} = x,\ B_{L,1} = R-a$	$f_{L,2}(y),\ A_{L,2} = R-a,\ B_{L,2} = R+a$	$f_{N,1}(y),\ A_{N,1} = x^{\frac{\alpha_L}{\alpha_N}},\ B_{N,1} = R-a$	$f_{N,2}(y),\ A_{N,2} = R-a,\ B_{N,2} = R+a$
$(R-a) < x < (R+a)$	$f_{L,2}(y),\ A_{L,1} = x,\ B_{L,1} = R+a$	—	"	"

TABLE 4.2: Conditioned on serving BS being NLOS for the case $(R-a)^{\frac{\alpha_N}{\alpha_L}} > R+a$

	LOS interferers		**NLOS interferers**	
	$A_{L,1} < y < B_{L,1}$	$A_{L,2} < y < B_{L,2}$	$A_{N,1} < y < B_{N,1}$	$A_{N,2} < y < B_{N,2}$
$0 < x < (R-a)^{\frac{\alpha_L}{\alpha_N}}$	$f_{L,1}(y),\ A_{L,1} = x^{\frac{\alpha_N}{\alpha_L}},\ B_{L,1} = R-a$	$f_{L,2}(y),\ A_{L,2} = R-a,\ B_{L,2} = R+a$	$f_{N,1}(y),\ A_{N,1} = x,\ B_{N,1} = R-a$	$f_{N,2}(y),\ A_{N,2} = R-a,\ B_{N,2} = R+a$
$(R-a)^{\frac{\alpha_L}{\alpha_N}} < x < (R+a)^{\frac{\alpha_L}{\alpha_N}}$	$f_{L,2}(y),\ A_{L,1} = x^{\frac{\alpha_N}{\alpha_L}},\ B_{L,1} = R+a$	—	"	"
$(R+a)^{\frac{\alpha_L}{\alpha_N}} < x < R-a$	$f_{L,2}(R+a),\ A_{L,1} = x^{\frac{\alpha_N}{\alpha_L}},\ B_{L,1} = R+a$	—	"	"
$R-a < x < R+a$	"	—	$f_{N,2}(y),\ A_{N,1} = x,\ B_{N,1} = R+a$	—

TABLE 4.3: Conditioned on serving BS being LOS for the case $(R-a)^{\frac{\alpha_N}{\alpha_L}} < R+a$

	LOS interferers		**NLOS interferers**	
	$\mathrm{A}_{L,1} < y < B_{L,1}$	$\mathrm{A}_{L,2} < y < B_{L,2}$	$\mathrm{A}_{N,1} < y < B_{N,1}$	$\mathrm{A}_{N,2} < y < B_{N,2}$
$0 < x < (R-a)$	$f_{L,1}(y),\ A_{L,1} = x,\ B_{L,1} = R-a$	$f_{L,2}(y),\ A_{L,2} = R-a,\ B_{L,2} = R+a$	$f_{N,1}(y),\ A_{N,1} = x^{\frac{\alpha_L}{\alpha_N}},\ B_{N,1} = R-a$	$f_{N,2}(y),\ A_{N,2} = R-a,\ B_{N,2} = R+a$
$(R-a) < x < (R-a)^{\frac{\alpha_N}{\alpha_L}}$	$f_{L,2}(y),\ A_{L,1} = x,\ B_{L,1} = R+a$	—	"	"
$(R-a)^{\frac{\alpha_N}{\alpha_L}} < x < R+a$	"	—	$f_{N,2}(y),\ A_{N,1} = x^{\frac{\alpha_L}{\alpha_N}},\ B_{N,1} = R+a$	—

TABLE 4.4: Conditioned on serving BS being NLOS for the case $(R-a)^{\frac{\alpha_N}{\alpha_L}} < R+a$

	LOS interferers		**NLOS interferers**	
	$A_{L,1} < y < B_{L,1}$	$A_{L,2} < y < B_{L,2}$	$A_{N,1} < y < B_{N,1}$	$A_{N,2} < y < B_{N,2}$
$0 < x < (R-a)^{\frac{\alpha_L}{\alpha_N}}$	$f_{L,1}(y),\ A_{L,1} = x^{\frac{\alpha_N}{\alpha_L}}, B_{L,1} = R-a$	$f_{L,2}(y),\ A_{L,2} = R-a,\ B_{L,2} = R+a$	$f_{N,1}(y),\ A_{N,1} = x,\ B_{N,1} = R-a$	$f_{N,2}(y),\ A_{N,2} = R-a,\ B_{N,2} = R+a$
$(R-a)^{\frac{\alpha_L}{\alpha_N}} < x < R-a$	$f_{L,2}(y),\ A_{L,1} = x^{\frac{\alpha_N}{\alpha_L}}, B_{L,1} = R+a$	—	"	"
$R-a < x < (R+a)^{\frac{\alpha_L}{\alpha_N}}$	"	—	$f_{N,2}(y),\ A_{N,1} = x,\ B_{N,1} = R+a$	—
$(R+a)^{\frac{\alpha_L}{\alpha_N}} < x < R+a$	$f_{L,2}(R+a),\ A_{L,1} = x^{\frac{\alpha_N}{\alpha_L}},\ B_{L,1} = R+a$	—	"	—

4.2.4 Coverage Analysis

With the above defined distance distributions for the serving and interfering BSs, now we can define the SINR coverage probability as presented in this section. Conditioning on the nearest BS being at a distance x from the reference receiver, the probability of coverage relative to an SINR threshold τ can be written as

$$\overset{(\mathrm{u})}{\mathbb{P}}_c(\tau) = Y_{L,u}\,\overset{(\mathrm{u})}{\mathbb{P}}_{c,L}(\tau) + Y_{N,u}\,\overset{(\mathrm{u})}{\mathbb{P}}_{c,N}(\tau);\ \ u = \{1,2\}, \tag{4.26}$$

where $u = 1$ and $u = 2$ corresponds to the cases $(R-a)^{\frac{\alpha_N}{\alpha_L}} > (R+a)$ and $(R-a)^{\frac{\alpha_N}{\alpha_L}} < (R+a)$ respectively. $\overset{(\mathrm{u})}{\mathbb{P}}_{c,L}(\tau)$ and $\overset{(\mathrm{u})}{\mathbb{P}}_{c,N}(\tau)$ are the conditional coverage probabilities given that the user is associated with a LOS BS and an NLOS BS respectively. Further $\overset{(\mathrm{u})}{\mathbb{P}}_{c,L}(\tau)$ and $\overset{(\mathrm{u})}{\mathbb{P}}_{c,N}(\tau)$ can be evaluated as

$$\overset{(\mathrm{u})}{\mathbb{P}}_{c,L}(\tau) = \int_0^{R+a} \mathbb{P}[\mathrm{SINR} > \tau]\ \overset{(\mathrm{SER})}{f}_{L,u}(x)dx = \int_0^{R+a} \mathbb{P}\left[\frac{x^{-\alpha_L} h_{\boldsymbol{X}} p_t N}{(\sigma^2 + I)} > \tau\right] \overset{(\mathrm{SER})}{f}_{L,u}(x)dx. \tag{4.27}$$

The inner probability term can be further simplified as

$$\begin{aligned}\mathbb{P}\left[\frac{x^{-\alpha_L} h_{\boldsymbol{X}} p_t N}{(\sigma^2 + I)} > \tau\right] &= \mathbb{P}\left[h_{\boldsymbol{X}} > \frac{x^{\alpha_L}\tau(\sigma^2 + I)}{p_t N}\right] \\ &\overset{(\mathrm{a})}{=} 1 - \mathbb{E}_I\left[\left(1 - \exp\left(\frac{-\eta_L \tau x^{\alpha_L}(\sigma^2 + I)}{p_t N}\right)\right)^{\beta_L}\right] \\ &\overset{(\mathrm{b})}{=} \sum_{n=1}^{\beta_L} (-1)^{n+1} \binom{\beta_L}{n} \exp\left(\frac{-n\eta_L \tau x^{\alpha_L}\sigma^2}{p_t N}\right) \overset{(u)}{\mathcal{L}}_{I|L}\left(\frac{n\eta_L \tau x^{\alpha_L}}{p_t N}\right)\end{aligned} \tag{4.28}$$

where (a) follows from, for a normalised gamma random variable γ with parameter β_L, the probability $P(\gamma < C\epsilon R^+)$ is upper bounded by $P(\gamma < C\epsilon R^+) < [1 - \exp -\eta_L C]^{\beta_L}$, where $\eta_L = \beta_L(\beta_L!)^{(\frac{-1}{\beta_L})}$ [51] and (b) follows from binomial theorem expansion.

Similarly the conditional coverage probability given that the reference user is served by an NLOS BS can be expressed as

$$\overset{(u)}{\mathbb{P}}_{c,N}(\tau) = \int_0^{R+a} \sum_{n=1}^{\beta_N} (-1)^{n+1} \binom{\beta_N}{n} \exp\left(\frac{-n\eta_N \tau x^{\alpha_N} \sigma^2}{p_t N}\right) \overset{(u)}{\mathcal{L}}_{I|N}\left(\frac{n\eta_N \tau x^{\alpha_N}}{p_t N}\right) \overset{(\mathrm{SER})}{f}_{N,u}(x)dx \quad (4.29)$$

where $\eta_N = \beta_N(\beta_N!)^{(\frac{-1}{\beta_N})}$. The Laplace transform of interference $\overset{(u)}{\mathcal{L}}_{I|s}(.)$ can be written as follows.

Theorem 4.6. *The Laplace transform of interference is given as*

$$\begin{aligned}
&\overset{(u)}{\mathcal{L}}_{I|s}\left(\frac{n\eta_s \tau x^{\alpha_s}}{p_t N}\right) = \\
&\frac{1}{\int_{A_{L,1}}^{B_{L,1}} f_{L,k}(q)dq + \int_{A_{L,2}}^{B_{L,2}} f_{L,k}(q)dq + \int_{A_{N,1}}^{B_{N,1}} f_{N,k}(q)dq + \int_{A_{N,2}}^{B_{N,2}} f_{N,k}(q)dq} \times \\
&\left(\int_{A_{L,1}}^{B_{L,1}} \frac{1}{\left(1 + \frac{n\eta_s \tau x^{\alpha_s} y^{-\alpha_L} p_t \mathbb{E}_{G_i}[(G_i)]}{p_t N \beta_L}\right)^{\beta_L}} f_{L,k}(y)dy + \right. \\
&\int_{A_{L,2}}^{B_{L,2}} \frac{1}{\left(1 + \frac{n\eta_s \tau x^{\alpha_s} y^{-\alpha_L} p_t \mathbb{E}_{G_i}[(G_i)]}{p_t N \beta_L}\right)^{\beta_L}} f_{L,k}(y)dy \\
&+ \int_{A_{N,1}}^{B_{N,1}} \frac{1}{\left(1 + \frac{n\eta_s \tau x^{\alpha_s} y^{-\alpha_N} p_t \mathbb{E}_{G_i}[(G_i)]}{p_t N \beta_N}\right)^{\beta_N}} f_{N,k}(y)dy + \\
&\left. \int_{A_{N,2}}^{B_{N,2}} \frac{1}{\left(1 + \frac{n\eta_s \tau x^{\alpha_s} y^{-\alpha_N} p_t \mathbb{E}_{G_i}[(G_i)]}{p_t N \beta_N}\right)^{\beta_N}} f_{N,k}(y)dy \right)^{N_t - 1}; \\
&\qquad u = \{1,2\}, k = \{1,2\} \text{ and } s = \{L,N\} \quad (4.30)
\end{aligned}$$

where $u = 1$ and $u = 2$ corresponds to the above defined cases and $s = L$ and $s = N$ corresponds to the LOS and NLOS serving BS. In (4.30), the Laplace transform of interference corresponding to different ranges of x can be computed by substituting the corresponding values of $A_{L,1}, A_{L,2}, A_{N,1}, A_{N,2}, B_{L,1}, B_{L,2}, B_{N,1}, B_{N,2}$

and k, given in Tables 4.1, 4.2, 4.3 and 4.4. Furthermore, by using the proposed multi-cosine antenna model, an expression for the expectation of the array gain $\mathbb{E}_{G_i}[(G_i)]$ in (4.30) can be derived as[4]

$$\mathbb{E}_{G_i}[(G_i)] =$$
$$\int_{-0.5}^{0.5} G_i d\varphi_i = \int_{-\frac{1}{N}}^{\frac{1}{N}} G_0 \cos^2\left(\frac{\pi N \varphi_i}{2}\right) d\varphi_i + 2\sum_{k=1}^{\frac{N}{2}-1} \int_{\frac{k}{N}}^{\frac{k+1}{N}} G_k \cos^2(\pi N(\varphi_i - \varphi_k)) d\varphi_i$$
$$= \frac{4}{\pi}\int_0^{\frac{\pi}{2}} \cos^2(m) dm + \frac{4G_k}{\pi N}\sum_{k=1}^{\frac{N}{2}-1} \int_0^{\frac{\pi}{2}} \cos^2(m) dm = 1 + \frac{1}{N}\sum_{k=1}^{\frac{N}{2}-1} G_k. \quad (4.31)$$

Proof: See Appendix A.4.

This concludes the SINR coverage probability derivations for the model specified in Section 4.1. In the coming sections (Section 4.2.4.1 and Section 4.2.4.2), we provide the SINR coverage probabilities for simplified cases for which manageable analytical expressions are obtained.

4.2.4.1 SINR Coverage Probability of a Centre UE

The SINR coverage probability in (4.26) can be simplified further for a centre reference UE (i.e., $a = 0$). The aforementioned two cases are not applicable in this scenario.

Corollary 4.1. *The SINR coverage probability of a centre UE can be written as*

$$\mathbb{P}_c(\tau) = Y_L \mathbb{P}_{c,L}(\tau) + Y_N \mathbb{P}_{c,N}(\tau) \quad (4.32)$$

where Y_L, Y_N, $\mathbb{P}_{c,L}(\tau)$ and $\mathbb{P}_{c,N}(\tau)$ can be written as

$$Y_L = N_t\left(\int_0^R \left(1 - F_{N,1}(x^{\frac{\alpha_L}{\alpha_N}})\right)^{N_t} (1 - F_{L,1}(x))^{(N_t-1)} f_{L,1}(x) dx\right), \quad (4.33)$$

[4]The interferers array gain $G_{\text{mcos}}(\varphi_Y)$ and the spatial AoD φ_Y are abbreviated as G_i and φ_i, respectively.

$$Y_N = N_t\Bigg(\int_0^{(R)^{\frac{\alpha_L}{\alpha_N}}} \left(1 - F_{L,1}(x^{\frac{\alpha_N}{\alpha_L}})\right)^{N_t} (1 - F_{N,1}(x))^{(N_t-1)} f_{N,1}(x)dx + \int_{(R)^{\frac{\alpha_L}{\alpha_N}}}^{R} a_L (1 - F_{N,1}(x))^{(N_t-1)} f_{N,1}(x)dx \Bigg), \quad (4.34)$$

$$\mathbb{P}_{c,L}(\tau) = \int_0^R \sum_{n=1}^{\beta_L} (-1)^{n+1} \binom{\beta_L}{n} \exp\left(\frac{-n\eta_L \tau x^{\alpha_L} \sigma^2}{p_t N}\right) \mathcal{L}_{I|L}\left(\frac{n\eta_L \tau x^{\alpha_L}}{p_t N}\right) \overset{(\mathrm{SER})}{f}_L(x)dx, \quad (4.35)$$

and

$$\mathbb{P}_{c,N}(\tau) = \int_0^R \sum_{n=1}^{\beta_N} (-1)^{n+1} \binom{\beta_N}{n} \exp\left(\frac{-n\eta_N \tau x^{\alpha_N} \sigma^2}{p_t N}\right) \mathcal{L}_{I|N}\left(\frac{n\eta_N \tau x^{\alpha_N}}{p_t N}\right) \overset{(\mathrm{SER})}{f}_N(x)dx. \quad (4.36)$$

In (4.35) and (4.36), $\overset{(\mathrm{SER})}{f}_L(x)$, $\overset{(\mathrm{SER})}{f}_N(x)$, $\mathcal{L}_{I|L}$ and $\mathcal{L}_{I|N}$ can be written as

$$\overset{(\mathrm{SER})}{f}_L(x) = \frac{N_t}{Y_L} (1 - F_{L,1}(x))^{(N_t-1)} f_{L,1}(x) \left(1 - F_{N,1}(x^{\frac{\alpha_L}{\alpha_N}})\right)^{N_t}, \quad (4.37)$$

$$\overset{(\mathrm{SER})}{f}_{N,1}(x) = \begin{cases} \frac{N_t}{Y_N} (1 - F_{N,1}(x))^{(N_t-1)} f_{N,1}(x) \left(1 - F_{L,1}(x^{\frac{\alpha_N}{\alpha_L}})\right)^{N_t} & 0 < x < R^{\frac{\alpha_L}{\alpha_N}} \\ \frac{N_t}{Y_N} a_L (1 - F_{N,1}(x))^{(N_t-1)} f_{N,1}(x) & R^{\frac{\alpha_L}{\alpha_N}} < x < R, \end{cases} \quad (4.38)$$

$$\mathcal{L}_{I|L}\left(\frac{n\eta_L\tau x^{\alpha_L}}{p_tN}\right)=\frac{1}{\int_x^R f_{L,1}(q)dq+\int_{x^{\frac{\alpha_L}{\alpha_N}}}^R f_{N,1}(q)dq}\times \left(\int_x^R \frac{1}{\left(1+\frac{n\eta_s\tau x^{\alpha_L}y^{-\alpha_L}p_t\mathbb{E}_{G_i}[(G_i)]}{p_tN\beta_L}\right)^{\beta_L}}f_{L,1}(y)dy+ \int_{x^{\frac{\alpha_L}{\alpha_N}}}^R \frac{1}{\left(1+\frac{n\eta_L\tau x^{\alpha_L}y^{-\alpha_N}p_t\mathbb{E}_{G_i}[(G_i)]}{p_tN\beta_N}\right)^{\beta_N}}f_{N,1}(y)dy\right)^{N_t-1}, \quad (4.39)$$

and

$$\mathcal{L}_{I|N}\left(\frac{n\eta_N\tau x^{\alpha_N}}{p_tN}\right)= \begin{cases} \frac{1}{\int_{x^{\frac{\alpha_N}{\alpha_L}}}^R f_{L,1}(q)dq+\int_x^R f_{N,1}(q)dq}\times \\ \left(\int_{x^{\frac{\alpha_N}{\alpha_L}}}^R \frac{1}{\left(1+\frac{n\eta_N\tau x^{\alpha_N}y^{-\alpha_L}p_t\mathbb{E}_{G_i}[(G_i)]}{p_tN\beta_L}\right)^{\beta_L}}f_{L,1}(y)dy+ \right. \\ \left.\int_x^R \frac{1}{\left(1+\frac{n\eta_N\tau x^{\alpha_N}y^{-\alpha_N}p_t\mathbb{E}_{G_i}[(G_i)]}{p_tN\beta_N}\right)^{\beta_N}}f_{N,1}(y)dy\right)^{N_t-1} & 0<x<R^{\frac{\alpha_L}{\alpha_N}} \\ \left(\int_x^R \frac{1}{\left(1+\frac{n\eta_N\tau x^{\alpha_N}y^{-\alpha_N}p_t\mathbb{E}_{G_i}[(G_i)]}{p_tN\beta_N}\right)^{\beta_N}}\frac{f_{N,1}(y)}{\int_x^R f_{N,1}(q)dq}dy\right)^{N_t-1} & R^{\frac{\alpha_L}{\alpha_N}}<x<R. \end{cases} \quad (4.40)$$

Proof: The expressions in *Corollary* 4.1 can be derived by substituting $a = 0$ in the expressions provided for the association probabilities, distance distributions and the coverage probability in sections 4.2.1, 4.2.2, 4.2.3 and 4.2.4.

4.2.4.2 SINR Coverage Probability of Dense Networks

Coverage probability expressions of dense networks can be derived with the following two assumptions as presented in [38]. Firstly, we assume all BSs to be with LOS link, as the BS density increases the distance between a UE and a BS becomes smaller; thus it is highly unlikely to have NLOS links in such a scenario. Secondly,

we ignore the impact of noise, as the BS density increases the network becomes interference-limited; therefore, thermal noise can be ignored. Furthermore, the aforementioned two cases are not applicable in this scenario. With these assumptions, a dense network's downlink coverage probability can be written as follows.

Corollary 4.2. *SINR coverage probability of dense networks can be written as*

$$\mathbb{P}_c\left(\tau\right) = \int_0^{R+a} \sum_{n=1}^{\beta_L} (-1)^{n+1} \binom{\beta_L}{n} \mathcal{L}_I\left(\frac{n\eta_L \tau x^{\alpha_L}}{p_t N}\right) \overset{(\mathrm{SER})}{f_d}\left(x\right) dx \tag{4.41}$$

where $\overset{(\mathrm{SER})}{f_d}\left(x\right)$ can be written by substituting $p(t) = 1$ in (4.21) and given as

$$\overset{(\mathrm{SER})}{f_d}\left(x\right) = \begin{cases} N_t \left(1 - F_{d,1}(x)\right)^{(N_t-1)} f_{d,1}(x) & 0 < x < R - a \\ N_t \left(1 - F_{d,2}(x)\right)^{(N_t-1)} f_{d,2}(x) & R - a < x < R + a \end{cases} \tag{4.42}$$

where $F_{d,1}(x)$, $F_{d,2}(x)$, $f_{d,1}(x)$ and $f_{d,2}(x)$ can be written as substituting $p(t) = 1$ in (4.6) and (4.7). Furthermore $\mathcal{L}_I(.)$ can be written as

$$\begin{aligned} \mathcal{L}_I\left(\frac{n\eta_L \tau x^{\alpha_L}}{p_t N}\right) = & \frac{1}{\int_x^{R-a} f_{d,1}(q)\, dq + \int_{R-a}^{R+a} f_{d,2}\left(q\right) dq} \times \\ & \left(\int_x^{R-a} \frac{1}{\left(1 + \frac{n\eta_L \tau x^{\alpha_L} y^{-\alpha_L} p_t \mathbb{E}_{G_i}[(G_i)]}{p_t N \beta_L}\right)^{\beta_L}} f_{d,1}\left(y\right) dy + \right. \\ & \left. \int_{R-a}^{R+a} \frac{1}{\left(1 + \frac{n\eta_L \tau x^{\alpha_L} y^{-\alpha_L} p_t \mathbb{E}_{G_i}[(G_i)]}{p_t N \beta_L}\right)^{\beta_L}} f_{d,2}\left(y\right) dy \right)^{N_t - 1}. \end{aligned} \tag{4.43}$$

4.2.5 Rate Analysis

The rate coverage probability is defined as $\mathbb{P}[W \log_2(1+\mathrm{SINR}) > \gamma] = \overset{(\mathrm{u})}{\mathbb{P}}_c\left(2^{\frac{\gamma}{W}} - 1\right)$, where W is the bandwidth and γ is the rate threshold [38].

4.3 Results and Discussions

This section provides numerical results for the analytical model proposed in Section 4.2. The Nakagami fading parameters and path loss exponents of LOS and NLOS links are set to $\alpha_L = 2$, $\alpha_N = 4$, $\beta_L = 3$ and $\beta_N = 2$. Unless or otherwise stated, a fixed number of BSs $N_t = 50$ in a finite disk region with $R = 100$ m. All BSs operate at frequency 28 GHz with 100 MHz bandwidth and assumed to transmit with the same transmission power of 25 dBm. The blockage parameter ω is set to $\frac{1}{140}$. With the above-defined parameters, we have performed Monte Carlo simulations to validate the accuracy of our mathematical framework in MATLAB. The simulation results are obtained by averaging over 10,000 realisations. In each simulation run, a fixed number of BSs (N_t) and users are randomly placed, link status between a user and a base station is randomly determined based on the blockage parameter, and fading gains are modelled by gamma random variables.

Fig. 4.6 shows the SINR coverage probability of the reference receiver at different locations ($a = 10$ m, and $a = 80$ m) from the centre of the finite disk region. The number of array antenna elements has been set to 32. The performance improves as the user moves away from the centre. This figure verifies the accuracy of the analytical model proposed. It can be observed that the proposed analytical model shows excellent agreement with the simulation results. Here, in order to demonstrate the analytical model's accuracy, we have considered the multi-cosine antenna model in both theoretical and simulation results. The performance comparison between the multi-cosine and actual antenna models presented in Section 4.1.4, will be discussed in Figs. 4.7 and 4.8.

In Figs. 4.7 and 4.8, the validity of the assumptions made in the proposed antenna model has been presented. It can be observed that the accuracy improves as the number of BSs increases in the network. In Section 4.1.4 we assumed a uniform distribution for the antenna spatial AoD and as shown in these figures this accuracy of this assumption depends on the network's BS density. For example, in Fig. 4.7, for number of BSs $N_t = 10$, the uniform angle distribution assumption is not providing an acceptable accuracy. But for $N_t = 50$, the accuracy improves.

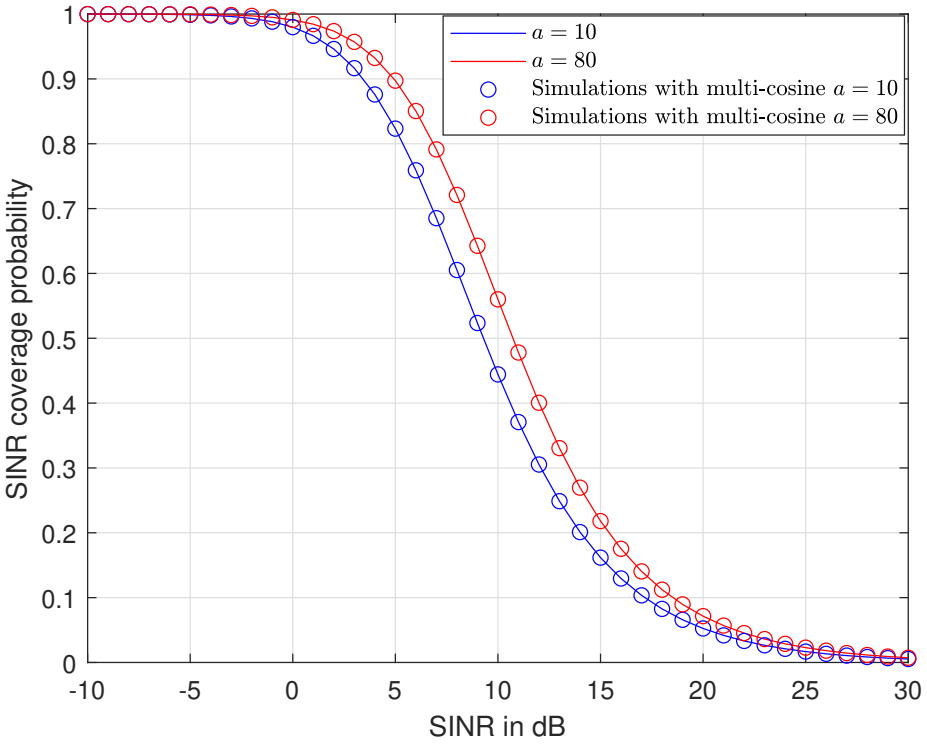

FIGURE 4.6: SINR coverage probability at different receiver locations ($N = 32$).

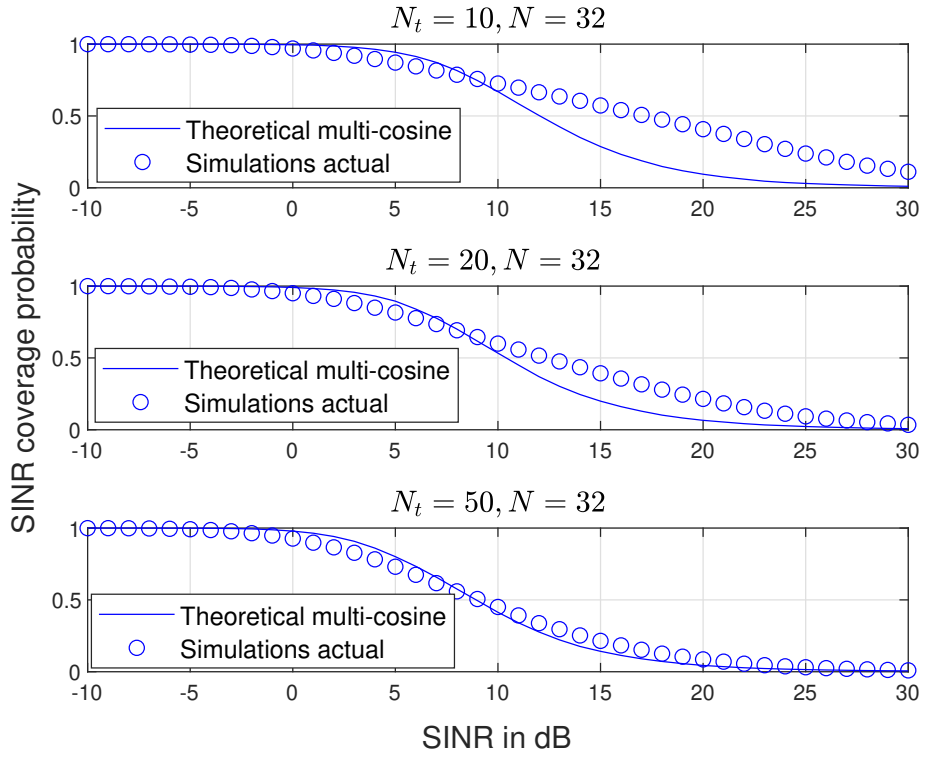

FIGURE 4.7: SINR coverage probability comparison between the actual and multi-cosine antenna models for different BS counts ($a = 10$ m, and $N = 32$).

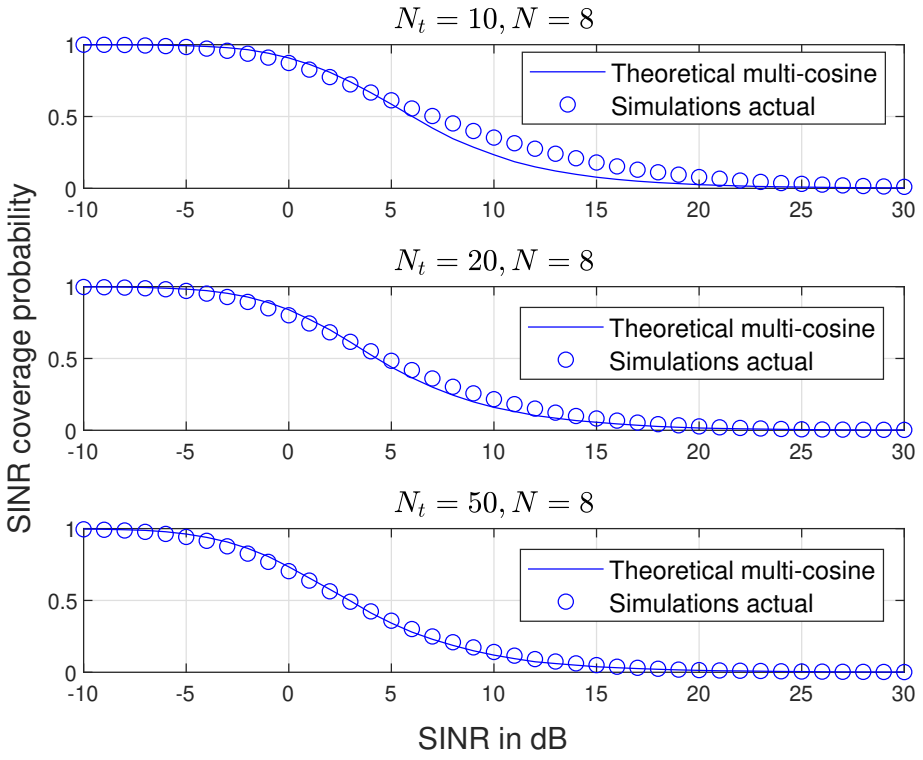

FIGURE 4.8: SINR coverage probability comparison between the actual and multi-cosine antenna models for different BS counts ($a = 10$ m, and $N = 8$).

Therefore, we can conclude that this AoD distribution assumption is valid for a network with high BS density. It is expected that mmWave cellular network will be deployed as an ultra dense network [14]. Hence, this assumptions seems to be a valid assumption for a dense mmWave cellular network. Furthermore, Fig. 4.8 shows the comparison between the simulated results with actual antenna and the theoretical model for array antenna elements $N = 8$. It can be observed that as the number of array elements decreases, the uniform angle distribution assumption provides a better accuracy even for a comparatively lower BS density.

Fig. 4.9 shows the comparison between the PPP and BPP models for a reference receiver located at the origin. We have considered the PPP's BS density equal to the number of BS in the BPP divided by the area of the finite disk region, i.e., $\frac{N_t}{\pi R^2}$. The PPP model provides a lower bound for the coverage probability compared to the BPP model. In the PPP model, we can only analyse the performance of a user located at the centre of the network. This emphasises the importance of the

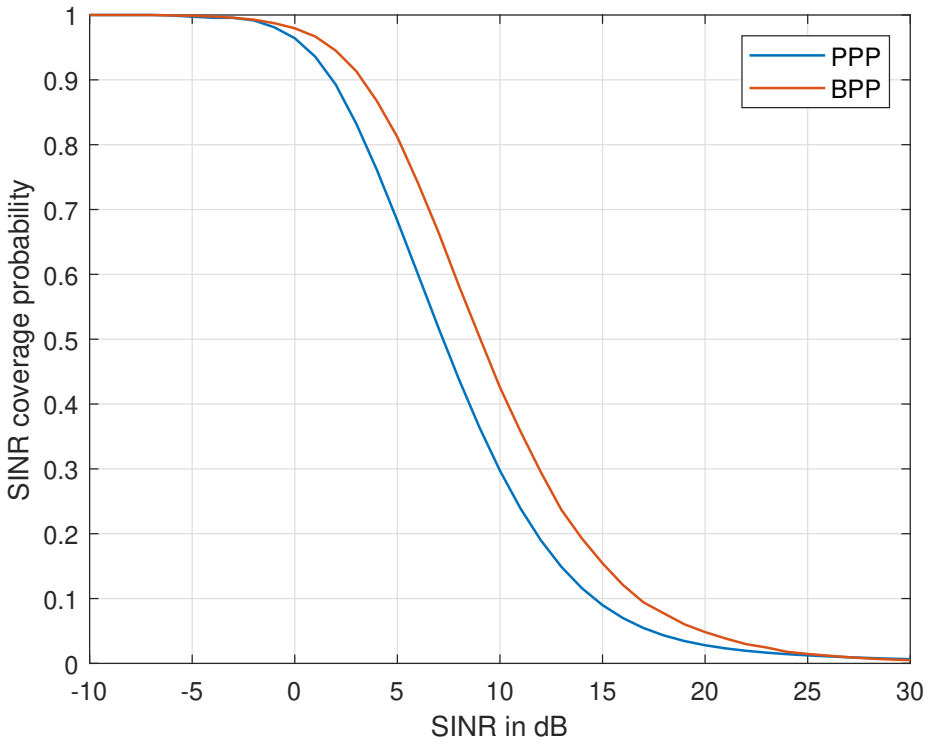

FIGURE 4.9: SINR downlink coverage probability for a BPP and PPP network ($a = 0$ m, and $N = 32$).

proposed BPP model, which allows the analysis of a user's performance at any arbitrary location in the given network.

In Fig. 4.10, the impact of antenna arrays in mmWave cellular networks has been investigated. The results illustrate considerable performance improvement as the number of antenna array elements increases. Increasing the array size, increases not only the maximum array gain of the serving BS but also narrows the beam of the interfering BSs, which reduces the interfering power towards the reference user. Furthermore, it can be observed that the flat-top antenna model underestimates the probability of coverage compared to the multi-cosine antenna model. Therefore this demonstrates the importance of incorporating a more realistic array antenna model in system analysis.

In Fig. 4.11, as the blockage parameter ω increases the coverage probability increases and reaches an optimum value and then declines. This can be interpreted

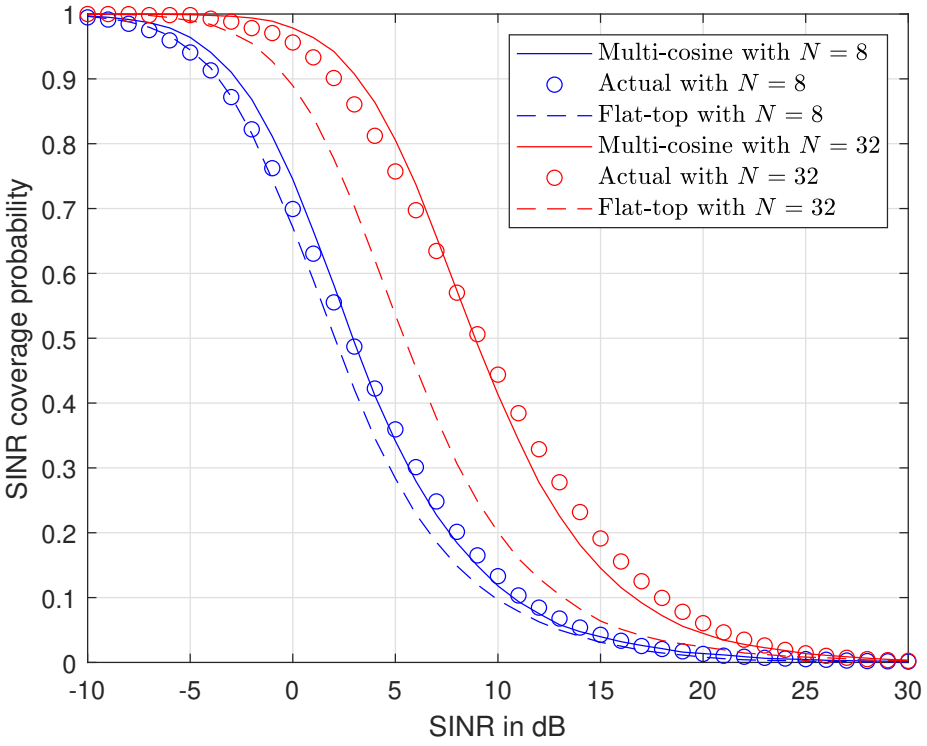

FIGURE 4.10: SINR downlink coverage probability comparison for different array elements ($a = 10$ m).

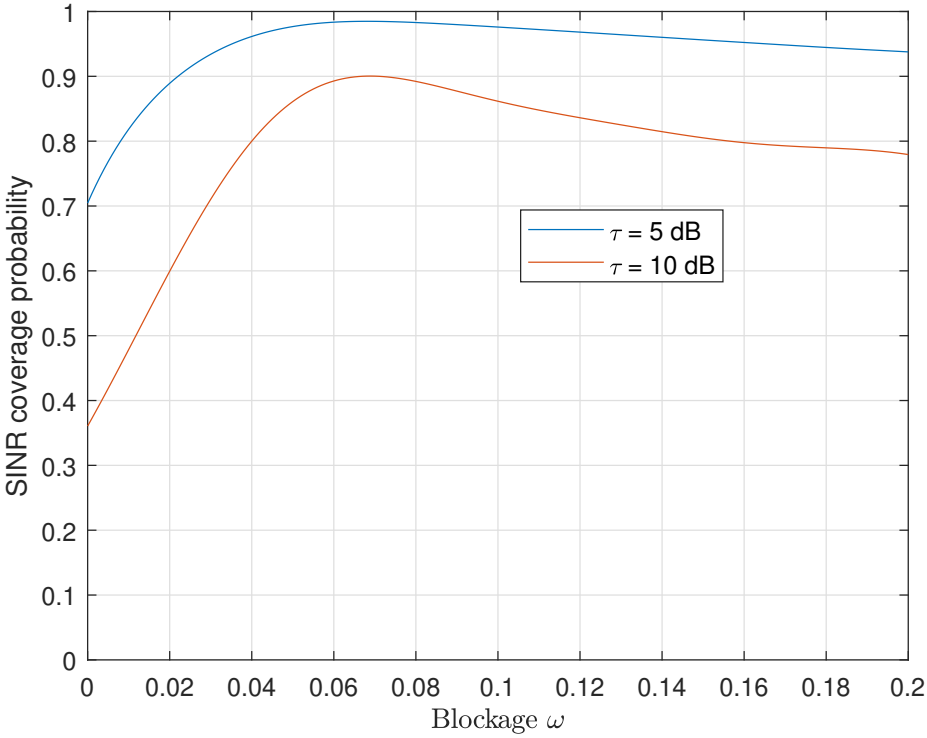

FIGURE 4.11: SINR coverage probability of a reference receiver as a function of the blockage parameter ω ($N = 32$ and $a = 10$ m).

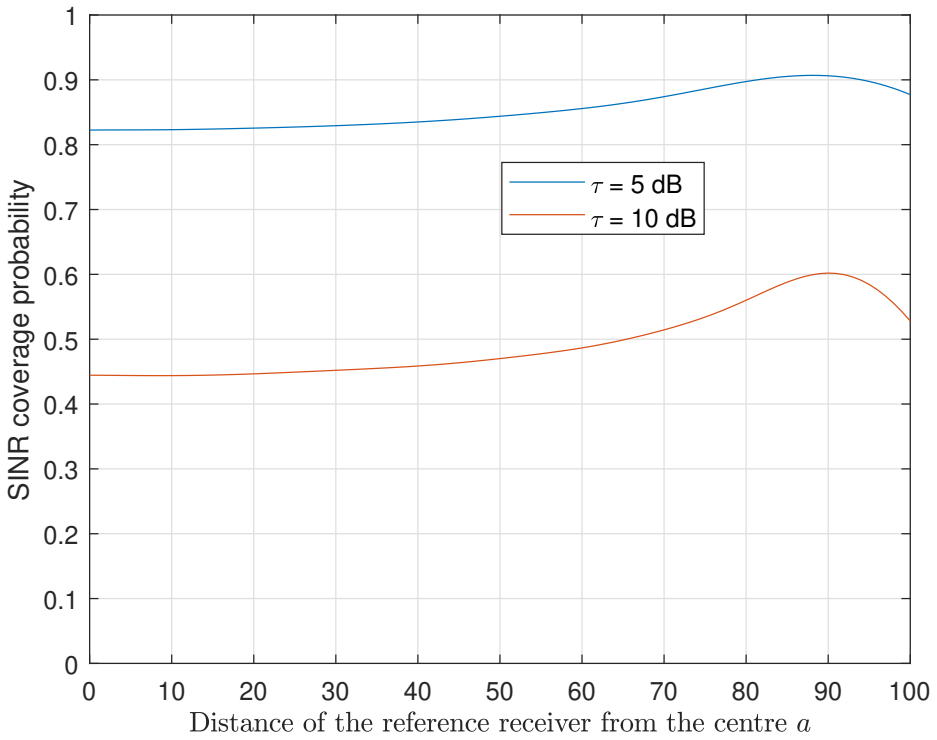

FIGURE 4.12: SINR coverage probability of a reference receiver as a function of its distance from the centre of the disk region ($N = 32$).

such that as ω increases, more BSs become NLOS resulting in decreased interference power. With further increases in ω, both the serving and interfering BSs might become NLOS, and the coverage probability degrades.

Fig. 4.12 shows that the minimum value of the coverage probability occurs when the reference receiver is located at the centre of the disk region. In contrast, the maximum value occurs somewhere closer to the circumference of the disk region. This might be due to, as the user moves farther from the centre of the finite region, more interferers become NLOS, thus results in reduce interference power. Further, it can be observed that, depending on the SINR threshold, there is an optimum distance for the receiver to experience the best possible coverage probability. In the given network setup the optimum distance is approximately 90 m from the centre of the disk region.

Fig. 4.13 illustrates that the coverage probability improves as the number of BSs increases, and starts to decline after an optimum number of BSs. This can be

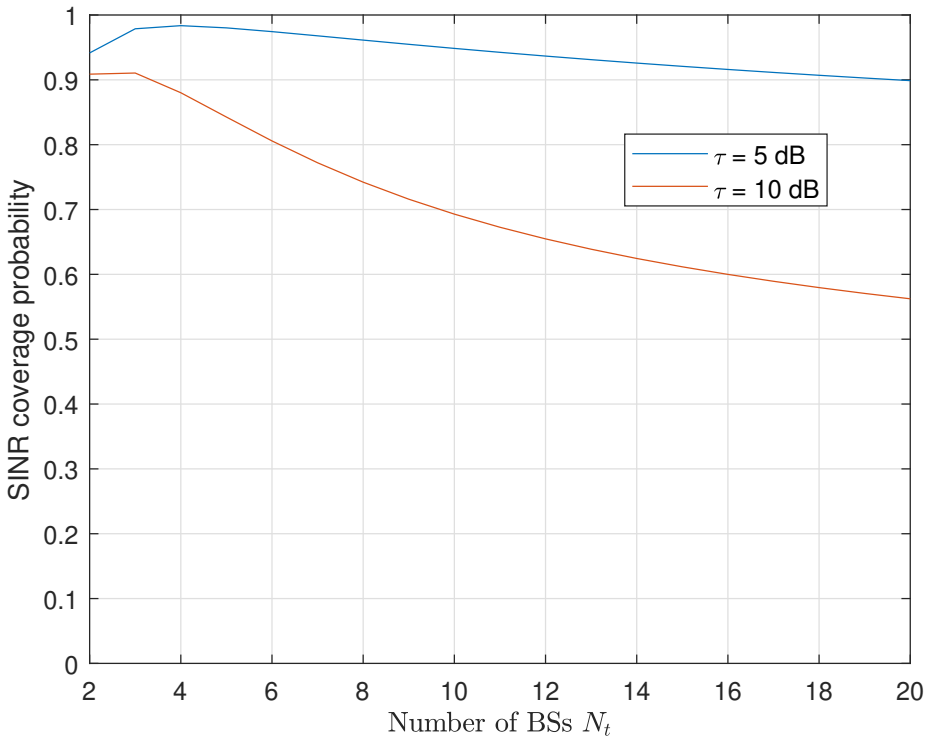

FIGURE 4.13: SINR coverage probability of a reference receiver as a function of number of BSs. ($N = 32$ and $a = 10$ m).

interpreted as, when the BS count increases, the distance between the user and BSs becomes smaller and it is more likely that a LOS BS will serve a user. However, increasing this count further might cause the user to see more LOS BSs, thus creating severe interference. As a result, the performance degrades.

Fig. 4.14 illustrates the rate coverage probability comparison for the BPP model for a different number of array antenna elements for mmWave cellular networks. Again, it can be seen that the performance significantly improves by increasing the number of array elements. It demonstrates that a significant number of array elements are required to achieve the expected high throughput in mmWave cellular networks successfully.

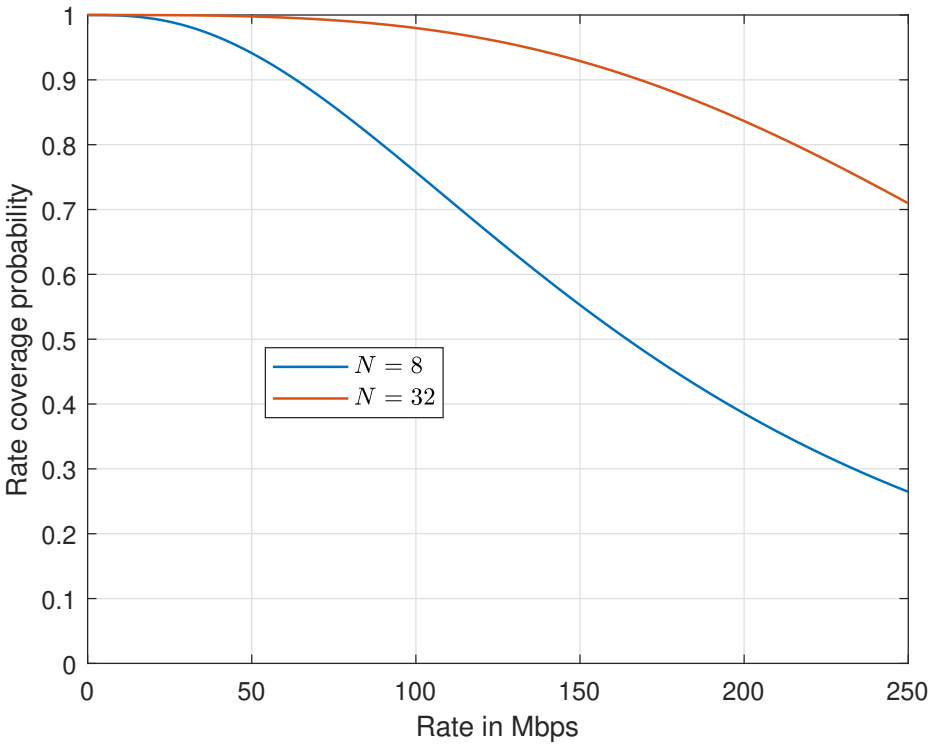

FIGURE 4.14: Rate coverage probability with different array antenna elements ($a = 10$ m).

4.4 Conclusions

This chapter presents a mathematical framework based on the binomial point process for analysing the performance of a downlink mmWave cellular network. This analysis enables us to analyse the downlink performance of a user located anywhere in a given network region. This is an important performance analysis requirement, in which it can be observed that a user closer to the boundary of the finite region experiences better performance compared to a user closer to the centre of the network. Also, it enables us to quantify the performance of a cellular system, given a fixed number of nodes. In contrast, these two possibilities of analysing a user's performance based on its location, given a fixed number of nodes are not possible with the commonly adopted PPP. Furthermore, the impact of antenna array size has been demonstrated by adopting a realistic array antenna model. The results show that the coverage and rate probability can be improved considerably by increasing the directional antenna array size. The impact of changes in the

blockage parameter ω have also been demonstrated. There is an optimum value of ω for a given network setup for which a user can experience the highest coverage probability. The coverage probability analysis as a function of number of BSs suggests that the SINR coverage probability improves for up to an optimum BS count, then thereafter performance declines.

Chapter 5

Downlink Coverage Analysis in a Regular L-Sided Convex Polygon

In this chapter, we generalise the coverage probability to an L-sided regular convex polygon. As similar in Chapter 4, we ave considered the unique features of millimetre wave communications and analysed the downlink performance. This chapter follows the exact modelling assumptions as in Chapter 4, the only difference is that the finite disk region has been generalised further, to an arbitrary shape. Numerical results are provided to validate the accuracy of the proposed analytical model. The remainder of the chapter is organised as follows. Section 5.1 describes the system modelling assumptions adopted in this chapter. Section 5.2 presents the technical derivations corresponding to the model proposed in Section 5.1. Section 5.3 presents numerical and simulation results. Finally, Section 5.4 concludes the chapter.

5.1 System Model

This section presents the system modelling assumptions we have incorporated to model the mmWave cellular systems' downlink communications in a L-sided regular convex polygon.

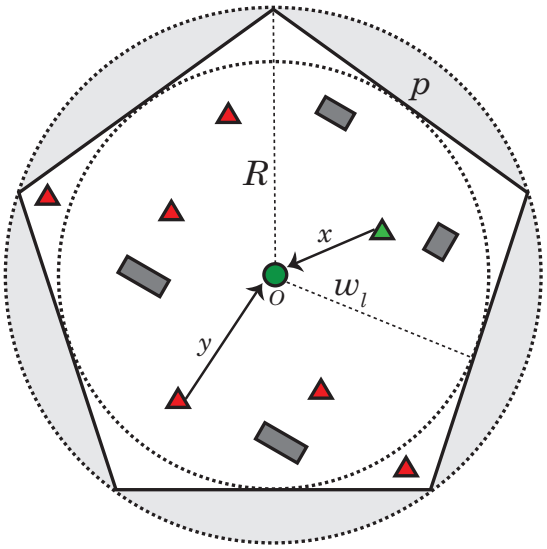

FIGURE 5.1: L-sided convex polygon ($L = 5$) with side length p inscribed in a circle of radius R. The green circle and the triangle are the reference UE and reference BS, respectively. The red triangles are the interfering BSs. The grey rectangles are the random blockages.

5.1.1 Network Model

This chapter focuses on downlink performance analysis of an outdoor mmWave cellular network in a two-dimensional finite L-sided regular convex polygon as shown in Fig. 5.1. It is assumed that N_t number of BSs are distributed according to a uniform BPP, Φ. The user of interest, referred to as the reference UE, is located at the origin $\boldsymbol{O}$. Here, we only consider a scenario in which the reference UE is at the centre of the polygon, as an arbitrarily located user would add greater complexity to the analysis [21]. The serving BS of the reference UE, referred to as the reference BS is located at $\boldsymbol{X}$ with distance x to the reference UE. Then the interfering BSs are located at $\boldsymbol{Y}$ with distance y to the reference UE.

5.1.2 Blockage and Channel Model

The blockage and channel models have been assumed for LOS and NLOS links as similar in Section 4.1.2.

5.1.3 Selection Strategy

As in Section 4.1.3 it is assumed that a user will be connected to the base station that provides the smallest path loss.

5.1.4 Antenna Model

The antenna model as given in Section 4.1.4 has been considered here.

5.2 Coverage Analysis

This section presents the coverage analysis for the proposed arbitrary shape polygon in Section 5.1. The intermediate definitions required to compute the coverage probability, namely the association probabilities and distance distributions of the serving and interfering BSs should be derived prior. These intermediate definitions' derivations follow a similar approach as in Chapter 4. Therefore we have omitted the proofs in this chapter.

5.2.1 Association Probabilities

A user can be associated with the nearest LOS or NLOS BS. A finite L-sided polygon that is inscribed in a circle of radius R is given in Fig. 5.1. The area $\mathcal{A}$ and the interior angle θ_i between two adjacent sides can then be written as

$$|\mathcal{A}| = \frac{1}{2} L R^2 \sin\left(\frac{2\pi}{L}\right) \tag{5.1}$$

and

$$\theta_i = \frac{\pi(L-2)}{L}. \tag{5.2}$$

In a scenario where the reference UE is at the centre of the polygon, the CDF for the LOS and NLOS links can be written as [67, 70]

$$F_L\left(x\right) = \begin{cases} F_{L,1}\left(x\right) = \frac{2\pi \int_0^x tp(t)dt}{\mathcal{A}} & 0 \leq x \leq w_l \\ F_{L,2}\left(x\right) = \frac{2\pi \int_0^{w_l} tp(t)dt + \int_{w_l}^x \left(2\pi t - 2Lt\arccos\left(\frac{w_l}{t}\right)\right)p(t)dt}{\mathcal{A}} & w_l < x \leq R, \end{cases} \tag{5.3}$$

and

$$F_N\left(x\right) = \begin{cases} F_{N,1}\left(x\right) = \frac{2\pi \int_0^x t(1-p(t))dt}{\mathcal{A}} & 0 \leq x \leq w_l \\ F_{N,2}\left(x\right) = \frac{2\pi \int_0^{w_l} t(1-p(t))dt + \int_{w_l}^x \left(2\pi t - 2Lt\arccos\left(\frac{w_l}{t}\right)\right)(1-p(t))dt}{\mathcal{A}} & \\ & w_l < x \leq R \end{cases} \tag{5.4}$$

where $w_l = R\sin\frac{\theta_i}{2}$. The corresponding PDFs can be written as

$$f_L\left(x\right) = \begin{cases} f_{L,1}\left(x\right) = \frac{dF_{L,1}(x)}{dx} & 0 \leq x \leq w_l \\ f_{L,2}\left(x\right) = \frac{dF_{L,2}(x)}{dx} & w_l < x \leq R, \end{cases} \tag{5.5}$$

and

$$f_N\left(x\right) = \begin{cases} f_{N,1}\left(x\right) = \frac{dF_{N,1}(x)}{dx} & 0 \leq x \leq w_l \\ f_{N,2}\left(x\right) = \frac{dF_{N,2}(x)}{dx} & w_l < x \leq R. \end{cases} \tag{5.6}$$

Based on these above-defined CDFs and PDFs, the LOS and NLOS association probabilities can be defined.

Theorem 5.1. *The probability that the reference user is associated with a LOS base station in the case* $w_l^{\frac{\alpha_N}{\alpha_L}} > R$ *is*

$$Y_{L,1} = N_t\Bigg(\int_0^{w_l} \Big(1 - F_{N,1}(x^{\frac{\alpha_L}{\alpha_N}})\Big)^{Nt} (1 - F_{L,1}(x))^{(N_t-1)} f_{L,1}(x)dx + \int_{w_l}^{R} \Big(1 - F_{N,1}(x^{\frac{\alpha_L}{\alpha_N}})\Big)^{Nt} (1 - F_{L,2}(x))^{(N_t-1)} f_{L,2}(x)dx \Bigg) \quad (5.7)$$

and in the case $w_l^{\frac{\alpha_N}{\alpha_L}} < R$ is

$$Y_{L,2} = N_t\Bigg(\int_0^{w_l} \Big(1 - F_{N,1}(x^{\frac{\alpha_L}{\alpha_N}})\Big)^{Nt} (1 - F_{L,1}(x))^{(N_t-1)} f_{L,1}(x)dx + \int_{w_l}^{w_l^{\frac{\alpha_N}{\alpha_L}}} \Big(1 - F_{N,1}(x^{\frac{\alpha_L}{\alpha_N}})\Big)^{Nt} (1 - F_{L,2}(x))^{(N_t-1)} f_{L,2}(x)dx + \int_{w_l^{\frac{\alpha_N}{\alpha_L}}}^{R} \Big(1 - F_{N,2}(x^{\frac{\alpha_L}{\alpha_N}})\Big)^{Nt} (1 - F_{L,2}(x))^{(N_t-1)} f_{L,2}(x)dx \Bigg). \quad (5.8)$$

Proof: The proof follows a similar approach to that seen in Appendix A.1; hence, it is skipped.

Similarly NLOS association probability can be defined as follows.

Theorem 5.2. *The probability that the reference user is associated with an NLOS base station in the case* $w_l^{\frac{\alpha_N}{\alpha_L}} > R$ *is*

$$Y_{N,1} = N_t\Bigg(\int_0^{w_l^{\frac{\alpha_L}{\alpha_N}}} \Big(1 - F_{L,1}(x^{\frac{\alpha_N}{\alpha_L}})\Big)^{Nt} (1 - F_{N,1}(x))^{(N_t-1)} f_{N,1}(x)dx + \int_{w_l^{\frac{\alpha_L}{\alpha_N}}}^{R^{\frac{\alpha_L}{\alpha_N}}} \Big(1 - F_{L,2}(x^{\frac{\alpha_N}{\alpha_L}})\Big)^{Nt} (1 - F_{N,1}(x))^{(N_t-1)} f_{N,1}(x)dx + \int_{R^{\frac{\alpha_L}{\alpha_N}}}^{w_l} (1 - F_{L,2}R)^{Nt} (1 - F_{N,1}(x))^{(N_t-1)} f_{N,1}(x)dx + \int_{w_l}^{R} (1 - F_{L,2}R)^{Nt} (1 - F_{N,2}(x))^{(N_t-1)} f_{N,2}(x)dx \Bigg) \quad (5.9)$$

and in the case $w_l^{\frac{\alpha_N}{\alpha_L}} < R$ is

$$Y_{N,2} = N_t\Bigg(\int_0^{w_l^{\frac{\alpha_L}{\alpha_N}}} \left(1 - F_{L,1}(x^{\frac{\alpha_N}{\alpha_L}})\right)^{Nt} (1 - F_{N,1}(x))^{(N_t-1)} f_{N,1}(x)dx + \int_{w_l^{\frac{\alpha_L}{\alpha_N}}}^{w_l} \left(1 - F_{L,2}(x^{\frac{\alpha_N}{\alpha_L}})\right)^{Nt} (1 - F_{N,1}(x))^{(N_t-1)} f_{N,1}(x)dx + \int_{w_l}^{R^{\frac{\alpha_L}{\alpha_N}}} \left(1 - F_{L,2}(x^{\frac{\alpha_N}{\alpha_L}})\right)^{Nt} (1 - F_{N,2}(x))^{(N_t-1)} f_{N,2}(x)dx + \int_{R^{\frac{\alpha_L}{\alpha_N}}}^{R} (1 - F_{L,2}R)^{Nt} (1 - F_{N,2}(x))^{(N_t-1)} f_{N,2}(x)dx \Bigg). \quad (5.10)$$

Proof: The proof follows a similar approach to that seen in Appendix A.1.

Based on the above-defined association probabilities, the serving BS's distance distributions are presented in the following section.

5.2.2 Serving BS's Distance Distributions

A user will be connected to a BS which provides the minimum path loss, referred to as the serving BS. This section presents the distance distributions of this serving BS conditioned on the serving BS's link status, i.e. either LOS or NLOS.

Theorem 5.3. *Given that the reference receiver is associated with a LOS base station, the PDF of the distance to its serving base station in the case* $w_l^{\frac{\alpha_N}{\alpha_L}} > R$ *is*

$$f_{L,1}^{(\mathrm{SER})}(x) = \begin{cases} \frac{N_t}{Y_{L,1}} (1 - F_{L,1}(x))^{(N_t-1)} f_{L,1}(x) \left(1 - F_{N,1}(x^{\frac{\alpha_L}{\alpha_N}})\right)^{N_t} & 0 < x < w_l \\ \frac{N_t}{Y_{L,1}} (1 - F_{L,2}(x))^{(N_t-1)} f_{L,2}(x) \left(1 - F_{N,1}(x^{\frac{\alpha_L}{\alpha_N}})\right)^{N_t} & w_l < x < R \end{cases} \quad (5.11)$$

and in the case $w_l^{\frac{\alpha_N}{\alpha_L}} < R$ is

$$\overset{(\mathrm{SER})}{f_{L,2}}(x) = \begin{cases} \frac{N_t}{Y_{L,2}} \left(1 - F_{L,1}(x)\right)^{(N_t-1)} f_{L,1}(x) \left(1 - F_{N,1}(x^{\frac{\alpha_L}{\alpha_N}})\right)^{N_t} & 0 < x < w_l \\ \frac{N_t}{Y_{L,2}} \left(1 - F_{L,2}(x)\right)^{(N_t-1)} f_{L,2}(x) \left(1 - F_{N,1}(x^{\frac{\alpha_L}{\alpha_N}})\right)^{N_t} & w_l < x < w_l^{\frac{\alpha_N}{\alpha_L}} \\ \frac{N_t}{Y_{L,2}} \left(1 - F_{L,2}(x)\right)^{(N_t-1)} f_{L,2}(x) \left(1 - F_{N,2}(x^{\frac{\alpha_L}{\alpha_N}})\right)^{N_t} & w_l^{\frac{\alpha_N}{\alpha_L}} < x < R. \end{cases} \tag{5.12}$$

Proof: The proof follows a similar approach to that seen in Appendix A.2.

Theorem 5.4. *Given that the reference receiver is associated with an NLOS base station, the PDF of the distance to its serving base station for the case* $w_l^{\frac{\alpha_N}{\alpha_L}} > R$ *is*

$$\overset{(\mathrm{SER})}{f_{N,1}}(x) = \begin{cases} \frac{N_t}{Y_{N,1}} \left(1 - F_{N,1}(x)\right)^{(N_t-1)} f_{N,1}(x) \left(1 - F_{L,1}(x^{\frac{\alpha_N}{\alpha_L}})\right)^{N_t} & 0 < x < w_l^{\frac{\alpha_L}{\alpha_N}} \\ \frac{N_t}{Y_{N,1}} \left(1 - F_{N,1}(x)\right)^{(N_t-1)} f_{N,1}(x) \left(1 - F_{L,2}(x^{\frac{\alpha_N}{\alpha_L}})\right)^{N_t} & w_l^{\frac{\alpha_L}{\alpha_N}} < x < w_l^{\frac{\alpha_L}{\alpha_N}} \\ \frac{N_t}{Y_{N,1}} \left(1 - F_{N,1}(x)\right)^{(N_t-1)} f_{N,1}(x) \left(1 - F_{L,2}(R)\right)^{N_t} & w_l^{\frac{\alpha_L}{\alpha_N}} < x < w_l \\ \frac{N_t}{Y_{N,1}} \left(1 - F_{N,2}(x)\right)^{(N_t-1)} f_{N,2}(x) \left(1 - F_{L,2}(R)\right)^{N_t} & w_l < x < R \end{cases} \tag{5.13}$$

and in the case $w_l^{\frac{\alpha_N}{\alpha_L}} < R$ is

$$\overset{(\mathrm{SER})}{f_{N,2}}(x) = \begin{cases} \frac{N_t}{Y_{N,2}} \left(1 - F_{N,1}(x)\right)^{(N_t-1)} f_{N,1}(x) \left(1 - F_{L,1}(x^{\frac{\alpha_N}{\alpha_L}})\right)^{N_t} & 0 < x < w_l^{\frac{\alpha_L}{\alpha_N}} \\ \frac{N_t}{Y_{N,2}} \left(1 - F_{N,1}(x)\right)^{(N_t-1)} f_{N,1}(x) \left(1 - F_{L,2}(x^{\frac{\alpha_N}{\alpha_L}})\right)^{N_t} & w_l^{\frac{\alpha_L}{\alpha_N}} < x < w_l \\ \frac{N_t}{Y_{N,2}} \left(1 - F_{N,2}(x)\right)^{(N_t-1)} f_{N,2}(x) \left(1 - F_{L,2}(x^{\frac{\alpha_N}{\alpha_L}})\right)^{N_t} & w_l < x < w_l^{\frac{\alpha_L}{\alpha_N}} \\ \frac{N_t}{Y_{N,2}} \left(1 - F_{N,2}(x)\right)^{(N_t-1)} f_{N,2}(x) \left(1 - F_{L,2}(R)\right)^{N_t} & w_l^{\frac{\alpha_L}{\alpha_N}} < x < R. \end{cases} \tag{5.14}$$

Proof: The proof follows a similar approach to that seen in Appendix A.2.

5.2.3 Interfering BSs' Distance Distributions

The interfering BSs can be of different types as shown in Fig. 5.2 and Fig. 5.3, which depends on both serving and interfering BSs' link statuses. Therefore,

the interfering BSs' distance distribution can be written by following the same approach as in Section 4.2.3.

Theorem 5.5. *The PDF of the distance to the interfering BSs from the reference receiver is given by*

$$\overset{(\mathrm{INT})}{f}_{s,u}(y) = \frac{f_{s,k}(y)}{\int_{\mathbb{A}}^{\mathbb{B}} f_{s,k}(q)dq};$$
$$u = \{1,2\}, \mathbb{A} = \{A_{s,1}, A_{s,2}\}, \mathbb{B} = \{B_{s,1}, B_{s,2}\}, k = \{1,2\} \text{ and } s = \{L, N\}. \quad (5.15)$$

where $u = 1$ and $u = 2$ corresponds to the cases $w_l^{\frac{\alpha_N}{\alpha_L}} > R$ and $w_l^{\frac{\alpha_N}{\alpha_L}} < R$, respectively. Also, s refers to the interferers type as LOS or NLOS. The interferers distance from the reference receiver can be in different distance ranges as given in Tables 5.1, 5.2, 5.3 and 5.4. Furthermore the symbols (") and (—) indicates the value above to be repeated, and a blank cell, respectively.

Proof: The proof follows a similar approach to that seen in Appendix A.3.

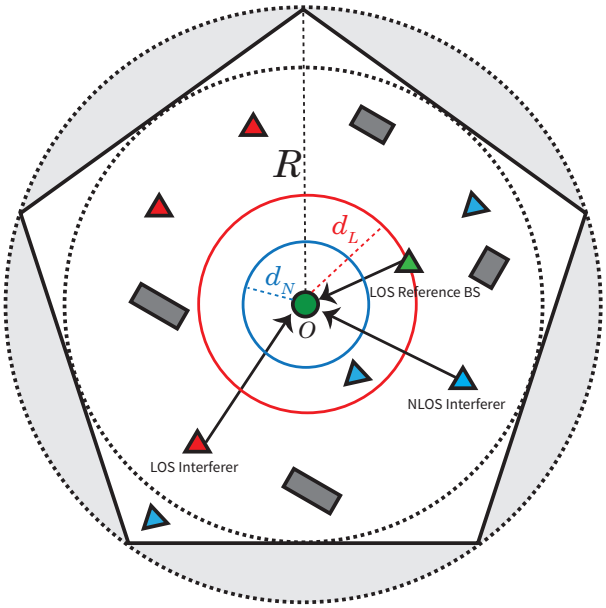

FIGURE 5.2: Given that the reference UE at the origin is served by an LOS BS with distance x to the user in an L-sided regular convex polygon. Then the LOS and the NLOS interfering BSs will be $d_L = x$ and $d_N = x^{\frac{\alpha_L}{\alpha_N}}$ away from the reference UE, respectively.

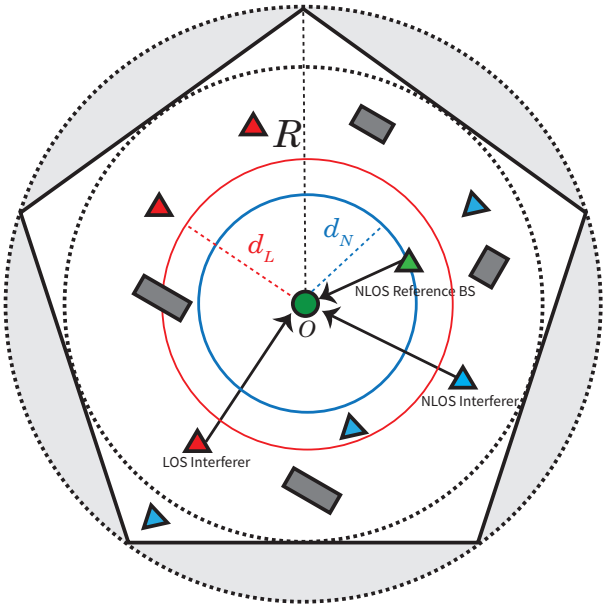

FIGURE 5.3: Given that the reference UE at the origin is served by an NLOS BS with distance x to the user in an L-sided regular convex polygon. Then the LOS and the NLOS interfering BSs will be $d_L = x^{\frac{\alpha_N}{\alpha_L}}$ and $d_N = x$ away from the reference UE, respectively.

TABLE 5.1: Conditioned on serving BS being LOS for the case $w_l^{\frac{\alpha_N}{\alpha_L}} > R$

	LOS interferers		**NLOS interferers**	
	$\mathrm{A}_{L,1} < y < B_{L,1}$	$\mathrm{A}_{L,2} < y < B_{L,2}$	$\mathrm{A}_{N,1} < y < B_{N,1}$	$\mathrm{A}_{N,2} < y < B_{N,2}$
$0 < x < w_l$	$f_{L,1}(y),\ A_{L,1} = x,\ B_{L,1} = w_l$	$f_{L,2}(y),\ A_{L,2} = w_l,\ B_{L,2} = R$	$f_{N,1}(y),\ A_{N,1} = x^{\frac{\alpha_L}{\alpha_N}},\ B_{N,1} = w_l$	$f_{N,2}(y),\ A_{N,2} = w_l,\ B_{N,2} = R$
$w_l < x < R$	$f_{L,2}(y),\ A_{L,1} = x,\ B_{L,1} = R$	—	"	"

TABLE 5.2: Conditioned on serving BS being NLOS for the case $w_l^{\frac{\alpha_N}{\alpha_L}} > R$

	LOS interferers		**NLOS interferers**	
	$\mathrm{A}_{L,1} < y < B_{L,1}$	$\mathrm{A}_{L,2} < y < B_{L,2}$	$\mathrm{A}_{N,1} < y < B_{N,1}$	$\mathrm{A}_{N,2} < y < B_{N,2}$
$0 < x < w_l^{\frac{\alpha_L}{\alpha_N}}$	$f_{L,1}(y),\ A_{L,1} = x^{\frac{\alpha_N}{\alpha_L}},\ B_{L,1} = w_l$	$f_{L,2}(y),\ A_{L,2} = w_l,\ B_{L,2} = R$	$f_{N,1}(y),\ A_{N,1} = x,\ B_{N,1} = w_l$	$f_{N,2}(y),\ A_{N,2} = w_l,\ B_{N,2} = R$
$w_l^{\frac{\alpha_L}{\alpha_N}} < x < R^{\frac{\alpha_L}{\alpha_N}}$	$f_{L,2}(y),\ A_{L,1} = x^{\frac{\alpha_N}{\alpha_L}},\ B_{L,1} = R$	—	"	"
$R^{\frac{\alpha_L}{\alpha_N}} < x < w_l$	$f_{L,2}R,\ A_{L,1} = x^{\frac{\alpha_N}{\alpha_L}},\ B_{L,1} = R$	—	"	"
$w_l < x < R$	"	—	$f_{N,2}(y),\ A_{N,1} = x,\ B_{N,1} = R$	—

TABLE 5.3: Conditioned on serving BS being LOS for the case $w_l^{\frac{\alpha_N}{\alpha_L}} < R$

	LOS interferers		**NLOS interferers**	
	$\mathrm{A}_{L,1} < y < B_{L,1}$	$\mathrm{A}_{L,2} < y < B_{L,2}$	$\mathrm{A}_{N,1} < y < B_{N,1}$	$\mathrm{A}_{N,2} < y < B_{N,2}$
$0 < x < w_l$	$f_{L,1}(y),\ A_{L,1} = x,\ B_{L,1} = w_l$	$f_{L,2}(y),\ A_{L,2} = w_l,\ B_{L,2} = R$	$f_{N,1}(y),\ A_{N,1} = x^{\frac{\alpha_L}{\alpha_N}},\ B_{N,1} = w_l$	$f_{N,2}(y),\ A_{N,2} = w_l,\ B_{N,2} = R$
$w_l < x < w_l^{\frac{\alpha_N}{\alpha_L}}$	$f_{L,2}(y),\ A_{L,1} = x,\ B_{L,1} = R$	—	"	"
$w_l^{\frac{\alpha_N}{\alpha_L}} < x < R$	"	—	$f_{N,2}(y),\ A_{N,1} = x^{\frac{\alpha_L}{\alpha_N}},\ B_{N,1} = R$	—

TABLE 5.4: Conditioned on serving BS being NLOS for the case $w_l^{\frac{\alpha_N}{\alpha_L}} < R$

	LOS interferers		**NLOS interferers**	
	$\mathrm{A}_{L,1} < y < B_{L,1}$	$\mathrm{A}_{L,2} < y < B_{L,2}$	$\mathrm{A}_{N,1} < y < B_{N,1}$	$\mathrm{A}_{N,2} < y < B_{N,2}$
$0 < x < w_l^{\frac{\alpha_L}{\alpha_N}}$	$f_{L,1}(y),\ A_{L,1} = x^{\frac{\alpha_N}{\alpha_L}},\ B_{L,1} = w_l$	$f_{L,2}(y),\ A_{L,2} = w_l,\ B_{L,2} = R$	$f_{N,1}(y),\ A_{N,1} = x,\ B_{N,1} = w_l$	$f_{N,2}(y),\ A_{N,2} = w_l,\ B_{N,2} = R$
$w_l^{\frac{\alpha_L}{\alpha_N}} < x < w_l$	$f_{L,2}(y),\ A_{L,1} = x^{\frac{\alpha_N}{\alpha_L}},\ B_{L,1} = R$	—	"	"
$w_l < x < R^{\frac{\alpha_L}{\alpha_N}}$	"	—	$f_{N,2}(y),\ A_{N,1} = x,\ B_{N,1} = R$	—
$R^{\frac{\alpha_L}{\alpha_N}} < x < R$	$f_{L,2}R,\ A_{L,1} = x^{\frac{\alpha_N}{\alpha_L}},\ B_{L,1} = R$	—	"	—

5.2.4 Coverage Probability

In this section, using the above defined association probabilities and the distance distributions the coverage probability of a central receiver in an L-sided polygon can defined as

$$\overset{(\mathrm{u})}{\mathbb{P}}_c(\tau) = Y_{L,u}\overset{(\mathrm{u})}{\mathbb{P}}_{c,L}(\tau) + Y_{N,u}\overset{(\mathrm{u})}{\mathbb{P}}_{c,N}(\tau);\ u = \{1,2\}, \tag{5.16}$$

where $u = 1$ and $u = 2$ corresponds to the cases $w_l^{\frac{\alpha_N}{\alpha_L}} > R$ and $w_l^{\frac{\alpha_N}{\alpha_L}} < R$, respectively. The LOS and NLOS conditional coverage probabilities $\overset{(\mathrm{u})}{\mathbb{P}}_{c,L}(\tau)$ and $\overset{(\mathrm{u})}{\mathbb{P}}_{c,N}(\tau)$ can be written as

$$\overset{(\mathrm{u})}{\mathbb{P}}_{c,L}(\tau) = \int_0^R \sum_{n=1}^{\beta_L} (-1)^{n+1}\binom{\beta_L}{n} exp\left(\frac{-n\eta_L\tau x^{\alpha_L}\sigma^2}{p_t N}\right) \overset{(u)}{\mathcal{L}}_{I|L}\left(\frac{n\eta_L\tau x^{\alpha_L}}{p_t N}\right) \overset{(\mathrm{SER})}{f}_{L,u}(x)dx \tag{5.17}$$

and

$$\overset{(\mathrm{u})}{\mathbb{P}}_{c,N}(\tau) = \int_0^R \sum_{n=1}^{\beta_N} (-1)^{n+1}\binom{\beta_N}{n} exp\left(\frac{-n\eta_N\tau x^{\alpha_N}\sigma^2}{p_t N}\right) \overset{(u)}{\mathcal{L}}_{I|N}\left(\frac{n\eta_N\tau x^{\alpha_N}}{p_t N}\right) \overset{(\mathrm{SER})}{f}_{N,u}(x)dx \tag{5.18}$$

where $\eta_L = \beta_L(\beta_L!)^{(\frac{-1}{\beta_L})}$ and $\eta_N = \beta_N(\beta_N!)^{(\frac{-1}{\beta_N})}$. The Laplace transform of interference $\overset{(u)}{\mathcal{L}}_{I|s}(.)$ is defined in the following theorem.

Theorem 5.6. *The Laplace transform of interference* $\overset{(u)}{\mathcal{L}}_{I|s}(.)$ *can be written as*

$$\overset{(u)}{\mathcal{L}}_{I|s}\left(\frac{n\eta_s\tau x^{\alpha_s}}{p_t N}\right) =$$

$$\frac{1}{\int_{A_{L,1}}^{B_{L,1}} f_{L,k}(q)dq + \int_{A_{L,2}}^{B_{L,2}} f_{L,k}(q)dq + \int_{A_{N,1}}^{B_{N,1}} f_{N,k}(q)dq + \int_{A_{N,2}}^{B_{N,2}} f_{N,k}(q)dq} \times$$

$$\left(\int_{A_{L,1}}^{B_{L,1}} \frac{1}{\left(1+\frac{n\eta_s\tau x^{\alpha_s} y^{-\alpha_L} p_t \mathbb{E}_{G_i}[(G_i)]}{p_t N \beta_L}\right)^{\beta_L}} f_{L,k}(y)dy + \right.$$

$$\int_{A_{L,2}}^{B_{L,2}} \frac{1}{\left(1+\frac{n\eta_s\tau x^{\alpha_s} y^{-\alpha_L} p_t \mathbb{E}_{G_i}[(G_i)]}{p_t N \beta_L}\right)^{\beta_L}} f_{L,k}(y)dy$$

$$+ \int_{A_{N,1}}^{B_{N,1}} \frac{1}{\left(1+\frac{n\eta_s\tau x^{\alpha_s} y^{-\alpha_N} p_t \mathbb{E}_{G_i}[(G_i)]}{p_t N \beta_N}\right)^{\beta_N}} f_{N,k}(y)dy +$$

$$\left. \int_{A_{N,2}}^{B_{N,2}} \frac{1}{\left(1+\frac{n\eta_s\tau x^{\alpha_s} y^{-\alpha_N} p_t \mathbb{E}_{G_i}[(G_i)]}{p_t N \beta_N}\right)^{\beta_N}} f_{N,k}(y)dy \right)^{N_t-1};$$

$$u = \{1,2\}, k = \{1,2\} \text{ and } s = \{L,N\}, \quad (5.19)$$

where u and s refers the above defined cases and link status conditions, respectively. Also the corresponding values of $A_{L,1}, A_{L,2}, A_{N,1}, A_{N,2}, B_{L,1}, B_{L,2}, B_{N,1}, B_{N,2}$ and k, given in Tables 5.1, 5.2, 5.3 and 5.4. The expectation of the antenna gain is given as

$$\mathbb{E}_{G_i}[(G_i)] = 1 + \frac{1}{N}\sum_{k=1}^{\frac{N}{2}-1} G_k \quad (5.20)$$

where proof is given in (4.31).

Proof: Proof of Theorem 5.6 follows on the same lines as that in Appendix A.4. Hence, skipped in this section.

5.3 Results and Discussions

This section presents the numerical results of the proposed analytical model given in Section 5.2. We kept the parameters consistent as similar is Chapter 4. In this section mainly, we produce the results similar as in Chapter 4 given that in Chapter 4 the analysis is a for disk region, whereas in this chapter the analysis is for a regular convex polygon. All BSs are assumed to be operating at 28 GHz with 100 MHz bandwidth. Nakagami fading parameters and the path loss exponents of LOS and NLOS links are set to $\alpha_L = 2$, $\alpha_N = 4$, $\beta_L = 3$ and $\beta_N = 2$. Transmit power of all BSs is set to 25 dBm. Number of BSs, array antenna elements, and the blockage parameter are considered as $N_t = 50$, $N = 32$, and $\omega = \frac{1}{140}$. Also, the analytical model's accuracy has been validated through Monte Carlo simulations by averaging over 10,000 realisations. The simulation environment has been modelled as similar in Chapter 4.

Fig. 5.4 shows the performance comparison between the analytical model presented in Section 5.2 and the Monte Carlo simulation result considering the multi-cosine antenna model. It validates the accuracy of the proposed analytical model considering a regular L-sided convex polygon with a number of sides equal to five $L = 5$.

Fig. 5.5 compares the SINR coverage probability of polygons with a different number of sides. The comparison also includes the SINR coverage probability in a disk region (this is equivalent to considering the number of sides of the polygon as infinity, i.e., $L \to \infty$). The result shows a negligible performance difference between the polygons of different sides and the disk region. Therefore, we may assume the finite region to be a disk region, enabling more tractable results than an arbitrary shape.

In Figs. 5.6 and 5.7, the SINR coverage probability as a function of the blockage parameter, and the number of BSs have been presented, respectively. The results show a similar trend to that seen Chapter 4, where both the blockage parameter ω and the BS count N_t have an optimum value to provide the best coverage

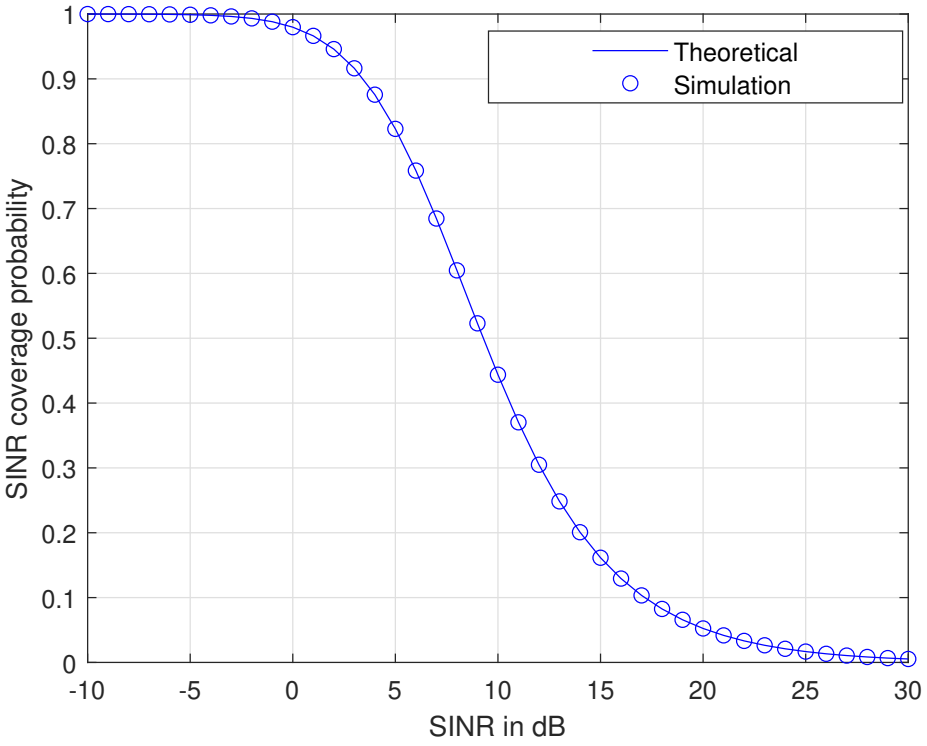

FIGURE 5.4: SINR coverage probability of a reference receiver in an L-sided regular convex polygon.

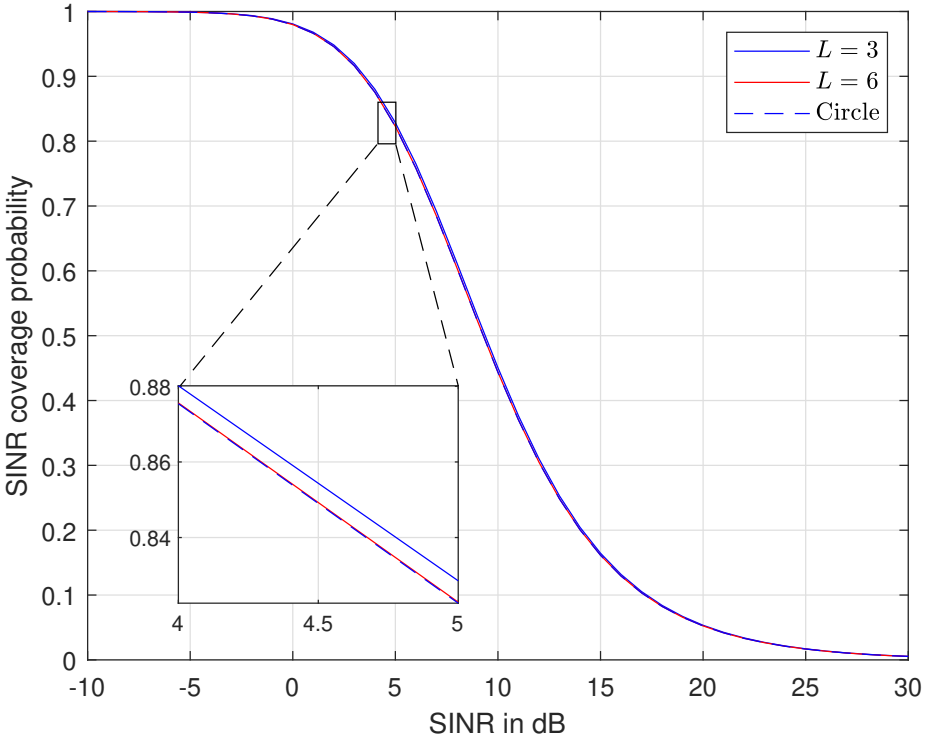

FIGURE 5.5: SINR coverage probability of polygons with different number of sides L.

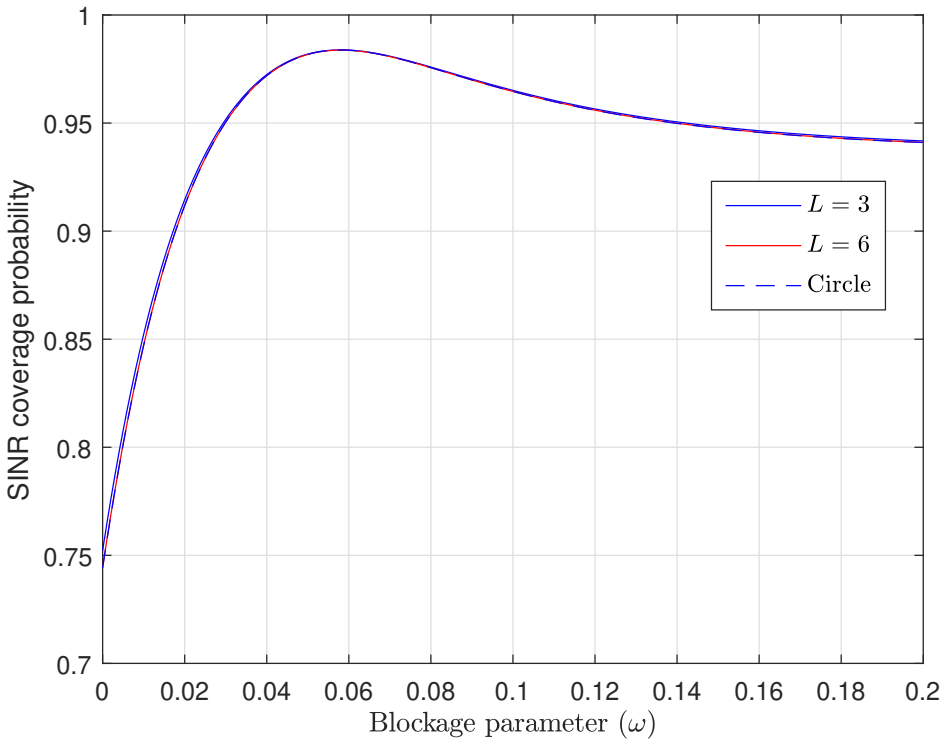

FIGURE 5.6: SINR coverage probability of a reference receiver as a function of blockage parameter for polygons with different number of sides.

probability. Also, the figures also compare the performance against a disk region, which again confirms the negligible performance gap between the polygons and the disk region.

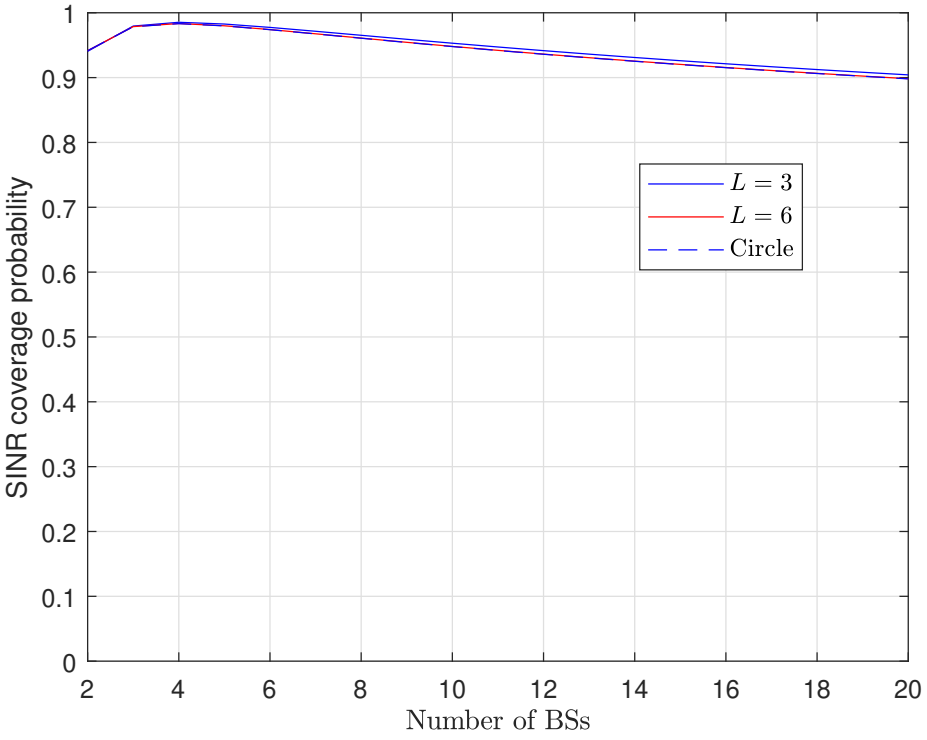

FIGURE 5.7: SINR coverage probability of a reference receiver as a function of number of BSs for polygons with different number of sides.

5.4 Conclusions

This chapter presented the SINR coverage probability performance analysis for a more generalised arbitrary polygonal region. As similar in Chapter 4, the results were produced to analyse the impact of blockage parameter and the BS count. This chapter presents an important conclusion that the performance gap between the polygon and the disk region is almost negligible for a user located at the centre of the network. Therefore, a mmWave cellular network's performance analysis in a disk region may be an acceptable model to represent the performance analysis of a centrally located user in a more general finite region. With this conclusion, in the next chapter, a disk region has been considered to analyse the uplink performance of a finite mmWave cellular network.

Chapter 6

Uplink Coverage Analysis on a Disk Region

Having analysed the downlink coverage analysis, next in this chapter, we focus on the uplink coverage analysis of an outdoor mmWave cellular network. As similar in previous chapters 4 and 5, by considering the unique features of mmWave communications such as different channel characteristics for the LOS and the NLOS links and high directional antenna gains provided by antenna arrays, we have developed a stochastic geometry framework to analyse the uplink coverage probability for a reference receiver. Furthermore, the fractional power control (FPC) has been applied to the UE in the system modelling process.

Unlike the downlink case, the uplink coverage analysis has additional challenges that need to be addressed. Firstly, the interference field in uplink communications is more challenging than that in downlink communications. In the downlink model, once a user chooses its serving base station based on the highest path gain. Then there is a definite exclusive region defined by the serving BS, whereas the BSs outside this region will become the interfering BSs. In uplink communications defining such exclusive regions are more challenging. For example, in an uplink model, given that a BS chooses a user randomly, then an interfering user can be closer to the BS than the user of interest. Secondly, a common modelling

assumption in previous studies based on the PPP is to assume a single uplink active user per BS in a given resource channel, and then the PPP is thinned[1] to form a new PPP [18].

The PPP is defined as a number of points distributed randomly and independently in an infinite region. Given that only a single user is scheduled per BS in a resource channel, this thinning is not independent. This causes complications in the uplink analysis. By addressing these additional challenges, we are able to provide stochastic geometry frameworks to analyse the uplink performance of cellular systems. Finally, the impact of antenna array size, blockage parameter, BS count, network area and the FPC factor has been investigated with the proposed system model.

The rest of the chapter is organised as follows. Section 6.1 describes the system model; this includes the network model, blockage and channel model, selection strategy, antenna model, user fractional power control and the performance metric. Section 6.2 presents the main technical derivations of this chapter. It also presents the analytical results from the coverage probability analyses. Section 6.3 presents the numerical and simulation results. Finally, Section 6.4 concludes the chapter.

6.1 System Model

In this section, we introduce the system model for evaluating the performance of uplink mmWave cellular networks.

6.1.1 Network Model

This chapter focuses on uplink performance analysis of an outdoor mmWave cellular network in a 2-dimensional finite disk region $\mathcal{A}$ with radius R, as shown in Fig. 6.1. It is assumed that BSs and UEs are distributed according to a uniform BPP Φ_b and Φ_u, respectively. Although cellular systems operate across many

[1]Thinning refers to a process when some points are removed [71].

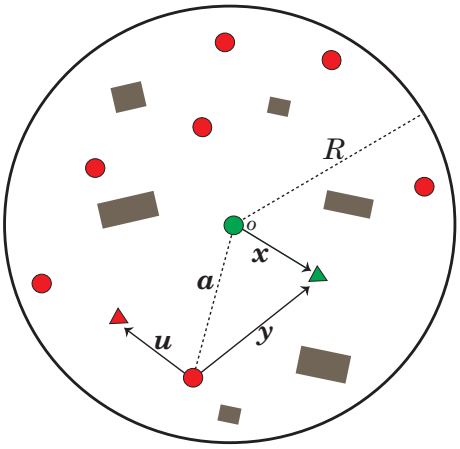

FIGURE 6.1: Finite disk region. The green circle and the triangle are the reference UE and reference BS, respectively. The red circle and the triangle are the interfering UE and its tagged BS, respectively. The grey rectangles are the random blockages.

channels, co-channel interference analysis is conducted for a single channel, recognising that other channels will be interfered in a similar way. Hence, in the analysis it is assumed that each BS has a single active uplink UE, which is scheduled using a round-robin scheduler. Hence, the UEs distribution Φ_u is thinned to get Φ_{ua}, which denotes the distribution of the active UEs. In harmony with [18, 72], it is assumed that active UEs also form a BPP even after associating with one UE per BS. Furthermore, the number of active UEs will be equal to the number of BSs N_t, since each BS serves a single UE. In our analysis, it is assumed that the reference UE at the origin $\boldsymbol{O}$ is connected to its tagged BS located at $\boldsymbol{X}$, this tagged BS will be referred as the reference BS. The interfering UEs are assumed to be located at $\boldsymbol{Y}$ with distance $y = ||\boldsymbol{Y} - \boldsymbol{X}||$ to the reference BS and with distance $a = ||\boldsymbol{Y} - \boldsymbol{O}||$ from the origin. Distance u is the distance of an interfering UE to its tagged BS.

6.1.2 Blockage and Channel Model

Blockage and channel model as similar in Section 4.1.2 has been considered. According to this model a UE can be LOS with probability $p(r) = e^{-\omega r}$ or NLOS with probability $1 - p(r)$ to its associated BS. Here r is the distance between the UE

and its associated BS and ω is referred to as the blockage parameter determined by the density and the average size of the buildings. Once the reference UE at the origin is connected to its reference BS, the set of interfering UEs can be divided into two sets as LOS interferers and NLOS interferers. Also, we assume a simple distance-dependent power law path loss $l = x^{\alpha}$, with different path loss exponents α_L and α_N for LOS and NLOS links, respectively. Furthermore, to compensate for the multi-path effects, the Nakagami fading has been considered with different Nakagami parameters for LOS and NLOS links, β_L and β_N, respectively.

6.1.3 Selection Strategy

It is assumed that a UE is served by a BS with the smallest path loss considering both the LOS and NLOS BS sets. This also means that a UE will be connected to the nearest LOS or NLOS BS.

6.1.4 Antenna Model

The antenna model is assumed as similar in Section 4.1.4.

6.1.5 User Fractional Power Control

It is assumed that UEs utilises a distance-proportional FPC in the uplink transmission. By employing the FPC method, the dynamic transmit power for the UE is set as [18]

$$p_u = x^{\alpha\epsilon} \tag{6.1}$$

where x is the distance between the UE and its tagged BS, α is the path loss exponent and $\epsilon \in [0,1]$ is the power control factor. When $\epsilon = 0$, FPC reduces to the fixed power control scheme and all the UEs transmit with the same power. In

contrast, when $\epsilon = 1$ the FPC becomes the power control scheme with complete channel inversion. Therefore with the FPC scheme, as a UE moves closer to the BS, the transmit power of the UE decreases. This is an important consideration for power limited battery-operated devices such as mobile phones.

6.1.6 Performance Metric

This chapter focuses on the uplink transmission of a reference receiver at the origin. With the above-defined system parameters, the Signal-to-Interference-plus-Noise-Ratio (SINR) received by the reference BS at distance x from the reference receiver can be written as

$$\text{SINR} = \frac{x^{-\alpha} h_{\boldsymbol{O}} x^{\alpha\epsilon} G_{\text{mcos}}(\varphi_{\boldsymbol{O}})}{(\sigma^2 + I)} \tag{6.2}$$

$$I = \sum_{\boldsymbol{Y} \in \Phi_{ua} \setminus \boldsymbol{O}} h_{\boldsymbol{Y}} u^{\alpha\epsilon} G_{\text{mcos}}(\varphi_{\boldsymbol{Y}}) y^{-\alpha} \tag{6.3}$$

where I is the total interference from all interfering UEs except the reference UE at $\boldsymbol{O}$. The parameters $h_{\boldsymbol{O}}$ and $h_{\boldsymbol{Y}}$ are the fading gains of the desired and interfering signals representing random channel effects, $G_{\text{mcos}}(\varphi_{\boldsymbol{O}}) = N$ and $G_{\text{mcos}}(\varphi_{\boldsymbol{Y}})$ are the antenna gains of the desired and interfering signals, ϵ is the FPC factor and σ^2 is the thermal noise power.

6.2 Coverage Analysis

This section presents the probability of coverage for the proposed millimetre wave cellular network in Section 6.1. To compute the coverage probability, the following intermediate definitions should be derived: (i) association probabilities; (ii) distributions of the distance between a UE and its tagged BS; (iii) interfering UEs' distance distributions, and (iv) the Laplace transform of interference.

6.2.1 Association Probabilities

As specified in Section 6.1.3 each UE will be associated with either the nearest LOS or NLOS BS. We have already derived the association probabilities in a disk region in Chapter 4. Therefore it can be used here directly for the uplink coverage analysis.

The association probabilities can be written as defined in Section 4.2.1.

LOS Association Probability: *The probability that a UE is associated with a LOS base station in the case* $(R-a)^{\frac{\alpha_N}{\alpha_L}} > R+a$ *is*

$$Y_{L,1} = N_t\Bigg(\int_0^{R-a} \Big(1 - F_{N,1}(u^{\frac{\alpha_L}{\alpha_N}})\Big)^{N_t} (1 - F_{L,1}(u))^{(N_t-1)} f_{L,1}(u)du + \int_{R-a}^{R+a} \Big(1 - F_{N,1}(u^{\frac{\alpha_L}{\alpha_N}})\Big)^{N_t} (1 - F_{L,2}(u))^{(N_t-1)} f_{L,2}(u)du \Bigg) \tag{6.4}$$

and in the case $(R-a)^{\frac{\alpha_N}{\alpha_L}} < R+a$ is

$$\begin{aligned} Y_{L,2} = N_t\Bigg(&\int_0^{R-a} \Big(1 - F_{N,1}(u^{\frac{\alpha_L}{\alpha_N}})\Big)^{N_t} (1 - F_{L,1}(u))^{(N_t-1)} f_{L,1}(u)du + \\ &\int_{R-a}^{(R-a)^{\frac{\alpha_N}{\alpha_L}}} \Big(1 - F_{N,1}(u^{\frac{\alpha_L}{\alpha_N}})\Big)^{N_t} (1 - F_{L,2}(u))^{(N_t-1)} f_{L,2}(u)du + \\ &\int_{(R-a)^{\frac{\alpha_N}{\alpha_L}}}^{R+a} \Big(1 - F_{N,2}(u^{\frac{\alpha_L}{\alpha_N}})\Big)^{N_t} (1 - F_{L,2}(u))^{(N_t-1)} f_{L,2}(u)du \Bigg). \end{aligned} \tag{6.5}$$

NLOS Association Probability: *The probability that a UE is associated with an NLOS base station in the case* $(R-a)^{\frac{\alpha_N}{\alpha_L}} > R+a$ *is*

$$Y_{N,1} = 1 - Y_{L,1} \tag{6.6}$$

and in the case $(R-a)^{\frac{\alpha_N}{\alpha_L}} < R+a$ is

$$Y_{N,2} = 1 - Y_{L,2}. \tag{6.7}$$

6.2.2 Distance Distributions between a UE and its Tagged BS

This section presents the distance distributions between a UE and its tagged BS at distance u, conditioned on the link status between the UE and its tagged BS. Here we assume a UE can be anywhere in the given finite disk region with distance a from the centre of the disk. Note that the distance u is identically distributed but not independent in general, this is due to having one user per BS, it is shown in [44], that this dependency is weak. Therefore the PDF of the distance distributions of u is derived with the assumption that the distance u is independent and identically distributed. The distance distributions between a UE and its tagged BS have been provided in Section 4.2.2. We directly use those theorems in this section to analyse the uplink coverage probability.

LOS Distance Distributions: *The PDF of distance between a LOS UE and its tagged BS in the case* $(R-a)^{\frac{\alpha_N}{\alpha_L}} > R + a$ *is given by*

$$\overset{(\mathrm{SER})}{f}_{L,1}(u) = \begin{cases} \frac{N_t}{Y_{L,1}} \left(1 - F_{L,1}(u)\right)^{(N_t-1)} f_{L,1}(u) \left(1 - F_{N,1}(u^{\frac{\alpha_L}{\alpha_N}})\right)^{N_t} & 0 < u < R - a \\ \frac{N_t}{Y_{L,1}} \left(1 - F_{L,2}(u)\right)^{(N_t-1)} f_{L,2}(u) \left(1 - F_{N,1}(u^{\frac{\alpha_L}{\alpha_N}})\right)^{N_t} & R - a < u < R + a \end{cases} \tag{6.8}$$

and in the case $(R-a)^{\frac{\alpha_N}{\alpha_L}} < R + a$ is

$$
\overset{(\mathrm{SER})}{f}_{L,2}(u) =
$$

$$
\begin{cases}
\frac{N_t}{Y_{L,2}} \left(1 - F_{L,1}(u)\right)^{(N_t-1)} f_{L,1}(u) \left(1 - F_{N,1}(u^{\frac{\alpha_L}{\alpha_N}})\right)^{N_t} & 0 < u < R - a \\
\frac{N_t}{Y_{L,2}} \left(1 - F_{L,2}(u)\right)^{(N_t-1)} f_{L,2}(u) \left(1 - F_{N,1}(u^{\frac{\alpha_L}{\alpha_N}})\right)^{N_t} & R - a < u < (R-a)^{\frac{\alpha_N}{\alpha_L}} \\
\frac{N_t}{Y_{L,2}} \left(1 - F_{L,2}(u)\right)^{(N_t-1)} f_{L,2}(u) \left(1 - F_{N,2}(u^{\frac{\alpha_L}{\alpha_N}})\right)^{N_t} & (R-a)^{\frac{\alpha_N}{\alpha_L}} < u < R + a.
\end{cases}
\tag{6.9}
$$

NLOS Distance Distributions: *The PDF of distance between an NLOS UE and its tagged BS in the case* $(R-a)^{\frac{\alpha_N}{\alpha_L}} > R + a$ *is given by*

$$
\overset{(\mathrm{SER})}{f}_{N,1}(u) =
$$

$$
\begin{cases}
\frac{N_t}{Y_{N,1}} \left(1 - F_{N,1}(u)\right)^{(N_t-1)} f_{N,1}(u) \left(1 - F_{L,1}(u^{\frac{\alpha_N}{\alpha_L}})\right)^{N_t} & \\
\qquad\qquad 0 < u < (R-a)^{\frac{\alpha_L}{\alpha_N}} & \\
\frac{N_t}{Y_{N,1}} \left(1 - F_{N,1}(u)\right)^{(N_t-1)} f_{N,1}(u) \left(1 - F_{L,2}(u^{\frac{\alpha_N}{\alpha_L}})\right)^{N_t} & \\
\qquad\qquad (R-a)^{\frac{\alpha_L}{\alpha_N}} < u < (R+a)^{\frac{\alpha_L}{\alpha_N}} & \\
\frac{N_t}{Y_{N,1}} \left(1 - F_{N,1}(u)\right)^{(N_t-1)} f_{N,1}(u) \left(1 - F_{L,2}(R+a)\right)^{N_t} & \\
\qquad\qquad (R+a)^{\frac{\alpha_L}{\alpha_N}} < u < R - a & \\
\frac{N_t}{Y_{N,1}} \left(1 - F_{N,2}(u)\right)^{(N_t-1)} f_{N,2}(u) \left(1 - F_{L,2}(R+a)\right)^{N_t} & \\
\qquad\qquad R - a < u < R + a &
\end{cases}
\tag{6.10}
$$

and in the case $(R-a)^{\frac{\alpha_N}{\alpha_L}} < R + a$ is

$$
\overset{(\mathrm{SER})}{f}_{N,2}(u) =
$$

$$
\begin{cases}
\frac{N_t}{Y_{N,2}} \left(1 - F_{N,1}(u)\right)^{(N_t-1)} f_{N,1}(u) \left(1 - F_{L,1}(u^{\frac{\alpha_N}{\alpha_L}})\right)^{N_t} & 0 < u < (R-a)^{\frac{\alpha_L}{\alpha_N}} \\
\frac{N_t}{Y_{N,2}} \left(1 - F_{N,1}(u)\right)^{(N_t-1)} f_{N,1}(u) \left(1 - F_{L,2}(u^{\frac{\alpha_N}{\alpha_L}})\right)^{N_t} & (R-a)^{\frac{\alpha_L}{\alpha_N}} < u < R-a \\
\frac{N_t}{Y_{N,2}} \left(1 - F_{N,2}(u)\right)^{(N_t-1)} f_{N,2}(u) \left(1 - F_{L,2}(u^{\frac{\alpha_N}{\alpha_L}})\right)^{N_t} & R-a < u < (R+a)^{\frac{\alpha_L}{\alpha_N}} \\
\frac{N_t}{Y_{N,2}} \left(1 - F_{N,2}(u)\right)^{(N_t-1)} f_{N,2}(u) \left(1 - F_{L,2}(R+a)\right)^{N_t} & (R+a)^{\frac{\alpha_L}{\alpha_N}} < u < R+a.
\end{cases}
\tag{6.11}
$$

6.2.3 Interfering UEs' Distance Distributions

Interfering UEs can be partitioned into four major categories, namely (i) LOS interfering UEs given that the reference BS is connected to a LOS reference UE, (ii) NLOS interfering UEs given that the reference BS is connected to a LOS reference UE, (iii) LOS interfering UEs given that the reference BS is connected to an NLOS reference UE and (iv) NLOS interfering UEs given that the reference BS is connected to an NLOS reference UE. Furthermore, each of these categories can be divided into two further divisions depending on the interfering UE's link to its tagged BS. Fig. 6.2 and (6.3) show these different interfering UE categories. As similar in [44, 46], we have included LOS and NLOS exclusive regions around the reference BS, which ensures no LOS and NLOS interferers in these regions, respectively. Therefore the distance distributions of the interfering UEs depend on both the link statuses of the reference UE and the interfering UEs. Hence, the distance distributions of the interfering UEs can be written as follows.

Theorem 6.1. *Given that the reference BS is associated with a LOS UE, the PDF of the distance to its LOS interfering UEs is given by*

$$
f_{L|L}(y) = \frac{f_{\text{int}}(y)p(y)}{\int_x^{R+x} f_{\text{int}}(q)p(q)dq} \tag{6.12}
$$

and the PDF of the distance to its NLOS interfering UEs is given by

$$f_{N|L}(y) = \frac{f_{\text{int}}(y)(1-p(y))}{\int_{x\frac{\alpha_L}{\alpha_N}}^{R+x} f_{\text{int}}(q)(1-p(q))dq}. \tag{6.13}$$

Proof: See Appendix B.1.

Theorem 6.2. *Given that the reference BS is associated with an NLOS UE, the PDF of the distance to its LOS interfering UEs is given by*

$$f_{L|N}(y) = \frac{f_{\text{int}}(y)p(y)}{\int_{x\frac{\alpha_N}{\alpha_L}}^{R+x} f_{\text{int}}(q)p(q)dq} \tag{6.14}$$

and the PDF of the distance to its NLOS interfering UEs is given by

$$f_{N|N}(y) = \frac{f_{\text{int}}(y)(1-p(y))}{\int_{x}^{R+x} f_{\text{int}}(q)(1-p(q))dq}. \tag{6.15}$$

Proof: Proof follows similar approach as Appendix B.1.

In Theorems 6.26 and 6.2 the distance distributions between two random nodes in a circle $f_{\text{int}}(.)$ is given by [73], equation 42.

$$f_{\text{int}}(y) = \frac{4y}{\pi R^2}\left(\arccos\left(\frac{y}{2R}\right) - \frac{y}{2R}\sqrt{1-\left(\frac{y}{2R}\right)^2}\right). \tag{6.16}$$

With these defined interfering UEs distance distributions, the Laplace transform of interference can be defined.

6.2.4 Laplace Transform of Interference

Laplace transform of the aggregate interference conditioned on the link status (either LOS or NLOS) between the reference BS and the reference UE can be written as in the following theorem.

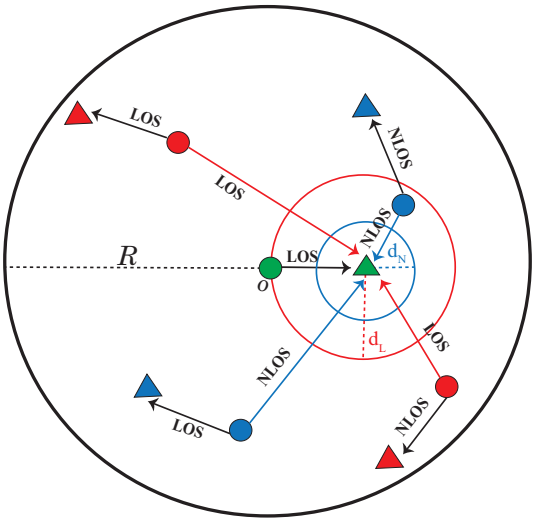

FIGURE 6.2: Interfering UEs distribution conditioned on LOS link between reference UE (green circle) and reference BS (green triangle). It can be observed that LOS interferes in red are distance $\mathrm{d}_L = x$ away from the reference BS and the NLOS interferes in blue are distance $\mathrm{d}_N = x^{\frac{\alpha_L}{\alpha_N}}$ away from the reference BS. Also, LOS and NLOS interferers can be further categorised based on their tagged BS.

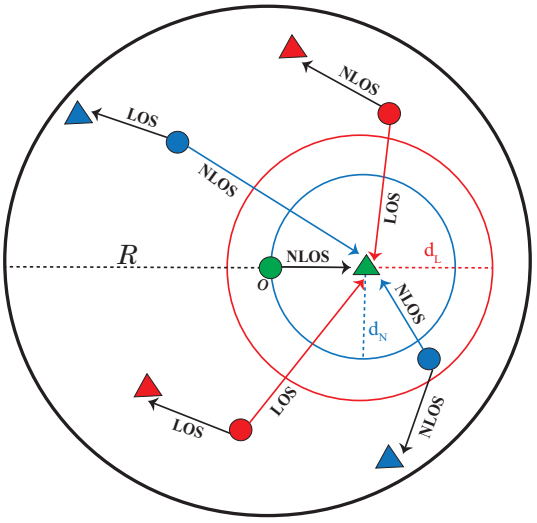

FIGURE 6.3: Interfering UEs distribution conditioned on NLOS link between reference UE (green circle) and reference BS (green triangle). It can be observed that LOS interferes in red are distance $\mathrm{d}_L = x^{\frac{\alpha_N}{\alpha_L}}$ away from the reference BS and the NLOS interferes in blue are distance $\mathrm{d}_N = x$ away from the reference BS. Also, LOS and NLOS interferers can be further categorised based on their tagged BS.

Theorem 6.3. *Given that the reference BS is connected with a reference LOS UE or NLOS UE, the Laplace transform of the total LOS interference $\mathcal{L}_{I|L}(.)$ and the total NLOS interference $\mathcal{L}_{I|N}(.)$ can be written as*

$$\mathcal{L}_{I|L}\left(\frac{n\eta_L\tau}{N}\right) = \left(\frac{1}{\int_x^{R+x} f_{\text{int}}(u)p(u)du + \int_{x^{\frac{\alpha_L}{\alpha_N}}}^{R+x} f_{\text{int}}(u)(1-p(u))du}\left(\int_x^{R+x} (\overset{(L)}{\mathcal{F}}_{LL} + \overset{(L)}{\mathcal{F}}_{LN}) f_{\text{int}}(y)p(y)dy + \int_{x^{\frac{\alpha_L}{\alpha_N}}}^{R+x} (\overset{(L)}{\mathcal{F}}_{NL} + \overset{(L)}{\mathcal{F}}_{NN}) f_{\text{int}}(y)(1-p(y))dy\right)\right)^{N_t-1}, \quad (6.17)$$

and

$$\mathcal{L}_{I|N}\left(\frac{n\eta_N\tau}{N}\right) = \left(\frac{1}{\int_{x^{\frac{\alpha_N}{\alpha_L}}}^{R+x} f_{\text{int}}(u)p(u)du + \int_x^{R+x} f_{\text{int}}(u)(1-p(u))du}\left(\int_{x^{\frac{\alpha_N}{\alpha_L}}}^{R+x} (\overset{(N)}{\mathcal{F}}_{LL} + \overset{(N)}{\mathcal{F}}_{LN}) f_{\text{int}}(y)p(y)dy + \int_x^{R+x} (\overset{(N)}{\mathcal{F}}_{NL} + \overset{(N)}{\mathcal{F}}_{NN}) f_{\text{int}}(y)(1-p(y))dy\right)\right)^{N_t-1}. \quad (6.18)$$

In (6.17) and (6.18) the terms $\overset{(s)}{\mathcal{F}}_{LL}$, $\overset{(s)}{\mathcal{F}}_{LN}$, $\overset{(s)}{\mathcal{F}}_{NL}$ and $\overset{(s)}{\mathcal{F}}_{NN}$ can be written as

$$\overset{(s)}{\mathcal{F}}_{LL} = \int_0^{a_d} Y_{L,1} \int_0^{R+a} \frac{1}{\left(1+\frac{n\eta_s\tau x^{\alpha_s(1-\epsilon)}u^{\alpha_L\epsilon}y^{-\alpha_L}\mathbb{E}_{G_i}[(G_i)]}{N\beta_L}\right)^{\beta_L}} \overset{(\text{SER})}{f}_{L,1}(u)du\frac{2a}{R^2}da + \int_{a_d}^{R} Y_{L,2} \int_0^{R+a} \frac{1}{\left(1+\frac{n\eta_s\tau x^{\alpha_s(1-\epsilon)}u^{\alpha_L\epsilon}y^{-\alpha_L}\mathbb{E}_{G_i}[(G_i)]}{N\beta_L}\right)^{\beta_L}} \overset{(\text{SER})}{f}_{L,2}(u)du\frac{2a}{R^2}da, \quad (6.19)$$

$$\overset{(s)}{\mathcal{F}}_{LN}= \int_0^{a_d} Y_{N,1} \int_0^{R+a} \frac{1}{\left(1+\frac{n\eta_s \tau x^{\alpha_s(1-\epsilon)} u^{\alpha_N \epsilon} y^{-\alpha_L} \mathbb{E}_{G_i}[(G_i)]}{N\beta_L}\right)^{\beta_L}} \overset{(\mathrm{SER})}{f}_{N,1}(u)du\frac{2a}{R^2}da+ \int_{a_d}^{R} Y_{N,2} \int_0^{R+a} \frac{1}{\left(1+\frac{n\eta_s \tau x^{\alpha_s(1-\epsilon)} u^{\alpha_N \epsilon} y^{-\alpha_L} \mathbb{E}_{G_i}[(G_i)]}{N\beta_L}\right)^{\beta_L}} \overset{(\mathrm{SER})}{f}_{N,2}(u)du\frac{2a}{R^2}da, \quad (6.20)$$

$$\overset{(s)}{\mathcal{F}}_{NL}= \int_0^{a_d} Y_{L,1} \int_0^{R+a} \frac{1}{\left(1+\frac{n\eta_s \tau x^{\alpha_s(1-\epsilon)} u^{\alpha_L \epsilon} y^{-\alpha_N} \mathbb{E}_{G_i}[(G_i)]}{N\beta_N}\right)^{\beta_N}} \overset{(\mathrm{SER})}{f}_{L,1}(u)du\frac{2a}{R^2}da+ \int_{a_d}^{R} Y_{L,2} \int_0^{R+a} \frac{1}{\left(1+\frac{n\eta_s \tau x^{\alpha_s(1-\epsilon)} u^{\alpha_L \epsilon} y^{-\alpha_N} \mathbb{E}_{G_i}[(G_i)]}{N\beta_N}\right)^{\beta_N}} \overset{(\mathrm{SER})}{f}_{L,2}(u)du\frac{2a}{R^2}da, \quad (6.21)$$

and

$$\overset{(s)}{\mathcal{F}}_{NN}= \int_0^{a_d} Y_{N,1} \int_0^{R+a} \frac{1}{\left(1+\frac{n\eta_s \tau x^{\alpha_s(1-\epsilon)} u^{\alpha_N \epsilon} y^{-\alpha_N} \mathbb{E}_{G_i}[(G_i)]}{N\beta_N}\right)^{\beta_N}} \overset{(\mathrm{SER})}{f}_{N,1}(u)du\frac{2a}{R^2}da+ \int_{a_d}^{R} Y_{N,2} \int_0^{R+a} \frac{1}{\left(1+\frac{n\eta_s \tau x^{\alpha_s(1-\epsilon)} u^{\alpha_N \epsilon} y^{-\alpha_N} \mathbb{E}_{G_i}[(G_i)]}{N\beta_N}\right)^{\beta_N}} \overset{(\mathrm{SER})}{f}_{N,2}(u)du\frac{2a}{R^2}da. \quad (6.22)$$

Here $s = L$ and $s = N$ represents LOS and NLOS reference UE, respectively. Furthermore, the term a_d can be written as

$$a_d = \mathrm{Re}\{\min(\mathrm{solve}(g(R,a),a))\} \quad (6.23)$$

where

$$g(R,a) = (R-a)^{\frac{\alpha_N}{\alpha_L}} - (R+a).$$

The term a_d can be interpreted as solving the function $g(R,a)$ for a, i.e, the solution of $g(R,a)=0$ and, then finding the minimum real value for a.

Then the expectation of the array gain has already been presented in (4.31).

Proof: See Appendix B.2.

6.2.5 Coverage Analysis

SINR coverage probability in the uplink communications is defined as the probability that the SINR received by a reference BS at $\boldsymbol{X}$ is greater than a threshold value τ dB ($\mathbb{P}_c(\tau) = \mathbb{P}(\text{SINR} > \tau)$). Conditioning on the nearest reference BS at distance x from the reference UE at the origin the SINR coverage probability can be written as

$$\mathbb{P}_c(\tau) = Y_L \mathbb{P}_{c,L}(\tau) + Y_N \mathbb{P}_{c,N}(\tau) \tag{6.24}$$

where $\mathbb{P}_{c,L}(\tau)$ and $\mathbb{P}_{c,N}(\tau)$ are the conditional coverage probabilities given that the reference BS is connected to LOS UE and NLOS UE, respectively. Furthermore, Y_L and Y_N can be evaluated by substituting $a = 0$ in (6.4) and (6.6). Next, these conditional coverage probabilities can be evaluated as

$$\mathbb{P}_{c,L}(\tau) = \int_0^R \mathbb{P}[\text{SINR} > \tau] \hat{f}_{L,1}(x) dx = \int_0^R \mathbb{P}\left[\frac{x^{-\alpha_L} h_{\boldsymbol{O}} x^{\alpha_L \epsilon} N}{(\sigma^2 + I)} > \tau\right] \overset{(\text{SER})}{f}_L(x) dx \tag{6.25}$$

where $\overset{(\text{SER})}{f}_L(x)$ can be evaluated by substituting $a = 0$ in (6.8). The inner probability term can be further simplified as

$$\begin{aligned}
\mathbb{P}\left[\frac{x^{-\alpha_L} h_{\boldsymbol{O}} x^{\alpha_L \epsilon} N}{(\sigma^2 + I)} > \tau\right] &= \mathbb{P}\left[h_{\boldsymbol{O}} > \frac{x^{\alpha_L(1-\epsilon)} \tau (\sigma^2 + I)}{N}\right] \\
&\overset{(a)}{=} 1 - \mathbb{E}_I\left[\left(1 - exp\left(\frac{-\eta_L \tau x^{\alpha_L(1-\epsilon)}(\sigma^2 + I)}{N}\right)\right)^{\beta_L}\right] \\
&\overset{(b)}{=} \sum_{n=1}^{\beta_L} (-1)^{n+1} \binom{\beta_L}{n} exp\left(\frac{-n\eta_L \tau x^{\alpha_L(1-\epsilon)} \sigma^2}{N}\right) \mathcal{L}_{I|L}\left(\frac{n\eta_L \tau x^{\alpha_L(1-\epsilon)}}{N}\right)
\end{aligned} \tag{6.26}$$

where (a) follows from, for a normalised gamma random variable γ with parameter β_L, the probability $P(\gamma < C\epsilon R^+)$ is upper bounded by $P(\gamma < C\epsilon R^+) < [1 - \exp -\eta_L C]^{\beta_L}$, where $\eta_L = \beta_L(\beta_L!)^{\left(\frac{-1}{\beta_L}\right)}$ [51] and (b) follows from binomial theorem expansion.

Similarly, the conditional coverage probability given that the reference BS is connected to an NLOS reference UE can be expressed as

$$\mathbb{P}_{c,N}(\tau) = \int_0^R \sum_{n=1}^{\beta_N} (-1)^{n+1} \binom{\beta_N}{n} exp\left(\frac{-n\eta_N \tau x^{\alpha_N(1-\epsilon)}\sigma^2}{N}\right) \mathcal{L}_{I|N}\left(\frac{n\eta_N \tau x^{\alpha_N(1-\epsilon)}}{N}\right) \overset{(\text{SER})}{f}_{N,1}(x)dx \quad (6.27)$$

where $\eta_N = \beta_N(\beta_N!)^{(\frac{-1}{\beta_N})}$. The Laplace transform of interference $\mathcal{L}_{I|s}(.)$ in (6.26) and (6.27) is given by (6.17) and (6.18). As similar in Chapter 4, more simplified cases for the SINR coverage probability for the uplink case can be evaluated.

6.2.5.1 Coverage Analysis with Fixed User Transmit Power

The SINR coverage probability in (6.24) can be simplified further for the fixed transmit power (i.e. $\epsilon = 0$). So we assume, all the UEs transmit with a constant power.

Corollary 6.1. *SINR coverage probability under the fixed transmit power condition can be expressed as*

$$\mathbb{P}_c(\tau) = Y_L \mathbb{P}_{c,L}(\tau) + Y_N \mathbb{P}_{c,N}(\tau) \quad (6.28)$$

where $\mathbb{P}_{c,L}(\tau)$ and $\mathbb{P}_{c,N}(\tau)$ for fixed transmit power can be written as

$$\mathbb{P}_{c,L}(\tau) = \int_0^R \sum_{n=1}^{\beta_L} (-1)^{n+1} \binom{\beta_L}{n} exp\left(\frac{-n\eta_L \tau x^{\alpha_L}\sigma^2}{N}\right) \mathcal{L}_{I|L}\left(\frac{n\eta_L \tau x^{\alpha_L}}{N}\right) \overset{(\text{SER})}{f}_{L,1}(x)dx \quad (6.29)$$

and

$$\mathbb{P}_{c,N}(\tau) = \int_0^R \sum_{n=1}^{\beta_N} (-1)^{n+1} \binom{\beta_N}{n} exp\left(\frac{-n\eta_N \tau x^{\alpha_N}\sigma^2}{N}\right) \mathcal{L}_{I|N}\left(\frac{n\eta_N \tau x^{\alpha_N}}{N}\right) \overset{(\mathrm{SER})}{f}_{N,1}(x)x. \tag{6.30}$$

In (6.29) and (6.30) the Laplace transform of interference $\mathcal{L}_{I|s}(.)$ can be expressed as

$$\mathcal{L}_{I|L}\left(\frac{n\eta_L \tau}{N}\right) = \left(\frac{1}{\int_x^{R+x} f_{\mathrm{int}}(u)p(u)du + \int_{x^{\frac{\alpha_L}{\alpha_N}}}^{R+x} f_{\mathrm{int}}(u)(1-p(u))du}\left(\int_x^{R+x} \frac{1}{\left(1+\frac{n\eta_L \tau x^{\alpha_L} y^{-\alpha_L}\mathbb{E}_{G_i}[(G_i)]}{N\beta_L}\right)^{\beta_L}}\right.\right.$$
$$\left.\left. f_{\mathrm{int}}(y)p(y)dy + \int_{x^{\frac{\alpha_L}{\alpha_N}}}^{R+x} \frac{1}{\left(1+\frac{n\eta_L \tau x^{\alpha_L} y^{-\alpha_N}\mathbb{E}_{G_i}[(G_i)]}{N\beta_N}\right)^{\beta_N}} f_{\mathrm{int}}(y)(1-p(y))dy\right)\right)^{N_t-1}, \tag{6.31}$$

and

$$\mathcal{L}_{I|N}\left(\frac{n\eta_N \tau}{N}\right) = \left(\frac{1}{\int_{x^{\frac{\alpha_N}{\alpha_L}}}^{R+x} f_{\mathrm{int}}(u)p(u)du + \int_x^{R+x} f_{\mathrm{int}}(u)(1-p(u))du}\left(\int_{x^{\frac{\alpha_N}{\alpha_L}}}^{R+x} \frac{1}{\left(1+\frac{n\eta_N \tau x^{\alpha_N} y^{-\alpha_L}\mathbb{E}_{G_i}[(G_i)]}{N\beta_L}\right)^{\beta_L}}\right.\right.$$
$$\left.\left. f_{\mathrm{int}}(y)p(y)dy + \int_x^{R+x} \frac{1}{\left(1+\frac{n\eta_N \tau x^{\alpha_N} y^{-\alpha_N}\mathbb{E}_{G_i}[(G_i)]}{N\beta_N}\right)^{\beta_N}} f_{\mathrm{int}}(y)(1-p(y))dy\right)\right)^{N_t-1}. \tag{6.32}$$

6.2.5.2 Coverage Analysis of Dense Network

In a similar manner to Section 4.2.4.2, coverage analysis for dense networks can be derived with two assumptions that are,

- No NLOS UEs: As the BS density increases, distance between UEs and BSs become smaller. Thus chances of a link between a UE and a BS being NLOS is highly unlikely.
- No Noise: Thermal noise can be ignored as the network becomes interference limited with strong LOS components.

With the above assumptions the uplink coverage probability of a dense network can be written.

Corollary 6.2. *SINR uplink coverage analysis for a dense network can be written as*

$$\mathbb{P}_c(\tau) = \int_0^R \sum_{n=1}^{\beta_L} (-1)^{n+1} \binom{\beta_L}{n} \mathcal{L}_I \left(\frac{n\eta_L \tau x^{\alpha_L(1-\epsilon)}}{N} \right) \overset{(\mathrm{SER})}{f_r}(x) dx. \tag{6.33}$$

In (6.33) $\overset{(\mathrm{SER})}{f_r}(x)$ and $\mathcal{L}_I(.)$ can be written as in (6.34) and (6.35).

$$\overset{(\mathrm{SER})}{f_r}(x) = N_t \left(1 - \frac{x^2}{R^2}\right)^{(N_t-1)} \frac{2x}{R^2}, \tag{6.34}$$

and

$$\mathcal{L}_I \left(\frac{n\eta_L \tau x^{\alpha_L(1-\epsilon)}}{N} \right) = \left(\int_x^{R+x} \int_0^R \int_0^{R+a} \frac{1}{\left(1 + \frac{n\eta_L \tau x^{\alpha_L(1-\epsilon)} u^{\alpha_L \epsilon} y^{-\alpha_L} \mathbb{E}_{G_i}[(G_i)]}{N\beta_L}\right)^{\beta_L}} \overset{(\mathrm{SER})}{f_d}(u) \frac{2a}{R^2} \frac{f_{\mathrm{int}}(y)}{\int_x^{R+x} f_{\mathrm{int}}(q) dq} du dy dy \right)^{N_t-1}. \tag{6.35}$$

In (6.35), $\overset{(\mathrm{SER})}{f_d}(u)$ can be written as

$$\overset{(\mathrm{SER})}{f_d}(u) = \begin{cases} N_t \left(1 - F_1(u)\right)^{(N_t-1)} f_1(u) & 0 < u < R - a \\ N_t \left(1 - F_2(u)\right)^{(N_t-1)} f_2(u) & R - a < u < R + a \end{cases} \tag{6.36}$$

where $F_1(u)$, $F_2(u)$, $f_1(u)$ and $f_2(u)$ can be found by substituting $p(t) = 1$ in (4.6) and (4.7) and can be written as

$$F(u) = \begin{cases} F_1(u) = \frac{u^2}{R^2} & 0 \leq u \leq R - a \\ F_2(u) = \frac{Ju^2 + \int_J^{2\pi - J} \int_0^{R_\theta} t dt d\theta}{\pi R^2} & R - a < u \leq R + a, \end{cases} \tag{6.37}$$

and

$$f(u) = \begin{cases} f_1(u) = \frac{dF_1(u)}{du} & 0 \leq u \leq R - a \\ f_2(u) = \frac{dF_2(u)}{du} & R - a < u \leq R + a \end{cases} \tag{6.38}$$

where $J = \cos^{-1}(\frac{a^2 + u^2 - R^2}{2au})$, and $R_\theta = \sqrt{R^2 - a^2 \sin^2 \theta} + a \cos \theta$.

This concludes the derivations of the uplink coverage probability in a disk region. Next section presents the results produced for the modelled uplink cellular network.

6.3 Results and Discussions

This section presents the numerical results to illustrate our analytical findings proposed in Section 6.2. Unless otherwise stated, we set the number of BSs $N_t = 50$ (this is equivalent to number of active UEs), Nakagami fading parameters and path loss exponents of LOS and NLOS links are set to $\beta_L = 3$, $\beta_N = 2$, $\alpha_L = 2$ and $\alpha_N = 4$. Furthermore, a finite disk region with radius $R = 100$m is considered. Also, it is assumed that the mmWave network is operated at 28 GHz frequency with a bandwidth of 100 MHz allocated to each UE. Additionally Monte Carlo simulations are obtained by averaging over 10,000 realisations to validate the accuracy of the results.

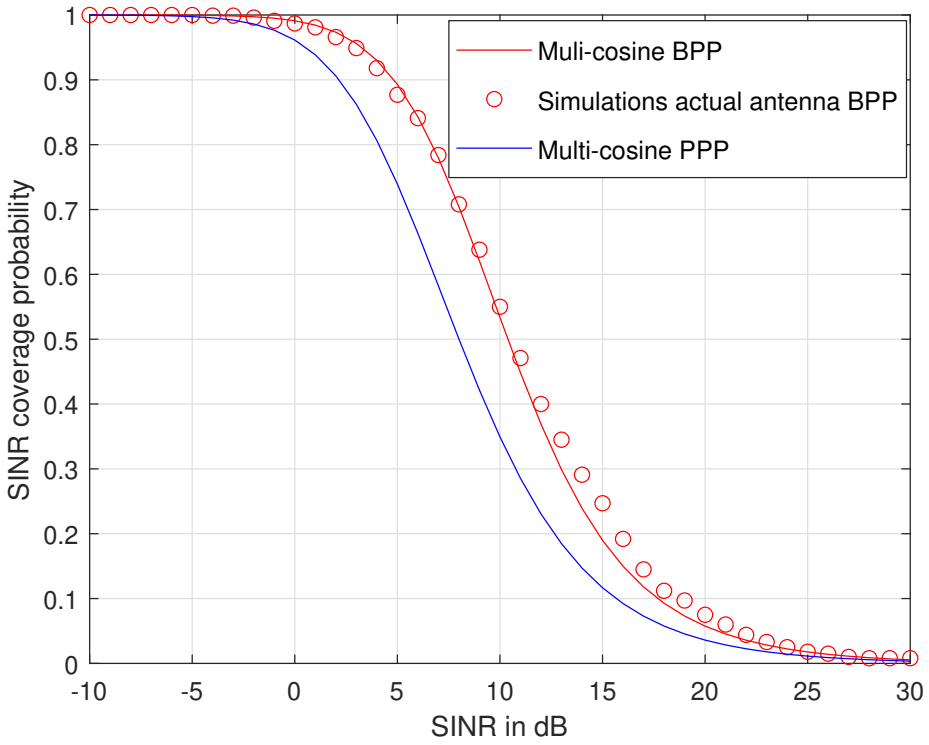

FIGURE 6.4: SINR uplink coverage probability for a BPP and PPP network ($N = 32$ and $\epsilon = 0$).

Fig. 6.4 shows the uplink SINR coverage probability of the reference receiver at the centre of the disk region. The blockage parameter w and the array antenna elements N are set to 1/140 and 32, respectively. The graphs for the power control factor $\epsilon = 0$ verifies the accuracy of the proposed analytical model by showing a close match with the simulation results with the actual antenna model. This result validates the assumption made in Section 4.1.4. An important limitation with this assumption is the accuracy depends on the BS density, whereas it is expected that mmWave networks will be deployed with very high BS density. Therefore this assumption is valid for a high dense mmWave cellular networks. In [62] a very high BS density of 0.004 m^{-2} has been considered to model a mmWave cellular network. Also, we compared the performance of an infinite PPP against our network by considering a BS density equals the density of our BPP model. It can be observed that PPP provides a lower bound compared to the BPP model. It has been demonstrated in [18] that one can use the PPP for analysis and then add a calibrated horizontal SINR shift of 1–3 dB. Interestingly the performance

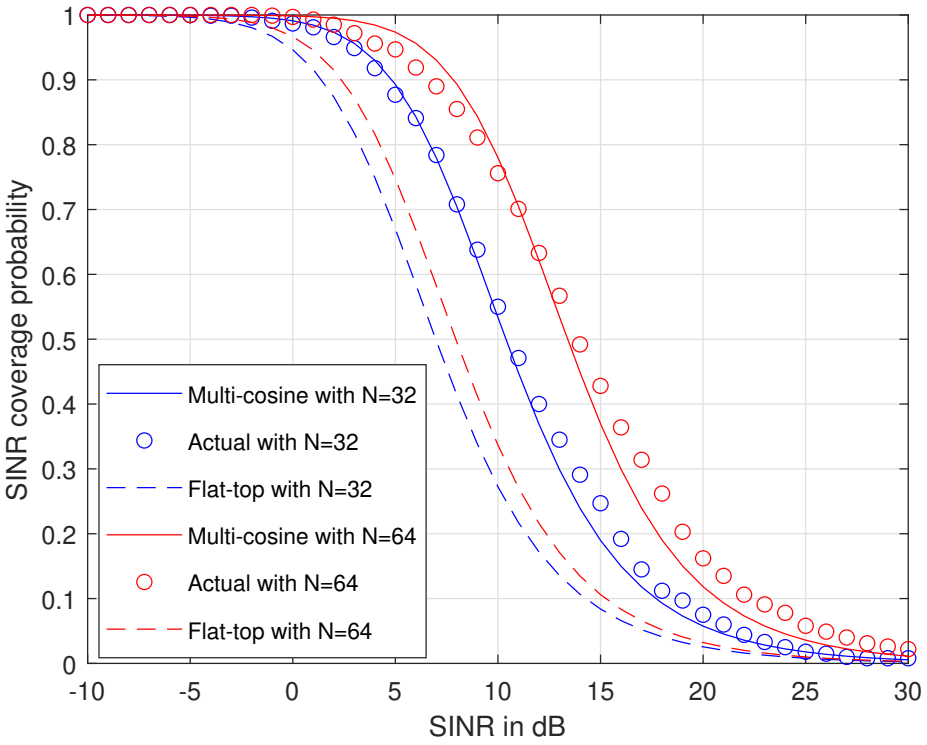

FIGURE 6.5: SINR uplink coverage probability comparison for different array elements ($\epsilon = 0$).

difference between the PPP and the BPP model also varies by approximately 1–2 dB. Therefore we can conclude that the BPP model provides more accuracy and can represent the practical cellular network more closely than the PPP model.

Fig. 6.5 shows the impact of the number of array antenna elements in the SINR coverage probability. It can be seen that increasing the array size results in significant improvement in the SINR coverage probability. Furthermore, it is evident that the flat-top antenna model underestimates the coverage probability compared to the multi-cosine model by 1–5 dB (horizontal gap) and the gap increases with the increase of N. This demonstrates the importance of incorporating a more realistic array antenna model to predict the system performance accurately. We can also observe that the uniform distribution assumption we made in the multi-cosine model provides better approximation, as it closely matches the actual antenna model.

Fig. 6.6 shows the impact of various fractional power control factors ϵ for two

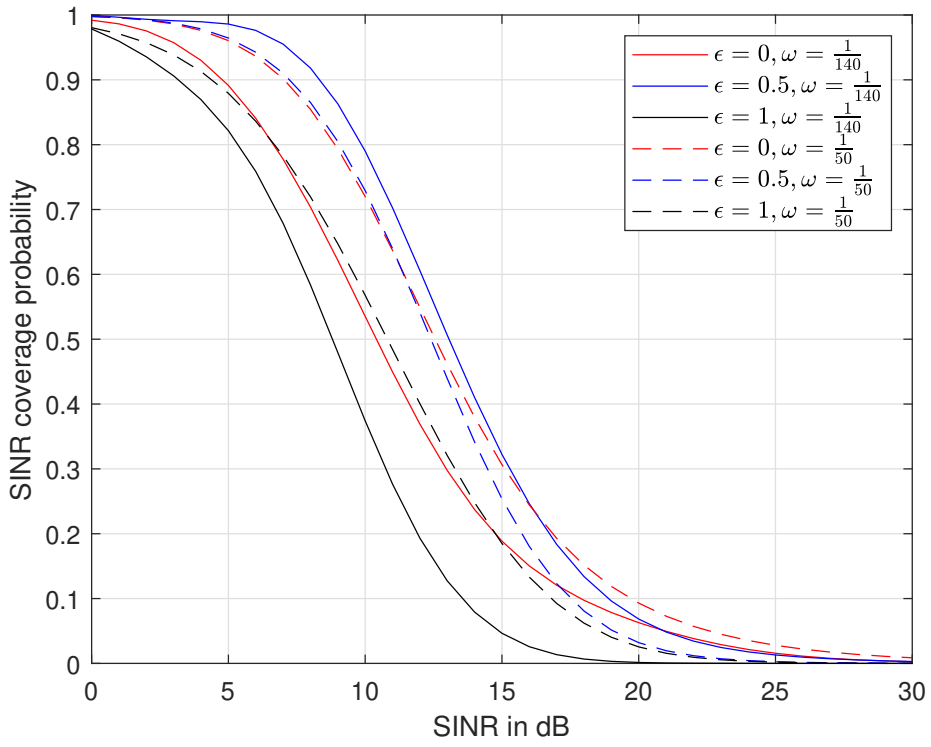

FIGURE 6.6: SINR uplink coverage probability for various FPC factors ($N = 32$).

different blockage parameters $\omega = \frac{1}{140}$ and $\omega = \frac{1}{50}$. We also plot the baseline case of fixed transmit power ($\epsilon = 0$) for all UEs. As it can be seen in both sparse blockage ($\omega = \frac{1}{140}$) and dense blockage networks ($\omega = \frac{1}{50}$), the full path loss compensation $\epsilon = 1$ provides the least SINR coverage probability. Considering the network with $\omega = \frac{1}{140}$, the largest coverage probability for almost all the UEs is provided by $\epsilon = 0.5$, followed by the fixed transmit power. In the case of network with $\omega = \frac{1}{50}$, for τ <12 dB, both the fixed transmit power and $\epsilon = 0.5$ provide similar values for the coverage probability. For SINR greater than 12 dB, the fixed transmit power case provides slightly better performance than $\epsilon = 0.5$. The benefit of such an uplink model is that engineers can carefully choose the operating thresholds for a given set of parameters.

Fig. 6.7 shows the variations of the SINR coverage probability with the blockage parameter ω. It can be observed that the coverage probability improves as the blockage parameter increases, reaching an optimum value for $\omega = 0.075$ and then the coverage probability starts to decline. This trend can be interpreted as the

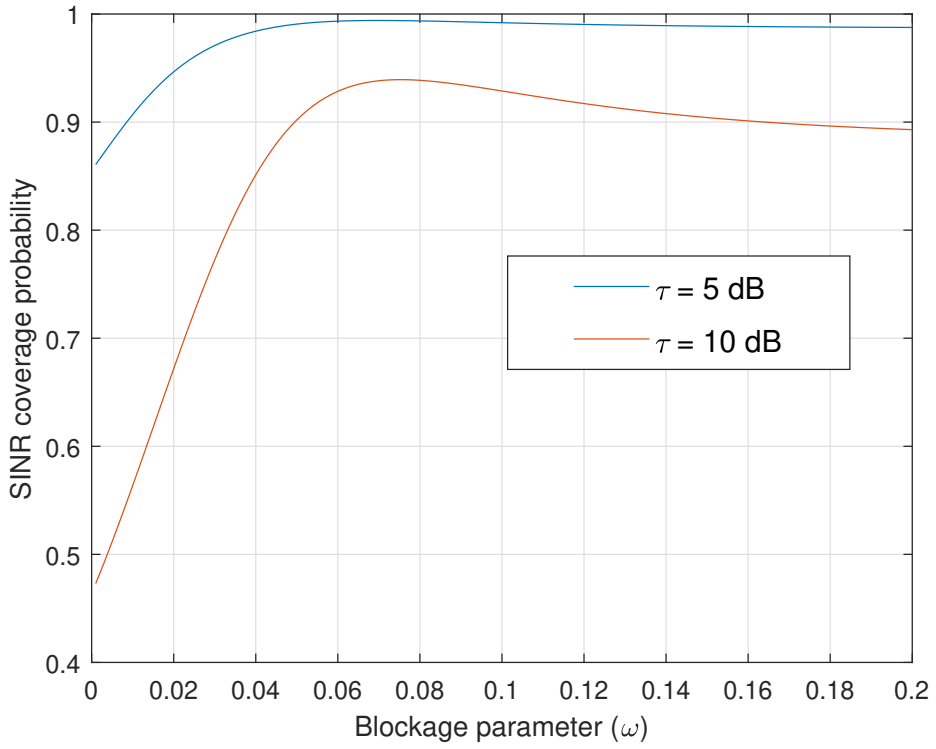

FIGURE 6.7: SINR uplink coverage probability as a function of the blockage parameter ($N = 32$ and $\epsilon = 0$).

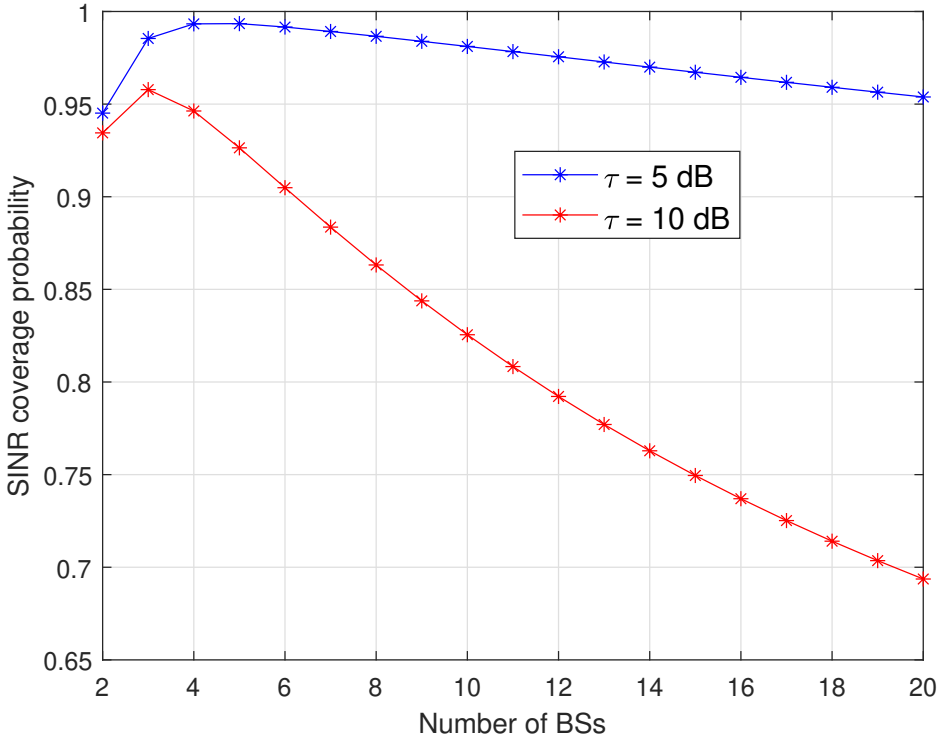

FIGURE 6.8: SINR uplink coverage probability as a function of number of BSs ($\epsilon = 0$ and $N = 32$).

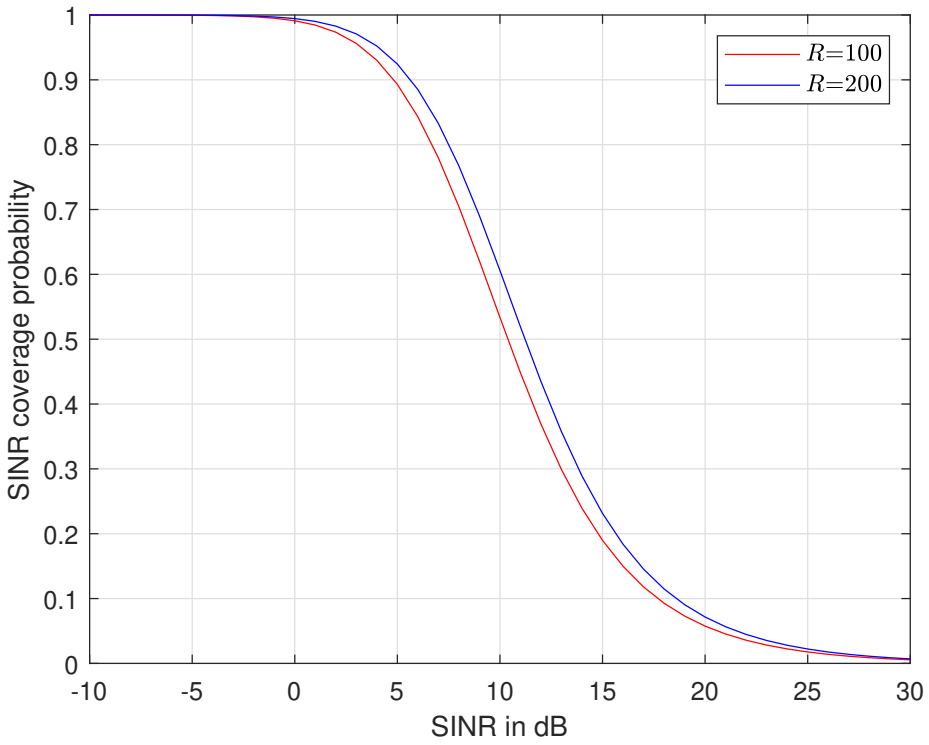

FIGURE 6.9: SINR uplink coverage probability as a function of radius ($N = 32$ and $\epsilon = 0$).

blockage parameter increases more BSs become NLOS and thus more interferers become NLOS and improves the performance. With further increase in the blockage parameter, both the serving and the interfering BSs might become NLOS and the coverage probability starts to decrease.

The impact of the number of BSs is illustrated in Fig. 6.8 for SINR thresholds $\tau = 5$dB and $\tau = 10$dB and FPC factor $\epsilon = 0$. The blockage parameter is set to $\omega = \frac{1}{140}$. Focusing on the performance variation of the SINR coverage probability with the number of BSs, it can be observed that the performance improves as the number of BSs increases and then performance starts to degrade. This can be interpreted as, as the BSs count increases, the performance starts to improve in the noise-limited regime. But on the other hand, keep on increasing the BS count leads to more LOS BSs in the networks, results in more severe interference. Thus the performance degrades.

Fig. 6.9 shows the effect of the area of the network region. It can be observed

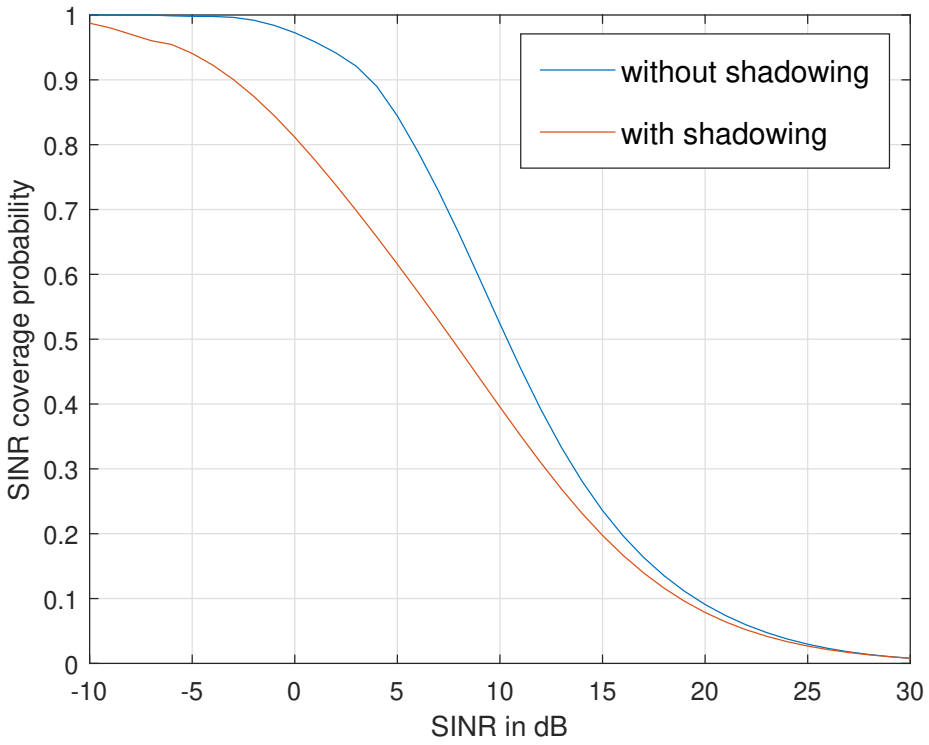

FIGURE 6.10: The impact of shadowing ($N = 32$ and $\epsilon = 0$).

that as the network region's radius increases, the performance improves. This is because as the area increases the UE - BS distance becomes larger, thus reduction in the interference power, which leads to improved performance.

Fig. 6.10 shows the coverage analysis for the composite fading scenario, that is combined Nakagami fading and log-normal shadowing. Different parameters for LOS and NLOS links have been considered per the guidelines provided in [58]. LOS links are assumed to be with Nakagami parameter β_L=3 and log-normal shadowing of zero mean and 5.8 dB of standard deviation. NLOS links are assumed to be with Nakagami parameter β_L=2 and log-normal shadowing of zero mean and 8.7 dB of standard deviation. The result shows that for lower SINR values, the effect of composite fading becomes significant, whereas no shadowing scenario results in an upper bounded coverage probability. But for high SINR values, there is negligible performance gap and this can be due to for high SINR the desired signal must be large enough to overcome the losses due to shadowing and fading. These shadowing results were presented via simulations for the proposed mathematical

model. Incorporating the log-normal shadowing along with Nakagami fading into our mathematical model becomes tedious, whereas the mathematical derivations become extremely complicated. Therefore, we have not considered in this work.

6.4 Conclusions

This chapter presents a stochastic geometry approach to model the uplink communications of a finite mmWave cellular network using the binomial point process. The system model incorporates the unique features of mmWave communications, such as the blockage environment, high directional beamforming and different channel models for LOS and NLOS links. Also, per-user fractional power control has been incorporated into the system model. A more realistic multi-cosine array antenna model has been incorporated to represent the actual antenna pattern compared to the flat-top antenna model. The results demonstrate that increasing the array size improves the performance considerably. Further flat-top antenna model underestimates the performance compared to the multi-cosine model. The significance of incorporating fractional power control has been demonstrated. It is essential to choose an optimum fractional power control factor that can provide acceptable performance for the majority of the UEs, which leads to overall high system capacity. Also, there is an optimum blockage parameter for a given set of parameters to experience the best coverage probability. Similarly, there is an optimum BS density for a given network set up.

Chapter 7

Conclusions and Recommendations

This thesis presents stochastic geometry based frameworks for analysing the system level performance of millimetre wave outdoor cellular networks. This chapter summarises the general conclusions drawn from this thesis and provides some future research directions.

7.1 Conclusions

The deficiencies in the existing millimetre cellular network models based on a PPP have been identified through a comprehensive literature review. To address these deficiencies, a refined model based on the BPP has been proposed.

Firstly, in Chapter 4, we proposed stochastic geometry frameworks based on the binomial point process to analyse the downlink performance of a millimetre wave cellular network. In contrast to the PPP, the BPP allows performance analysis to be conducted in a finite region and with a fixed number of nodes. In this chapter, we considered a disk region to represent the cellular geographical region. We proposed stochastic geometry frameworks that incorporate millimetre wave communications' unique features and a more realistic array antenna model, thereby

representing the actual radiation pattern. The presented results showed the importance of adopting a more realistic antenna model, named multi-cosine; whereas a more commonly used sectored antenna model provides a lower bound than the multi-cosine model. These frameworks also allow us to analyse the user's location dependant performance, and the results show the performance improves as the user moves farther from the centre. Furthermore, the results also demonstrate the effect of the blockage parameter and the BS count, indicating that there is an optimum value for both that provides the best coverage probability for a given network.

We then extend the coverage analysis to more generalised arbitrary shape in Chapter 5, compared to the disk shape in Chapter 4. As in Chapter 4, we proposed stochastic geometry frameworks to analyse the downlink performance in an L-sided regular convex polygon. The results indicate that the performance difference between a polygon and a disk is almost negligible for a centrally located reference receiver. Therefore, we believe that it is acceptable to assume that the finite region can be a disk shape, representing any arbitrarily shaped geographical region to analyse the performance of a centre user. Assuming the network region as a simple disk region enables us to produce more tractable analytical results.

Finally, in Chapter 6 we conducted an uplink analysis of a mmWave cellular network. With the conclusions derived in Chapter 5, we fix the network region as a a disk region. Similar to previous chapters, we proposed a stochastic geometry framework considering the peculiar features of millimetre wave communications. We have also enabled the fractional power control at the user devices. Similar conclusion as in Chapter 4 has been derived representing the impact of array antenna elements, blockage parameter and the BS density. The results also demonstrate the importance of the proper selection of the power control factor to provide acceptable performance for the majority of the users.

7.2 Recommendations for Further Research

In addition to the contributions we have presented in this thesis, there are several areas this work can be extended. Firstly, in this thesis, we have incorporated the antenna array model only at the base stations, whereas the user devices are assumed to be having a single omnidirectional antenna. It is expected that in future millimetre wave cellular systems, the directional antenna arrays will be deployed both at the base stations and at mobile devices. Therefore, we recommend incorporating the array antenna models at both BSs and UEs and analysing the performance by using a similar approach as in chapters 4 to 6. Besides, we can also incorporate the impact of beam alignment errors. In [25, 72], the significance of incorporating beam alignment has been demonstrated, whereas relatively small alignment errors can lead to a significant reduction in the performance.

Another possible future extension to this thesis would be to consider a heterogeneous network deployment, wherein BSs with similar specifications (such as transmit power and coverage range) are grouped and form a tier in a heterogeneous network. We could then consider a two-tier approach, incorporating a conventional cellular network operating in the sub-6 GHz band (tier 1), and an mmWave network operating in the 28-GHz band (tier 2). Although the interference of these two frequencies is independent, the coverage analysis is correlated; the mmWave network's BS locations depend on the coverage footprint of the conventional cellular network's BSs. For example, we can assume the mmWave BSs to be highly populated in the cell-edge areas of a conventional cellular network BS, in order to provide better signal quality to the users located in the cell boundary region. These correlated deployment strategies, which consider the coexistence of the mmWave and microwave frequencies, can give us different insights into the results produced by this thesis. The heterogeneous network deployment using the PPP is presented in [74–76].

In this thesis, we have assumed our BSs and users to be stationary. A possible future extension would be to consider the mobility of the network nodes. We can expect that BSs will be static, but that users will be roaming, most of the time.

Therefore, it would be appropriate to incorporate mobility models such as random walk, random waypoint and Brownian motion [77, 78] into our system analysis process.

Finally, we recommend incorporating the non-orthogonal multiple access (NOMA) technique to the proposed stochastic geometry frameworks used in this work. NOMA is a promising radio access technique for future wireless systems that allows multiple users to access a given resource block simultaneously. This offers benefits such as enhanced spectrum efficiency and massive connectivity [79, 80].

Appendix A

Proofs for Chapter 4

A.1 Proof of Theorem 4.1

A user can be associated with a LOS BS by satisfying the following two conditions, which are, (i) there is at least one LOS BS exists in $\mathcal{A}$. This can be either all BSs being LOS or the network can contain both LOS and NLOS BSs, (ii) the nearest LOS BS's path loss ($R_L^{-\alpha_L}$) is smaller than the nearest NLOS BS's path loss ($R_N^{-\alpha_N}$). Hence it follows that

$$\begin{aligned} Y_{L,u} = \mathbb{P}(N_{tL} \geq 1 \& N_{tN} = 0) \times \\ \mathbb{P}(R_L^{-\alpha_L} > R_N^{-\alpha_N} \mid N_{tL} \geq 1 \& N_{tN} = 0) \\ + \mathbb{P}(N_{tL} \geq 1 \& N_{tN} \geq 1) \times \\ \mathbb{P}(R_L^{-\alpha_L} > R_N^{-\alpha_N} \mid N_{tL} \geq 1 \& N_{tN} \geq 1) \\ \overset{(a)}{=} (1 - a_L) a_N + \\ (1 - a_L)(1 - a_N) \int_0^{R+a} \mathbb{P}(R_N > x^{\frac{\alpha_L}{\alpha_N}}) \overset{(\text{NEA})}{f_L}(x) dx; \;\; u = \{1, 2\} \end{aligned} \tag{A.1}$$

where $\overset{(\text{NEA})}{f_L}(x)$ is given by (4.11), (a) follows from $\mathbb{P}(R_L^{-\alpha_L} \geq R_N^{-\alpha_N} \mid N_{tL} \geq 1 \& N_{tN} = 0) = 1$ and $u = 1, 2$ specifies the above defined Case 1 and Case 2.

Next, $\mathbb{P}(R_N > x^{\frac{\alpha_L}{\alpha_N}})$ can be interpreted as, there is no NLOS BSs in the region $\mathcal{B}(\boldsymbol{D}, x^{\frac{\alpha_L}{\alpha_N}})$. Therefore from (4.5), $\mathbb{P}(R_N > x^{\frac{\alpha_L}{\alpha_N}})$ can be written as

$$\mathbb{P}(R_N > x^{\frac{\alpha_L}{\alpha_N}}) = \frac{\left(1 - F_N(x^{\frac{\alpha_L}{\alpha_N}})\right)^{Nt} - a_N}{1 - a_N} \tag{A.2}$$

where $F_N(x^{\frac{\alpha_L}{\alpha_N}})$ and a_N are given by (4.14) and (4.16), respectively. Based on the values of R, a, α_L and α_N and the fact that $\alpha_N > \alpha_L$, there can be two different cases for the LOS association probability and these association probabilities can be computed by substituting (A.2) in (A.1) as follows.

Case 1: $(R-a)^{\frac{\alpha_N}{\alpha_L}} > R + a$

$$\begin{aligned} Y_{L,1} = (1 - a_L)(1 - a_N) \\ \Bigg[\int_0^{R-a} \frac{\left(\left(1 - F_{N,1}(x^{\frac{\alpha_L}{\alpha_N}})\right)^{Nt} - a_N\right)}{1 - a_N} f_{L,1}^{(\text{NEA})}(x)dx \\ + \int_{R-a}^{R+a} \frac{\left(\left(1 - F_{N,1}(x^{\frac{\alpha_L}{\alpha_N}})\right)^{Nt} - a_N\right)}{1 - a_N} f_{L,2}^{(\text{NEA})}(x)dx \Bigg] \\ + a_N(1 - a_L). \end{aligned} \tag{A.3}$$

Case 2: $(R-a)^{\frac{\alpha_N}{\alpha_L}} < R + a$

$$\begin{aligned} Y_{L,2} = (1 - a_L)(1 - a_N) \\ \Bigg[\int_0^{R-a} \frac{\left(\left(1 - F_{N,1}(x^{\frac{\alpha_L}{\alpha_N}})\right)^{Nt} - a_N\right)}{1 - a_N} f_{L,1}^{(\text{NEA})}(x)dx \\ + \int_{R-a}^{(R-a)^{\frac{\alpha_N}{\alpha_L}}} \frac{\left(\left(1 - F_{N,1}(x^{\frac{\alpha_L}{\alpha_N}})\right)^{Nt} - a_N\right)}{1 - a_N} f_{L,2}^{(\text{NEA})}(x)dx \\ + \int_{(R-a)^{\frac{\alpha_N}{\alpha_L}}}^{R+a} \frac{\left(\left(1 - F_{N,2}(x^{\frac{\alpha_L}{\alpha_N}})\right)^{Nt} - a_N\right)}{1 - a_N} f_{L,2}^{(\text{NEA})}(x)dx \Bigg] \\ + a_N(1 - a_L). \end{aligned} \tag{A.4}$$

By simplifying (A.3) and (A.4), (4.17) and (4.18) are obtained.

A.2 Proof of Theorem 4.3

Given that the reference receiver is associated with a LOS BS at distance R_L and to obtain the probability density function of this serving BS, as a first step the conditional cumulative distribution function of R_L should be defined. The conditional CDF can be written as

$$\overset{(\mathrm{SER})}{F}_{L,u}(x) = 1 - \frac{\mathbb{P}(R_L > x, R_L^{-\alpha_L} > R_N^{-\alpha_N})}{Y_{L,u}}; \;\; u = \{1, 2\} \tag{A.5}$$

where $u = 1, 2$ specifies the above defined Case 1 and Case 2.

Following similar approach as in Appendix A.1, $\mathbb{P}(R_L > x, R_L^{-\alpha_L} > R_N^{-\alpha_N})$ can be written as

$$\mathbb{P}(R_L > x, R_L^{-\alpha_L} > R_N^{-\alpha_N}) = (1 - a_L)a_N\mathbb{P}(R_L > x) + (1 - a_L)(1 - a_N)\int_x^{R+a} \mathbb{P}(R_N > w^{\frac{\alpha_L}{\alpha_N}}) \overset{(\mathrm{NEA})}{f}_L(w)dw. \tag{A.6}$$

Finally, by substituting (A.6) in (A.5), $\overset{(\mathrm{SER})}{F}_{L,u}(x)$ can be written as follows for the two cases

Case 1: $(R-a)^{\frac{\alpha_N}{\alpha_L}} > R+a$

$$\overset{(\text{SER})}{F}_{L,1}(x) = 1 - \frac{1}{Y_{L,1}}\Bigg[(1-a_L)a_N\frac{\left((1-F_{L,1}(x))^{Nt}-a_L\right)}{1-a_L} + (1-a_L)(1-a_N)$$
$$\Bigg\{\int_x^{R-a}\frac{\left(\left(1-F_{N,1}(w^{\frac{\alpha_L}{\alpha_N}})\right)^{Nt}-a_N\right)}{1-a_N}\overset{(\text{NEA})}{f}_{L,1}(w)dw$$
$$+\int_{R-a}^{R+a}\frac{\left(\left(1-F_{N,1}(w^{\frac{\alpha_L}{\alpha_N}})\right)^{Nt}-a_N\right)}{1-a_N}\overset{(\text{NEA})}{f}_{L,2}(w)dw\Bigg\}\Bigg]$$

if $0 < x < R-a$, and

$$\overset{(\text{SER})}{F}_{L,1}(x) = 1 - \frac{1}{Y_{L,1}}\Bigg[(1-a_L)a_N\frac{\left((1-F_{L,2}(x))^{Nt}-a_L\right)}{1-a_L} + (1-a_L)(1-a_N)$$
$$\Bigg\{\int_x^{R+a}\frac{\left(\left(1-F_{N,1}(w^{\frac{\alpha_L}{\alpha_N}})\right)^{Nt}-a_N\right)}{1-a_N}\overset{(\text{NEA})}{f}_{L,2}(w)dw\Bigg\}\Bigg] \quad \text{(A.7)}$$

if $R-a < x < R+a$, and

Case 2: $(R-a)^{\frac{\alpha_N}{\alpha_L}} < R+a$

$$\overset{(\text{SER})}{F}_{L,2}(x) = 1 - \frac{1}{Y_{L,2}}\Bigg[(1-a_L)a_N$$
$$\frac{\left((1-F_{L,1}(x))^{Nt}-a_L\right)}{1-a_L} + (1-a_L)(1-a_N)$$
$$\Bigg\{\int_x^{R-a}\frac{\left(\left(1-F_{N,1}(w^{\frac{\alpha_L}{\alpha_N}})\right)^{Nt}-a_N\right)}{1-a_N}\overset{(\text{NEA})}{f}_{L,1}(w)dw$$
$$+\int_{R-a}^{(R-a)^{\frac{\alpha_N}{\alpha_L}}}\frac{\left(\left(1-F_{N,1}(w^{\frac{\alpha_L}{\alpha_N}})\right)^{Nt}-a_N\right)}{1-a_N}\overset{(\text{NEA})}{f}_{L,2}(w)dw$$
$$+\int_{(R-a)^{\frac{\alpha_N}{\alpha_L}}}^{R+a}\frac{\left(\left(1-F_{N,2}(w^{\frac{\alpha_L}{\alpha_N}})\right)^{Nt}-a_N\right)}{1-a_N}\overset{(\text{NEA})}{f}_{L,2}(w)dw\Bigg\}\Bigg]$$

if $0 < x < R - a$,

$$\overset{(\text{SER})}{F}_{L,2}(x) = 1 - \frac{1}{Y_{L,2}}\Bigg[(1-a_L)a_N \frac{\left((1-F_{L,2}(x))^{Nt} - a_L\right)}{1-a_L} + (1-a_L)(1-a_N)\Bigg\{\int_x^{(R-a)^{\frac{\alpha_N}{\alpha_L}}} \frac{\left(\left(1-F_{N,1}(w^{\frac{\alpha_L}{\alpha_N}})\right)^{Nt} - a_N\right)}{1-a_N} \overset{(\text{NEA})}{f}_{L,2}(w)dw + \int_{(R-a)^{\frac{\alpha_N}{\alpha_L}}}^{R+a} \frac{\left(\left(1-F_{N,2}(w^{\frac{\alpha_L}{\alpha_N}})\right)^{Nt} - a_N\right)}{1-a_N} \overset{(\text{NEA})}{f}_{L,2}(w)dw\Bigg\}\Bigg]$$

if $R - a < x < (R-a)^{\frac{\alpha_N}{\alpha_L}}$, and

$$\overset{(\text{SER})}{F}_{L,2}(x) = 1 - \frac{1}{Y_{L,2}}\Bigg[(1-a_L)a_N \frac{\left((1-F_{L,2}(x))^{Nt} - a_L\right)}{1-a_L} + (1-a_L)(1-a_N)\Bigg\{\int_x^{R+a} \frac{\left(\left(1-F_{N,2}(w^{\frac{\alpha_L}{\alpha_N}})\right)^{Nt} - a_N\right)}{1-a_N} \overset{(\text{NEA})}{f}_{L,2}(w)dw\Bigg\}\Bigg] \quad \text{(A.8)}$$

if $(R-a)^{\frac{\alpha_N}{\alpha_L}} < x < R + a$.

The PDF can then be obtained by differentiating the CDF $\overset{(\text{SER})}{F}_{L,u}(x)$.

A.3 Proof of Theorem 4.5

Given that a user is served by a LOS BS at distance x, there can be interference from LOS and NLOS BSs. Let's assume a LOS interferer at $\boldsymbol{Y_L}$ with distance y_L to the reference user. Then the BS at $\boldsymbol{Y_L}$ can be an interferer only if the path gain of the LOS interferer is less than the serving BS, i.e., $y_L^{-\alpha_L} < x^{-\alpha_L}$. So then, the CDF of the LOS interferer conditioned on the LOS serving BS can be written as

$$F(y_L < y \mid y_L > x, \boldsymbol{Y_L}) = \frac{\mathbb{P}(x < y_L < y, \boldsymbol{Y_L})}{\mathbb{P}(y_L > x, \boldsymbol{Y_L})} = \frac{\int_x^y f_L(q)dq}{\int_x^{R+a} f_L(q)dq}. \quad \text{(A.9)}$$

The PDF can be obtained by differentiating the CDF and can be written as

$$f(y_L < y \mid y_L > x, \boldsymbol{Y_L}) = \frac{f_L(y)}{\int_x^{R+a} f_L(q)dq}. \tag{A.10}$$

Accordingly the general format can be written as in (4.25).

A.4 Proof of Theorem 4.6

An expression for the Laplace transform of the aggregate interference conditioned on the serving BS being LOS and the serving distance x is in the range $0 < x < R-a$ can be derived as follows. Here s_L and s_N denotes the set of LOS and NLOS interferers, respectively.

$$\begin{aligned}
\mathcal{L}_{I|L}\left(\frac{n\eta_L \tau x^{\alpha_L}}{p_t N}\right) = & \\
& \mathbb{E}_{h_i,G_i}\Bigg[\exp\left(\frac{-n\eta_L\tau x^{\alpha_L}\sum_{\boldsymbol{Y}\in s_L} h_i p_t G_i y^{-\alpha_L}}{p_t N}\right) \\
& \exp\left(\frac{-n\eta_L\tau x^{\alpha_L}\sum_{\boldsymbol{Y}\in s_N} h_i p_t G_i y^{-\alpha_N}}{p_t N}\right)\Bigg] \\
& \overset{(c)}{=} \prod_{\boldsymbol{Y}\in s_L} \frac{1}{\left(1+\frac{\mathcal{F}y^{-\alpha_L}}{\beta_L}\right)^{\beta_L}} \prod_{\boldsymbol{y}\in s_N} \frac{1}{\left(1+\frac{\mathcal{F}y^{-\alpha_N}}{\beta_N}\right)^{\beta_N}} \\
& \overset{(d)}{=} \Bigg(\mathbb{P}(\mathcal{E}_{L1}\mid\mathcal{E})\int_x^{R-a} \frac{1}{\left(1+\frac{\mathcal{F}y^{-\alpha_L}}{\beta_L}\right)^{\beta_L}} \frac{f_{L,1}(y)}{\int_x^{R-a} f_{L,1}(q)dq}dy + \\
& \mathbb{P}(\mathcal{E}_{L2}\mid\mathcal{E})\int_{R-a}^{R+a} \frac{1}{\left(1+\frac{\mathcal{F}y^{-\alpha_L}}{\beta_L}\right)^{\beta_L}} \frac{f_{L,2}(y)}{\int_{R-a}^{R+a} f_{L,2}(q)dq}dy + \\
& \mathbb{P}(\mathcal{E}_{N1}\mid\mathcal{E})\int_{x^{\frac{\alpha_L}{\alpha_N}}}^{R-a} \frac{1}{\left(1+\frac{\mathcal{F}y^{-\alpha_N}}{\beta_N}\right)^{\beta_N}} \frac{f_{N,1}(y)}{\int_{x^{\frac{\alpha_L}{\alpha_N}}}^{R-a} f_{N,1}(q)dq}dy + \\
& \mathbb{P}(\mathcal{E}_{N2}\mid\mathcal{E})\int_{R-a}^{R-a} \frac{1}{\left(1+\frac{\mathcal{F}y^{-\alpha_N}}{\beta_N}\right)^{\beta_N}} \frac{f_{N,2}(y)}{\int_{R-a}^{R+a} f_{N,2}(q)dq}dy\Bigg)^{N_t-1}
\end{aligned} \tag{A.11}$$

where

$$\mathcal{F} = \frac{n\eta_L \tau x^{\alpha_L} \mathbb{E}_{G_i}[(G_i)]}{N}. \tag{A.12}$$

In (A.11), (c) follows from the moment generating function of the gamma random variable, and (d) is obtained by converting from Cartesian to polar coordinates and substituting the corresponding interference distance distributions $\overset{(\text{INT})}{f_{s,u}}(y)$ as given in (4.25). The probabilities $\mathbb{P}(.)$ can be defined with the following arguments.

Assuming a LOS serving BS at distance x, the LOS and NLOS interferers will be x and $x^{\frac{\alpha_L}{\alpha_N}}$ away from the reference receiver, respectively. Along with these interpretations and depending on the locations of the interfering BSs, the following events can be defined:

- $\mathcal{E}_{L1}$: Interference from a LOS BS that is farther than x but smaller than $R-a$ to the reference receiver;
- $\mathcal{E}_{L2}$: Interference from a LOS BS that is farther than $R-a$ but smaller than $R+a$ to the reference receiver;
- $\mathcal{E}_{N1}$: Interference from an NLOS BS that is farther than $x^{\frac{\alpha_L}{\alpha_N}}$ but smaller than $R-a$ to the reference receiver; and
- $\mathcal{E}_{N1}$: Interference from an NLOS BS that is farther than $R-a$ but smaller than $R+a$ to the reference receiver.

Also, $\mathbb{P}(\mathcal{E})$ is the union of all events and is given by $\mathbb{P}(\mathcal{E}_{L1}) + \mathbb{P}(\mathcal{E}_{L2}) + \mathbb{P}(\mathcal{E}_{N1}) + \mathbb{P}(\mathcal{E}_{N2})$.

With these explanations, the probability $\mathbb{P}(\mathcal{E}_{L1} \mid \mathcal{E})$ can be derived as

$$\mathbb{P}(\mathcal{E}_{L1} \mid \mathcal{E}) = \frac{\mathbb{P}(\mathcal{E}_{L1}, \mathcal{E})}{\mathbb{P}(\mathcal{E})} \overset{(a)}{=} \frac{\mathbb{P}(\mathcal{E}_{L1})}{\mathbb{P}(\mathcal{E})} \tag{A.13}$$

where (a) is due to, all the events are mutually exclusive,

$$\mathbb{P}(\mathcal{E}_{L1}) = \int_{x}^{R-a} f_{L,1}(q)dq$$

and

$$\mathbb{P}(\mathcal{E}) = \int_{x}^{R-a} f_{L,1}(q)dq + \int_{R-a}^{R+a} f_{L,2}(q)dq + \int_{x\frac{\alpha_L}{\alpha_N}}^{R-a} f_{N,1}(q)dq + \int_{R-a}^{R+a} f_{N,2}(q)dq.$$

In similar way the other events' probabilities can be written. Then, the general format for the Laplace transform of the aggregate interference can be written as in (4.30).

Appendix B

Proofs for Chapter 6

B.1 Proof of Theorem 6.1

Interfering UEs distance distribution depends on the link characteristics of the reference UE and the interfering UEs. Given that a reference BS is associated with a LOS reference receiver at distance x, there can be interference from LOS and NLOS UEs. Let's assume a LOS interferer at $\boldsymbol{Y_L}$ with distance y_L to the reference BS. Then the user at $\boldsymbol{Y_L}$ can be an interferer if $y_L^{-\alpha_L} < x^{-\alpha_L}$. Therefore, the CDF of the LOS interfering UE conditioned on reference BS connected to a LOS reference UE can be written as

$$F(y_L < y \mid y_L > x, \boldsymbol{Y_L}) = \frac{\mathbb{P}(x < y_L < y, \boldsymbol{Y_L})}{\mathbb{P}(y_L > x, \boldsymbol{Y_L})} = \frac{\int_x^y f_{\text{int}}(q)p(q)dq}{\int_x^{R+x} f_{\text{int}}(q)p(q)dq} \tag{B.1}$$

where $f_{\text{int}}(.)$ is given by (6.16). The PDF can be obtained by differentiating the CDF in (B.1) and can be written as

$$f_{L|L}(y) = \frac{f_{\text{int}}(y)p(y)}{\int_x^{R+x} f_{\text{int}}(q)p(q)dq}. \tag{B.2}$$

Similarly, $f_{N|L}(y)$, $f_{L|N}(y)$ and $f_{N|N}(y)$ can be proved.

B.2 Proof of Theorem 6.3

This section provides the proof of the Laplace transform of the aggregate interference given that the reference UE at the origin is connected to a LOS BS at $\boldsymbol{X}$ with distance x from the reference UE. Based on this, the reference BS at $\boldsymbol{X}$ will get interference from a set of LOS s_L and NLOS s_N interfering UEs. Moreover, these interfering UEs can be divided further based on their connections to their tagged BSs. So, it can be concluded that the interfering UEs can be categorised into four categories as (i) A set of LOS interferers with LOS links to their tagged BS, s_{LL}, (ii) A set of LOS interferers with NLOS links to their tagged BS, s_{LN},(iii) A set of NLOS interferers with LOS links to their tagged BS, s_{NL}, and (iv) A set of NLOS interferers with NLOS links to their tagged BS, s_{NN}. With these understanding the Laplace transform of aggregate interference conditioned on the LOS reference UE can be proved as in (B.3).

$$
\begin{aligned}
\mathcal{L}_{I|L}\left(\frac{n\eta_L\tau x^{\alpha_L(1-\epsilon)}}{N}\right) &= \mathcal{E}_{h_{\mathbf{y}},G_i,u,y}\left[\exp\left(\frac{-n\eta_L\tau x^{\alpha_L(1-\epsilon)}\sum_{\boldsymbol{Y}\in s_{LL}} h_{\mathbf{y}}u^{\alpha_{L\epsilon}}G_i y^{-\alpha_L}}{N}\right)\exp\left(\frac{-n\eta_L\tau x^{\alpha_L(1-\epsilon)}\sum_{\boldsymbol{Y}\in s_{LN}} h_{\mathbf{y}}u^{\alpha_{N\epsilon}}G_i y^{-\alpha_L}}{N}\right)\right.\\
&\left.\exp\left(\frac{-n\eta_L\tau x^{\alpha_L(1-\epsilon)}\sum_{\boldsymbol{Y}\in s_{NL}} h_{\mathbf{y}}u^{\alpha_{L\epsilon}}G_i y^{-\alpha_N}}{N}\right)\exp\left(\frac{-n\eta_L\tau x^{\alpha_L(1-\epsilon)}\sum_{\boldsymbol{Y}\in s_{NN}} h_{\mathbf{y}}u^{\alpha_{N\epsilon}}G_i y^{-\alpha_N}}{N}\right)\right]\\
&\overset{(c)}{=} \prod_{\boldsymbol{Y}\in s_{LL}}\frac{1}{\left(1+\frac{\mathcal{C}y^{-\alpha_L}u^{\alpha_{L\epsilon}}}{\beta_L}\right)^{\beta_L}}\prod_{\boldsymbol{Y}\in s_{LN}}\frac{1}{\left(1+\frac{\mathcal{C}y^{-\alpha_L}u^{\alpha_{N\epsilon}}}{\beta_L}\right)^{\beta_L}}\prod_{\boldsymbol{Y}\in s_{NL}}\frac{1}{\left(1+\frac{\mathcal{C}y^{-\alpha_N}u^{\alpha_{L\epsilon}}}{\beta_N}\right)^{\beta_N}}\prod_{\boldsymbol{Y}\in s_{NN}}\frac{1}{\left(1+\frac{\mathcal{C}y^{-\alpha_N}u^{\alpha_{N\epsilon}}}{\beta_N}\right)^{\beta_N}}\\
&\overset{(d)}{=} \left(\mathbb{P}(\mathcal{E}_1\mid\mathcal{E})A_L\int_x^{R+x}\frac{1}{\left(1+\frac{\mathcal{C}y^{-\alpha_L}u^{\alpha_{L\epsilon}}}{\beta_L}\right)^{\beta_L}}\hat{f}_L(u)f_{L|L}(y)dudy \;+\; \mathbb{P}(\mathcal{E}_1\mid\mathcal{E})A_N\int_x^{R+x}\frac{1}{\left(1+\frac{\mathcal{C}y^{-\alpha_L}u^{\alpha_{N\epsilon}}}{\beta_L}\right)^{\beta_L}}\hat{f}_N(u)f_{L|L}(y)dudy\right.\\
&\left.+\; \mathbb{P}(\mathcal{E}_2\mid\mathcal{E})A_L\int_{x^{\frac{\alpha_L}{\alpha_N}}}^{R+x}\frac{1}{\left(1+\frac{\mathcal{C}y^{-\alpha_N}u^{\alpha_{L\epsilon}}}{\beta_N}\right)^{\beta_N}}\hat{f}_L(u)f_{N|L}(y)dudy \;+\; \mathbb{P}(\mathcal{E}_2\mid\mathcal{E})A_N\int_{x^{\frac{\alpha_L}{\alpha_N}}}^{R+x}\frac{1}{\left(1+\frac{\mathcal{C}y^{-\alpha_N}u^{\alpha_{N\epsilon}}}{\beta_N}\right)^{\beta_N}}\hat{f}_N(u)f_{N|L}(y)dudy\right)\\
&\overset{(e)}{=} \left(\mathbb{P}(\mathcal{E}_1\mid\mathcal{E})\int_x^{R+x}\left\{\int_0^{a_d}A_{L,1}\int_0^{R+a}\frac{1}{\left(1+\frac{\mathcal{C}y^{-\alpha_L}u^{\alpha_{L\epsilon}}}{\beta_L}\right)^{\beta_L}}\hat{f}_{L,1}(u)\frac{2a}{R^2}duda \;+\; \int_{a_d}^{R}A_{L,2}\int_0^{R+a}\frac{1}{\left(1+\frac{\mathcal{C}y^{-\alpha_L}u^{\alpha_{L\epsilon}}}{\beta_L}\right)^{\beta_L}}\hat{f}_{L,2}(u)\frac{2a}{R^2}duda\right.\right.\\
&\quad+\int_0^{a_d}A_{N,1}\int_0^{R+a}\frac{1}{\left(1+\frac{\mathcal{C}y^{-\alpha_L}u^{\alpha_{N\epsilon}}}{\beta_L}\right)^{\beta_L}}\hat{f}_{N,1}(u)\frac{2a}{R^2}duda \;+\; \int_{a_d}^{R}A_{N,2}\int_0^{R+a}\frac{1}{\left(1+\frac{\mathcal{C}y^{-\alpha_L}u^{\alpha_{N\epsilon}}}{\beta_L}\right)^{\beta_L}}\hat{f}_{N,2}(u,a)\frac{2a}{R^2}duda\left.\right\}f_{L|L}(y)dy\\
&\quad+\;\mathbb{P}(\mathcal{E}_2\mid\mathcal{E})\int_{x^{\frac{\alpha_L}{\alpha_N}}}^{R+x}\left\{\int_0^{a_d}A_{L,1}\int_0^{R+a}\frac{1}{\left(1+\frac{\mathcal{C}y^{-\alpha_N}u^{\alpha_{L\epsilon}}}{\beta_N}\right)^{\beta_N}}\hat{f}_{L,1}(u)\frac{2a}{R^2}duda \;+\; \int_{a_d}^{R}A_{L,2}\int_0^{R+a}\frac{1}{\left(1+\frac{\mathcal{C}y^{-\alpha_N}u^{\alpha_{L\epsilon}}}{\beta_N}\right)^{\beta_N}}\hat{f}_{L,2}(u)\frac{2a}{R^2}duda\right.\\
&\left.\left.\quad+\int_0^{a_d}A_{N,1}\int_0^{R+a}\frac{1}{\left(1+\frac{\mathcal{C}y^{-\alpha_N}u^{\alpha_{N\epsilon}}}{\beta_N}\right)^{\beta_N}}\hat{f}_{N,1}(u)\frac{2a}{R^2}duda \;+\; \int_{a_d}^{R}A_{N,2}\int_0^{R+a}\frac{1}{\left(1+\frac{\mathcal{C}y^{-\alpha_N}u^{\alpha_{N\epsilon}}}{\beta_N}\right)^{\beta_N}}\hat{f}_{N,2}(u,a)\frac{2a}{R^2}duda\right\}f_{N|L}(y)dy\right)^{N_t-1}.
\end{aligned}
\tag{B.3}
$$

In (B.3), $\mathcal{C}$ is given by

$$\mathcal{C} = \frac{n\eta_L \tau x^{\alpha_L(1-\epsilon)} \mathcal{E}_{G_i}[(G_i)]}{N}. \tag{B.4}$$

In (B.3), (c) follows from the moment generating function of the gamma random variable, and (d) is obtained by converting from Cartesian to polar coordinates and evaluating the function with respect to u, recall that an interfering UE at distance a from the origin will connect to its reference BS as per the PDF given in (6.8) or (6.9) or (6.10) or (6.11). Then (e) follows from depending on the position of the interfering UE from the centre (distance a) the PDFs can be either case (1) or case (2). So a distance a_d is defined in such way that case (1) derivations are applicable for the UEs in between 0 and a_d and case (2) derivations are applicable for the UEs in between a_d and R. This distance a_d can be determined by solving for a in $(R-a)^{\frac{\alpha_N}{\alpha_L}} - (R+a)$ and finding the minimum real solution. For example for $R = 100$ m, $\alpha_L = 2$ and $\alpha_N = 4$, a_d becomes 86.35 m. Also the PDF of a from the origin of the disk region can be written as $\frac{2a}{R^2}$ [21].

The probabilities $\mathbb{P}(\mathcal{E}_1 \mid \mathcal{E})$ and $\mathbb{P}(\mathcal{E}_2 \mid \mathcal{E})$ can be defined with the following arguments. Assuming a LOS UE at the origin and its reference BS at distance x, the LOS and NLOS interfering UEs will be x and $x^{\frac{\alpha_L}{\alpha_N}}$ away from the reference BS, respectively. With these interpretations, the following events can be defined:

- $\mathcal{E}_1$: Reference BS at $\boldsymbol{X}$ is interfered by a LOS UE at $\boldsymbol{Y}$, which is father than distance x from the reference BS at $\boldsymbol{X}$; and
- $\mathcal{E}_2$: Reference BS at $\boldsymbol{X}$ is interfered by an NLOS UE at $\boldsymbol{Y}$, which is father than distance $x^{\frac{\alpha_L}{\alpha_N}}$ from the reference BS at $\boldsymbol{X}$.

Further the union of both the events $\mathbb{P}(\mathcal{E})$ is given by $\mathbb{P}(\mathcal{E}_1) + \mathbb{P}(\mathcal{E}_2)$.

Next, the probabilities $\mathbb{P}(\mathcal{E}_1 \mid \mathcal{E})$ and $\mathbb{P}(\mathcal{E}_2 \mid \mathcal{E})$ can be defined as

$$\mathbb{P}(\mathcal{E}_1 \mid \mathcal{E}) = \frac{\mathbb{P}(\mathcal{E}_1, \mathcal{E})}{\mathbb{P}(T)} \overset{(a)}{=} \frac{\mathbb{P}(\mathcal{E}_1)}{\mathbb{P}(\mathcal{E})}$$
$$= \frac{\int_x^{R+x} f_{\text{int}}(q)p(q)dq}{\int_x^{R+x} f_{\text{int}}(q)p(q)dq + \int_{x\frac{\alpha_L}{\alpha_N}}^{R+x} f_{\text{int}}(q)(1-p(q))dq} \quad \text{(B.5)}$$

where (a) follows from mutually exclusive events.

Similarly $\mathbb{P}(\mathcal{E}_2 \mid \mathcal{E})$ can be written as

$$\mathbb{P}(\mathcal{E}_2 \mid \mathcal{E}) = \frac{\int_{x\frac{\alpha_L}{\alpha_N}}^{R+x} f_{\text{int}}(q)(1-p(q))dq}{\int_x^{R+x} f_{\text{int}}(q)p(q)dq + \int_{x\frac{\alpha_L}{\alpha_N}}^{R+x} f_{\text{int}}(q)(1-p(q))dq}. \quad \text{(B.6)}$$

In a similar way, the Laplace transform of the aggregate interference given that the reference UE at the origin is connected to an NLOS BS can be proved.

Bibliography

[1] "Secure spectrum sharing and coexistence of heterogeneous wireless systems — wireless.ece.arizona.edu," http://wireless.ece.arizona.edu/secure-spectrum-sharing-and-coexistence-heterogeneous-wireless-systems, (Accessed on 02/16/2021).

[2] N. Heuveldop, "Ericsson mobility report," Nov 2017. [Online]. Available: https://www.ericsson.com/49de7e/assets/local/mobility-report/documents/2017/ericsson-mobility-report-november-2017.pdf

[3] J. Guo *et al.*, "Stochastic geometry for modeling, analysis and design of future wireless networks," 2016.

[4] A. F. Cattoni, H. T. Nguyen, J. Duplicy, D. Tandur, B. Badic, R. Balraj, F. Kaltenberger, I. Latif, A. Bhamri, G. Vivier *et al.*, "Multi-user MIMO and carrier aggregation in 4G systems: The SAMURAI approach," in *2012 IEEE Wireless Communications and Networking Conference Workshops (WCNCW)*. IEEE, 2012, pp. 288–293.

[5] "Carrier aggregation explained," https://www.3gpp.org/technologies/keywords-acronyms/101-carrier-aggregation-explained, (Accessed on 02/16/2021).

[6] H. S. Dhillon, "Fundamentals of heterogeneous cellular networks," Ph.D. dissertation, 2013.

[7] C. Cano and D. J. Leith, "Coexistence of WiFi and LTE in unlicensed bands: A proportional fair allocation scheme," in *2015 IEEE International Conference on Communication Workshop (ICCW)*. IEEE, 2015, pp. 2288–2293.

[8] C. Gartenberg, "T-Mobile rolls out LTE-U support in sixnbsp;cities," Jun 2017. [Online]. Available: https://www.theverge.com/2017/6/26/15876884/t-mobile-lte-u-support-six-cities-licensedassisted-access

[9] T. S. Rappaport, R. W. Heath Jr, R. C. Daniels, and J. N. Murdock, *Millimeter wave wireless communications*. Pearson Education, 2015.

[10] T. S. Rappaport, S. Sun, R. Mayzus, H. Zhao, Y. Azar, K. Wang, G. N. Wong, J. K. Schulz, M. Samimi, and F. Gutierrez, "Millimeter wave mobile communications for 5G cellular: It will work!" *IEEE Access*, vol. 1, pp. 335–349, 2013.

[11] M. Kamel, W. Hamouda, and A. Youssef, "Ultra-dense networks: A survey," *IEEE Communications Surveys & Tutorials*, vol. 18, no. 4, pp. 2522–2545, 2016.

[12] D. López-Pérez, M. Ding, H. Claussen, and A. H. Jafari, "Towards 1 Gbps/UE in cellular systems: Understanding ultra-dense small cell deployments," *IEEE Communications Surveys & Tutorials*, vol. 17, no. 4, pp. 2078–2101, 2015.

[13] M. Ding, D. López-Pérez, G. Mao, P. Wang, and Z. Lin, "Will the area spectral efficiency monotonically grow as small cells go dense?" in *2015 IEEE Global Communications Conference (GLOBECOM)*. IEEE, 2015, pp. 1–7.

[14] R. Baldemair, T. Irnich, K. Balachandran, E. Dahlman, G. Mildh, Y. Selén, S. Parkvall, M. Meyer, and A. Osseiran, "Ultra-dense networks in millimeter-wave frequencies," *IEEE Communications Magazine*, vol. 53, no. 1, pp. 202–208, 2015.

[15] J. G. Andrews, F. Baccelli, and R. K. Ganti, "A tractable approach to coverage and rate in cellular networks," *IEEE Transactions on Communications*, vol. 59, no. 11, pp. 3122–3134, 2011.

[16] A. D. Wyner, "Shannon-theoretic approach to a gaussian cellular multiple-access channel," *IEEE Transactions on Information Theory*, vol. 40, no. 6, pp. 1713–1727, 1994.

[17] J. Xu, J. Zhang, and J. G. Andrews, "On the accuracy of the Wyner model in cellular networks," *IEEE Transactions on Wireless Communications*, vol. 10, no. 9, pp. 3098–3109, 2011.

[18] J. G. Andrews, A. K. Gupta, and H. S. Dhillon, "A primer on cellular network analysis using stochastic geometry," *arXiv preprint arXiv:1604.03183*, 2016.

[19] M. Haenggi, *Stochastic Geometry for Wireless Networks*. Cambridge University Press, 2012.

[20] Y. Li, "Modeling and analyzing the evolution of cellular networks using stochastic geometry," Ph.D. dissertation, 2017.

[21] M. Afshang and H. S. Dhillon, "Fundamentals of modeling finite wireless networks using binomial point process," *IEEE Transactions on Wireless Communications*, vol. 16, no. 5, pp. 3355–3370, 2017.

[22] "A novel approximate antenna pattern for directional antenna arrays, author=Deng, Na and Haenggi, Martin," *IEEE Wireless Communications Letters*, vol. 7, no. 5, pp. 832–835, 2018.

[23] T. S. Rappaport, G. R. MacCartney, M. K. Samimi, and S. Sun, "Wideband millimeter-wave propagation measurements and channel models for future wireless communication system design," *IEEE Transactions on Communications*, vol. 63, no. 9, pp. 3029–3056, 2015.

[24] M. Di Renzo, "Stochastic geometry modeling and analysis of multi-tier millimeter wave cellular networks," *IEEE Transactions on Wireless Communications*, vol. 14, no. 9, pp. 5038–5057, 2015.

[25] E. Turgut and M. C. Gursoy, "Coverage in heterogeneous downlink millimeter wave cellular networks," *IEEE Transactions on Communications*, vol. 65, no. 10, pp. 4463–4477, 2017.

[26] T. S. Rappaport, F. Gutierrez, E. Ben-Dor, J. N. Murdock, Y. Qiao, and J. I. Tamir, "Broadband millimeter-wave propagation measurements and models using adaptive-beam antennas for outdoor urban cellular communications,"

IEEE Transactions on Antennas and Propagation, vol. 61, no. 4, pp. 1850–1859, 2012.

[27] S. Rajagopal, S. Abu-Surra, and M. Malmirchegini, "Channel feasibility for outdoor non-line-of-sight mmwave mobile communication," in *2012 IEEE Vehicular Technology Conference (VTC Fall)*. IEEE, 2012, pp. 1–6.

[28] Z. Pi and F. Khan, "An introduction to millimeter-wave mobile broadband systems," *IEEE Communications Magazine*, vol. 49, no. 6, pp. 101–107, 2011.

[29] C. R. Anderson and T. S. Rappaport, "In-building wideband partition loss measurements at 2.5 and 60 GHz," *IEEE Transactions on Wireless Communications*, vol. 3, no. 3, pp. 922–928, 2004.

[30] K. Allen, N. DeMinco, J. Hoffman, Y. Lo, and P. Papazian, "Building penetration loss measurements at 900 MHz, 11.4 GHz, and 28.8 GHz," *NTIA Report*, pp. 94–306, 1994.

[31] A. V. Alejos, M. G. Sanchez, and I. Cuinas, "Measurement and analysis of propagation mechanisms at 40 GHz: Viability of site shielding forced by obstacles," *IEEE Transactions on Vehicular Technology*, vol. 57, no. 6, pp. 3369–3380, 2008.

[32] S. Joshi and S. Sancheti, "Foliage loss measurements of tropical trees at 35 GHz," in *2008 International Conference on Recent Advances in Microwave Theory and Applications*. IEEE, 2008, pp. 531–532.

[33] A. Y. Nashashibi, K. Sarabandi, S. Oveisgharan, M. C. Dobson, W. S. Walker, and E. Burke, "Millimeter-wave measurements of foliage attenuation and ground reflectivity of tree stands at nadir incidence," *IEEE Transactions on Antennas and Propagation*, vol. 52, no. 5, pp. 1211–1222, 2004.

[34] J. S. Lu, D. Steinbach, P. Cabrol, and P. Pietraski, "Modeling human blockers in millimeter wave radio links," *ZTE Communications*, vol. 10, no. 4, pp. 23–28, 2012.

[35] M. Gapeyenko, A. Samuylov, M. Gerasimenko, D. Moltchanov, S. Singh, E. Aryafar, S.-p. Yeh, N. Himayat, S. Andreev, and Y. Koucheryavy, "Analysis of human-body blockage in urban millimeter-wave cellular communications," in *2016 IEEE International Conference on Communications (ICC)*. IEEE, 2016, pp. 1–7.

[36] A. Grami, *Introduction to digital communications*. Academic Press, 2015.

[37] M. K. Simon and M.-S. Alouini, *Digital communication over fading channels*. John Wiley & Sons, 2005, vol. 95.

[38] T. Bai and R. W. Heath, "Coverage and rate analysis for millimeter-wave cellular networks," *IEEE Transactions on Wireless Communications*, vol. 14, no. 2, pp. 1100–1114, 2014.

[39] Y. Yang, "Ultra-densification for future cellular networks: Performance analysis and design insights," Ph.D. dissertation, KTH Royal Institute of Technology, 2018.

[40] B. Błaszczyszyn, M. Haenggi, P. Keeler, and S. Mukherjee, *Stochastic geometry analysis of cellular networks*. Cambridge University Press, 2018.

[41] S. N. Chiu, D. Stoyan, W. S. Kendall, and J. Mecke, *Stochastic geometry and its applications*. John Wiley & Sons, 2013.

[42] J. G. Andrews, F. Baccelli, and R. K. Ganti, "A tractable approach to coverage and rate in cellular networks," *IEEE Transactions on Communications*, vol. 59, no. 11, pp. 3122–3134, 2011.

[43] S. Singh, M. N. Kulkarni, A. Ghosh, and J. G. Andrews, "Tractable model for rate in self-backhauled millimeter wave cellular networks," *IEEE Journal on Selected Areas in Communications*, vol. 33, no. 10, pp. 2196–2211, 2015.

[44] O. Onireti, A. Imran, and M. A. Imran, "Coverage, capacity, and energy efficiency analysis in the uplink of mmwave cellular networks," *IEEE Transactions on Vehicular Technology*, vol. 67, no. 5, pp. 3982–3997, 2018.

[45] O. Onireti, L. Zhang, A. Imran, and M. A. Imran, "Outage probability in the uplink of multitier millimeter wave cellular networks," *IEEE Systems Journal*, vol. 14, no. 2, pp. 2520–2531, 2020.

[46] N. A. Muhammad, N. I. A. Apandi, Y. Li, and N. Seman, "Uplink performance analysis for millimeter wave cellular networks with clustered users," *IEEE Transactions on Vehicular Technology*, vol. 69, no. 6, pp. 6178–6188, 2020.

[47] H. Elshaer, M. N. Kulkarni, F. Boccardi, J. G. Andrews, and M. Dohler, "Downlink and uplink cell association with traditional macrocells and millimeter wave small cells," *IEEE Transactions on Wireless Communications*, vol. 15, no. 9, pp. 6244–6258, 2016.

[48] F. Baccelli and B. Błaszczyszyn, *Stochastic geometry and wireless networks*. Now Publishers Inc, 2009, vol. 1.

[49] X. Lin and J. G. Andrews, "A general approach to SINR-based performance metrics with application to D2D and carrier aggregation," in *2013 Asilomar Conference on Signals, Systems and Computers*. IEEE, 2013, pp. 738–742.

[50] S. Mukherjee, *Analytical modeling of heterogeneous cellular networks*. Cambridge University Press, 2014.

[51] H. Alzer, "On some inequalities for the incomplete gamma function," *Mathematics of Computation*, vol. 66, no. 218, pp. 771–778, 1997.

[52] A. Goldsmith, *Wireless communications*. Cambridge university press, 2005.

[53] X. Yu, C. Li, J. Zhang, and K. B. Letaief, *Stochastic Geometry Analysis of Multi-Antenna Wireless Networks*. Springer, 2019.

[54] T. Baykas, C.-S. Sum, Z. Lan, J. Wang, M. A. Rahman, H. Harada, and S. Kato, "IEEE 802.15. 3c: The first IEEE wireless standard for data rates over 1 Gb/s," *IEEE Communications Magazine*, vol. 49, no. 7, pp. 114–121, 2011.

[55] W. Group *et al.*, "IEEE standard part 11: Wireless LAN MAC and PHY specifications," *IEEE Std 802.11-2012*, 2012.

[56] J. Horwitz, "FCC will auction 5G–ready 3.7-4.2GHz and mmwave spectrum–if Congress acts by May 13," Feb 2018. [Online]. Available: https://venturebeat.com/2018/02/26/fcc-will-auction-5g-ready-3-7-4-2ghz-and-mmwave-spectrum-if\congress-acts-by-may-13/

[57] S. Rangan, T. S. Rappaport, and E. Erkip, "Millimetre-wave cellular wireless networks: potentials and challenges," *Proceedings of the IEEE*, vol. 102, no. 3, pp. 366–385, 2014.

[58] M. R. Akdeniz, Y. Liu, M. K. Samimi, S. Sun, S. Rangan, T. S. Rappaport, and E. Erkip, "Millimeter wave channel modeling and cellular capacity evaluation," *IEEE Journal on Selected Areas in Communications*, vol. 32, no. 6, pp. 1164–1179, 2014.

[59] H. ElSawy, E. Hossain, and M. Haenggi, "Stochastic geometry for modeling, analysis, and design of multi-tier and cognitive cellular wireless networks: A survey," *IEEE Communications Surveys & Tutorials*, vol. 15, no. 3, pp. 996–1019, 2013.

[60] X. Yu, J. Zhang, M. Haenggi, and K. B. Letaief, "Coverage analysis for millimeter wave networks: The impact of directional antenna arrays," *IEEE Journal on Selected Areas in Communications*, vol. 35, no. 7, pp. 1498–1512, 2017.

[61] J. G. Andrews, T. Bai, M. N. Kulkarni, A. Alkhateeb, A. K. Gupta, and R. W. Heath, "Modelling and analysing millimetre wave cellular systems," *IEEE Transactions on Communications*, vol. 65, no. 1, pp. 403–430, 2017.

[62] S. M. Azimi-Abarghouyi, B. Makki, M. Nasiri-Kenari, and T. Svensson, "Stochastic geometry modeling and analysis of finite millimeter wave wireless networks," *IEEE Transactions on Vehicular Technology*, vol. 68, no. 2, pp. 1378–1393, 2019.

[63] A. Thornburg, T. Bai, and R. W. Heath, "Performance analysis of outdoor mmwave ad hoc networks," *IEEE Transactions on Signal Processing*, vol. 64, no. 15, pp. 4065–4079, 2016.

[64] S. Srinivasa and M. Haenggi, "Distance distributions in finite uniformly random networks: Theory and applications," *IEEE Transactions on Vehicular Technology*, vol. 59, no. 2, pp. 940–949, 2010.

[65] K. Venugopal, M. C. Valenti, and R. W. Heath, "Interference in finite-sized highly dense millimeter wave networks," in *2015 Information Theory and Applications Workshop (ITA)*. IEEE, 2015, pp. 175–180.

[66] J. Guo, S. Durrani, and X. Zhou, "Outage probability in arbitrarily-shaped finite wireless networks," *IEEE Transactions on Communications*, vol. 62, no. 2, pp. 699–712, 2014.

[67] Z. Khalid and S. Durrani, "Distance distributions in regular polygons," *IEEE Transactions on Vehicular Technology*, vol. 62, no. 5, pp. 2363–2368, 2013.

[68] X. Wang, H. Zhang, Y. Tian, and V. C. M. Leung, "Modeling and analysis of aerial base station-assisted cellular networks in finite areas under LoS and NLoS propagation," *IEEE Transactions on Wireless Communications*, vol. 17, no. 10, pp. 6985–7000, 2018.

[69] T. Bai, R. Vaze, and R. W. Heath, "Analysis of blockage effects on urban cellular networks," *IEEE Transactions on Wireless Communications*, vol. 13, no. 9, pp. 5070–5083, 2014.

[70] J. Guo, S. Durrani, and X. Zhou, "Performance analysis of arbitrarily-shaped underlay cognitive networks: Effects of secondary user activity protocols," *IEEE Transactions on Communications*, vol. 63, no. 2, pp. 376–389, 2014.

[71] A. Baddeley, I. Bárány, and R. Schneider, "Spatial point processes and their applications," *Stochastic Geometry: Lectures Given at the CIME Summer School Held in Martina Franca, Italy, September 13–18, 2004*, pp. 1–75, 2007.

[72] H. ElSawy and E. Hossain, "On stochastic geometry modeling of cellular uplink transmission with truncated channel inversion power control," *IEEE Transactions on Wireless Communications*, vol. 13, no. 8, pp. 4454–4469, 2014.

[73] D. Moltchanov, "Distance distributions in random networks," *Ad Hoc Networks*, vol. 10, no. 6, pp. 1146–1166, 2012.

[74] G. Yao, N. Liu, Z. Pan, and X. You, "Coverage and rate analysis for non-uniform millimeter-wave heterogeneous cellular network," in *2016 8th International Conference on Wireless Communications & Signal Processing (WCSP)*. IEEE, 2016, pp. 1–6.

[75] N. Deng, W. Zhou, and M. Haenggi, "Heterogeneous cellular network models with dependence," *IEEE Journal on Selected Areas in Communications*, vol. 33, no. 10, pp. 2167–2181, 2015.

[76] Z. Yazdanshenasan, H. S. Dhillon, M. Afshang, and P. H. Chong, "Poisson hole process: Theory and applications to wireless networks," *IEEE Transactions on Wireless Communications*, vol. 15, no. 11, pp. 7531–7546, 2016.

[77] M. Comisso and F. Babich, "Coverage analysis for 2D/3D millimeter wave peer-to-peer networks," *IEEE Transactions on Wireless Communications*, vol. 18, no. 7, pp. 3613–3627, 2019.

[78] F. Babich, M. Comisso, and A. Cuttin, "Impact of interference spatial distribution on line-of-sight millimeter-wave communications," in *European Wireless 2017; 23th European Wireless Conference*. VDE, 2017, pp. 1–6.

[79] Y. Liu, Z. Qin, M. Elkashlan, Z. Ding, A. Nallanathan, and L. Hanzo, "Non-orthogonal multiple access for 5G and beyond," *Proceedings of the IEEE*, vol. 105, no. 12, pp. 2347–2381, 2017.

[80] S. Kusaladharma, W.-P. Zhu, and W. Ajib, "Outage performance and average rate for large-scale millimeter-wave NOMA networks," *IEEE Transactions on Wireless Communications*, vol. 19, no. 2, pp. 1280–1291, 2019.